IDO-16752
September 1963

TRANSIENT TESTS OF THE SPERT I LOW-ENRICHMENT UO_2 CORE: DATA SUMMARY REPORT

718501

H.K. Peterson 12-15-83

R. Scott, Jr., A. A. Wasserman, and R. C. Schmitt

REPOSITORY INEL
COLLECTION PUBLIC READING ROOM
U.S. DOE PUBLIC READING ROOM IDO
BOX No. UNIVERSITY PLACE
FOLDER IDO-16752

PHILLIPS 66

NATIONAL REACTOR TESTING STATION
IDAHO OPERATIONS OFFICE

1133246

PRICE $2.00

Available from the
Office of Technical Services
U. S. Department of Commerce
Washington 25, D. C.

LEGAL NOTICE

This report was prepared as an account of Government sponsored work. Neither the United States, nor the Commission, nor any person acting on behalf of the Commission:

A. Makes any warranty or representation, express or implied, with respect to the accuracy, completeness, or usefulness of the information contained in this report, or that the use of any information, apparatus, method, or process disclosed in this report may not infringe privately owned rights; or

B. Assumes any liabilities with respect to the use of, or for damages resulting from the use of any information, apparatus, method, or process disclosed in this report.

As used in the above, "person acting on behalf of the Commission" includes any employee or contractor of the Commission, or employee of such contractor, to the extent that such employee or contractor of the Commission, or employee of such contractor prepares, disseminates, or provides access to, any information pursuant to his employment or contract with the Commission, or his employment with such contractor.

Printed in USA

1133247

IDO-16752
AEC Research and Development Report
Reactor Technology
TID-4500 (22nd Ed.)
Issued: September 3, 1963

TRANSIENT TESTS OF THE SPERT I LOW-ENRICHMENT UO_2 CORE: DATA SUMMARY REPORT

by

R. Scott, Jr.
A. A. Wasserman
R. C. Schmitt

PHILLIPS
PETROLEUM
COMPANY

Atomic Energy Division
Contract AT(10-1)-205
Idaho Operations Office
U. S. ATOMIC ENERGY COMMISSION

1133248

INTENTIONAL BLANK PAGE NO. ii

1133249

TRANSIENT TESTS OF THE SPERT I
LOW-ENRICHMENT UO_2 CORE: DATA SUMMARY REPORT

CONTENTS

I. INTRODUCTION 1

II. GENERAL TEST DESCRIPTION 2

III. CORE DESCRIPTION 4

IV. POWER CALIBRATION AND MEASUREMENT 5

V. TEMPERATURE AND PRESSURE MEASUREMENT 8

VI. PHOTOGRAPHIC MEASUREMENTS OF FUEL ROD MOVEMENT ... 11

VII. DATA-PROCESSING PROCEDURES 13

VIII. TEST DATA 14

IX. REFERENCES 16

APPENDIX A - PLOTS OF SURFACE TEMPERATURE, POWER, ENERGY, AND COMPENSATED REACTIVITY VS TIME, FOR UNCONSTRAINED SPERT I OXIDE CORE .. 19

APPENDIX B - PLOTS OF SURFACE TEMPERATURE, POWER, ENERGY, AND COMPENSATED REACTIVITY VS TIME, FOR CONSTRAINED SPERT I OXIDE CORE 49

APPENDIX C - PLOTS OF PEAK POWER, TOTAL ENERGY AT TIME OF PEAK POWER, AND COMPENSATED REACTIVITY AT TIME OF PEAK POWER VS INVERSE PERIOD, FOR CONSTRAINED AND UNCONSTRAINED SPERT I OXIDE CORES 77

APPENDIX D - SUMMARY TABLES OF KEY DATA, FOR THE CONSTRAINED AND UNCONSTRAINED SPERT I OXIDE CORES 83

FIGURES

1. Scheme for specifying transducers location in the core 9

2. Time-sequence photographs showing post-burst random movement of fuel rods 12

1133250

A-1. Run 64 - 15.2-sec-period test 21
A-2. Run 64 - 15.2-sec-period test 21
A-3. Run 3 - 10.5-sec-period test 22
A-4. Run 3 - 10.5-sec-period test 22
A-5. Run 5 - 5.9-sec-period test 23
A-6. Run 5 - 5.9-sec-period test 23
A-7. Run 63 - 4.3-sec-period test 24
A-8. Run 63 - 4.3-sec-period test 24
A-9. Run 6 - 2.3-sec-period test 25
A-10. Run 6 - 2.3-sec-period test 25
A-11. Run 7 - 1.2-sec-period test 26
A-12. Run 7 - 1.2-sec-period test 26
A-13. Run 8 - 822-msec-period test 27
A-14. Run 8 - 822-msec-period test 27
A-15. Run 9 - 542-msec-period test 28
A-16. Run 9 - 542-msec-period test 28
A-17. Run 10 - 273-msec-period test 29
A-18. Run 10 - 273-msec-period test 29
A-19. Run 11 - 150-msec-period test 30
A-20. Run 11 - 150-msec-period test 30
A-21. Run 12 - 114-msec-period test 31
A-22. Run 12 - 114-msec-period test 31
A-23. Run 13 - 84.2-msec-period test 32
A-24. Run 13 - 84.2-msec-period test 32
A-25. Run 14 - 51.8-msec-period test 33
A-26. Run 14 - 51.8-msec-period test 33
A-27. Run 15 - 45.2-msec-period test 34

1133251

A-28. Run 15 - 45.2-msec-period test 34
A-29. Run 16 - 35.5-msec-period test 35
A-30. Run 16 - 35.5-msec-period test 35
A-31. Run 17 - 31.2-msec-period test 36
A-32. Run 17 - 31.2-msec-period test 36
A-33. Run 62 - 27.4-msec-period test 37
A-34. Run 62 - 27.4-msec-period test 37
A-35. Run 18 - 25.8-msec-period test 38
A-36. Run 18 - 25.8-msec-period test 38
A-37. Run 19 - 20.4-msec-period test 39
A-38. Run 19 - 20.4-msec-period test 39
A-39. Run 21 - 17.2-msec-period test 40
A-40. Run 21 - 16.2-msec-period test 40
A-41. Run 22 - 15.7-msec-period test 41
A-42. Run 22 - 15.7-msec-period test 41
A-43. Run 27 - 14.2-msec-period test 42
A-44. Run 27 - 14.2-msec-period test 42
A-45. Run 28 - 11.2-msec-period test 43
A-46. Run 28 - 11.2-msec-period test 43
A-47. Run 29 - 10.1-msec-period test 44
A-48. Run 29 - 10.1-msec-period test 44
A-49. Run 65 - 9.7-msec-period test 45
A-50. Run 65 - 9.7-msec-period test 45
A-51. Run 66 - 9.7-msec-period test 46
A-52. Run 66 - 9.7-msec-period test 46
A-53. Run 75 - 9.7-msec-period test 47
A-54. Run 75 - 9.7-msec-period test 47

1133252

A-55. Run 30 - 8.5-msec-period test 48

A-56. Run 30 - 8.5-msec-period test 48

B-1. Run 47 - 15.0-sec-period test 51

B-2. Run 47 - 15.0-sec-period test 51

B-3. Run 41 - 10.5-sec-period test 52

B-4. Run 41 - 10.5-sec-period test 52

B-5. Run 56 - 8.1-sec-period test 53

B-6. Run 56 - 8.1-sec-period test 53

B-7. Run 45 - 4.8-sec-period test 54

B-8. Run 45 - 4.8-sec-period test 54

B-9. Run 48 - 1.8-sec-period test 55

B-10. Run 48 - 1.8-sec-period test 55

B-11. Run 42 - 957-msec-period test 56

B-12. Run 42 - 957-msec-period test 56

B-13. Run 49 - 416-msec-period test 57

B-14. Run 49 - 416-msec-period test 57

B-15. Run 43 - 273-msec-period test 58

B-16. Run 43 - 273-msec-period test 58

B-17. Run 40 - 144-msec-period test 59

B-18. Run 40 - 144-msec-period test 59

B-19. Run 52 - 108-msec-period test 60

B-20. Run 52 - 108-msec-period test 60

B-21. Run 39 - 73.9-msec-period test 61

B-22. Run 39 - 73.9-msec-period test 61

B-23. Run 53 - 44.1-msec-period test 62

B-24. Run 53 - 44.1-msec-period test 62

B-25. Run 68 - 33.5-msec-period test 63

1133253

B-26. Run 68 - 33.5-msec-period test 63

B-27. Run 50 - 29.2-msec-period test 64

B-28. Run 50 - 29.2-msec-period test 64

B-29. Run 29 - 17.6-msec-period test 65

B-30. Run 38 - 17.6-msec-period test 65

B-31. Run 51 - 14.0-msec-period test 66

B-32. Run 51 - 14.0-msec-period test 66

B-33. Run 54 - 10.2-msec-period test 67

B-34. Run 54 - 10.2-msec-period test 67

B-35. Run 55 - 9.4-msec-period test 68

B-36. Run 55 - 9.4-msec-period test 68

B-37. Run 59 - 7.9-msec-period test 69

B-38. Run 59 - 7.9-msec-period test 69

B-39. Run 69 - 7.0-msec-period test 70

B-40. Run 69 - 7.0-msec-period test 70

B-41. Run 61 - 6.8-msec-period test 71

B-42. Run 61 - 6.8-msec-period test 71

B-43. Run 70 - 6.3-msec-period test 72

B-44. Run 70 - 6.3-msec-period test 72

B-45. Run 71 - 5.6-msec-period test 73

B-46. Run 71 - 5.6-msec-period test 73

B-47. Run 72 - 4.8-msec-period test 74

B-48. Run 72 - 4.8-msec-period test 74

B-49. Run 73 - 3.8-msec-period test 75

B-50. Run 73 - 3.8-msec-period test 75

B-51. Run 74 - 3.2-msec-period test 76

B-52. Run 74 - 3.2-msec-period test 76

1133254

C-1. Peak power vs inverse reactor period 79

C-2. Energy at time of peak power vs inverse reactor period. 80

C-3. Compensated reactivity at time of peak power vs inverse reactor period 80

C-4. Dynamic shutdown coefficient vs inverse reactor period 81

C-5. Power-burst-shape plots (unconstrained oxide core) 81

C-6. Power-burst-shape plots (constrained oxide core) 82

TABLES

I. Specific Heat of UO_2 vs Temperature 6

II. Summary Table of Key Data, for Unconstrained Core 85

III. Summary Table of Key Data, for Constrained Core 86

1133255

TRANSIENT TESTS OF THE SPERT I LOW-ENRICHMENT UO_2 CORE: DATA SUMMARY REPORT

I. INTRODUCTION

This report is presented as a supplement to the report, "Self-Limiting Power Excursion Tests of a Water-Moderated, Low-Enrichment, UO_2 Core in Spert I", [1] which is a description of step-induced transient tests performed in the uranium oxide core in the Spert I reactor facility. The purposes of the present report are: (a) to present a complete set of graphs and tables of the data taken in these tests; (b) to describe the methods used in processing the data; and (c) to provide more complete information on the special instrumentation used for the excursion-test measurements of reactor power, temperature, and pressure.

The report is organized as follows: In Section II and III the principal features of the transient tests and of the reactor core design are reviewed briefly. In Sections IV and V the details of the reactor power and temperature measurement are discussed. In Section VI a brief description of photographic measurements of fuel rod bowing is presented. In Section VII a summary is given of the data-processing methods employed. Finally, in Section VIII an outline is given of the detailed data plots and tables which are presented in the appendices.

1133256

II. GENERAL TEST DESCRIPTION

The purpose of this test series was to investigate the dynamic behavior of a heterogeneous, light-water-moderated reactor, using low-enrichment-UO_2, rod-type fuel elements [1-12]. Self-limiting power excursion tests, initiated by stepwise insertions of reactivity, were conducted over a broad range of initial asymptotic reactor periods, from 30 seconds to 3.2 milliseconds. All tests were performed under the following system conditions: atmospheric pressure, ambient temperature, and no water flow other than that due to natural convection. (Although a water stirrer and a circulation pump were included in the system, they were used only during power calibrations.) The water level was approximately two feet above the top of the core.

In the long-period region, reactor shutdown was provided both by the various heat-transfer-dependent mechanisms effecting loss of moderator from the core and by Doppler broadening of the U-238 absorption resonances. In the short-period region, where the reactor period was short compared to the thermal time constant of the UO_2 fuel rods, reactor shutdown was provided essentially by the Doppler reactivity effect alone, permitting a direct measurement of the dynamic Doppler coefficient of the core.

In the oxide core tests, an additional positive reactivity effect was observed resulting from the systematic bowing of the fuel rods during the transient power burst. This effect introduced a significant change in power-burst shape compared to power-burst shapes observed when the fuel rods were restrained from lateral motion. The reactivity attributed to the fuel-rod bowing effect was separated from the other reactivity effects by performing two series of reactor transient experiments. The first of these was performed with the fuel rods restrained only at the ends, permitting some lateral rod motion at the ends and also allowing fuel-rod bowing and slight axial expansion to occur. This test series is referred to as the "unconstrained core" tests. The second test series was performed with a restraining grid placed within the core matrix. This had the effect of suppressing the fuel-rod bowing. The second test series is referred to as the "constrained core" tests. In both test series, photographic techniques were used to obtain a direct observation of the rod bowing.

1133257

The shortest asymptotic reactor period achieved in these tests was 3.2 msec. In this test a maximum power level of 7500 Mw was reached, the total energy released was about 107 Mw-sec, and the maximum steam pressure was 8 psi. No damage occurred as a consequence of this test.

III. CORE DESCRIPTION

The core used in the power-excursion test series in the Spert I facility consisted of 592 fuel pins in an octagonal configuration. Each fuel pin consisted of a stainless steel tube about 6 ft long and 0.5 in. OD with a 0.028-in. wall, containing 1600 g of 4%-enriched UO_2 powder compressed to a density of 9.45 g/cm^3. The core had an approximate diameter of 19 in., with a center-to-center rectangular pin spacing of 0.663 in. The core was divided into quadrants by a 0.75-in.-thick, aluminum rod-guide cross, which housed four blade-type control rods and a central, cruciform transient rod.

The control rods and transient rod were constructed in such a way that the control rods could be driven into the core and transient rod driven out of the bottom of the core in a very short time interval. The control rods could be dropped into the core in approximately 350 msec, while the transient rod could be dropped out in approximately 270 msec (the time interval from release until it hit the the shock absorber limits of the rod guide).

Criticality was achieved with 503 fuel pins arranged in a cylindrical geometry. This loading had an excess reactivity of 17¢. After criticality was reached the core was then loaded to 592 fuel pins, giving the core approximately 3.3$ excess reactivity.

IDO-16751 gives a more complete description of the Spert I oxide core [1].

1133259

IV. POWER CALIBRATION AND MEASUREMENT

Power data for the excursion tests in the oxide core were obtained by measurements of the neutron leakage from the core, utilizing a number of boron-lined ionization chambers located at various positions at the periphery of the reactor vessel. Some of the chambers were connected to linear-amplifier circuits, others to logarithmic-amplifier circuits. (The power data presented in this report were obtained solely from the linear circuits.) The data were transmitted from the amplifiers to optical recording galvanometers and then printed out on oscillograph charts. The following discussion is a description of the procedures that were followed to obtain the calibration constants for the ion chamber circuits. These procedures were similar to those used in earlier Spert transient test series [13].

Each chamber and its associated circuitry were subjected to a three-stage calibration procedure. First, the chambers were placed in a high neutron-flux field in the thermal column of the Materials Testing Reactor. Measurements were made of the linearity of the chamber current as a function of neutron flux, the value of the current at a given neutron flux, the upper limit to the current, and the operating voltage for current saturation; ie, the domain where the current was independent of the applied voltage. The neutron flux was measured by the gold foil irradiation technique.

Second, a calibration of the electronics circuitry associated with each chamber was performed by using a calibrated current source in place of the chamber. This was referred to as an instrumentation calibration. A relationship was determined between the input current of the source and the magnitude of the resultant deflection of the optical galvanometer record. In order to decrease the effect of drift in the electronic amplifiers and drivers, this calibration was performed weekly. The weekly calibration provided a continual measure of the sensitivity and the linearity of all the electronic circuitry. The sensitivity values obtained from the calibrations had a probable error of less than ± 1%.

Finally, the reactor power corresponding to a given deflection of the galvanometer trace was determined. With the reactor operating at some arbitrary power level, the rate of increase in the bulk system temperature was measured, along with the deflections of the galvanometers connected to the outputs of the ion-chamber circuits. From this measured rate of temperature rise and a calculated value for the system heat capacity, the thermal

1133260

power of the reactor was determined. The power, the deflections of the galvanometers connected to the outputs of the ion chambers circuits, and the results of the instrumentation calibration were then used to determine the chamber calibration constants, in terms of power per unit current from each ion chamber (Mw/μa).

The heat capacity of the system was calculated using the approximation that the entire volume of the reactor, except the UO_2, had the same heat capacity as water. The volumes of the window port and internal piping were included in this calculation, yielding a total reactor volume of 130.5 ft^3, excluding the UO_2. The total heat capacity of this volume of water was calculated to be 15.5 Mw-sec/°C. The UO_2 contribution to the heat capacity of the system was determined from the specific heat of UO_2 and the total mass of UO_2 in the system. The specific heat of UO_2 was taken to be 0.060 cal/g-°C at 24°C (obtained by extrapolation of the data in Table I. so that with a UO_2 mass of 947.2 kg in the core, the UO_2 heat capacity contribution was calculated to be 0.24 Mw-sec/°C at 24°C. The total system heat capacity, therefore, was taken to be 15.7 Mw-sec/°C.

TABLE I

SPECIFIC HEAT OF UO_2 VS TEMPERATURE[14]

Temperature (°C)	Specific Heat (cal/g-°C)	Specific Heat (Mw-sec/°C)
100	0.063	0.25
200	0.067	0.265
500	0.074	0.293
1000	0.078	0.31
1500	0.082	0.325

A four-junction, copper-constantan thermopile with a calibration constant of 0.16 mv/°C in the relevant temperature range was used to obtain the system heating rate. The water level in the reactor tank during this calibration was 2 ft above the top of the core, or 10.5 ft from the bottom of the vessel. The reactor was operated at a steady power of approximately 80 kw for about 15 min with both the stirrer and the circulation pump turned on. The contribution to the overall power arising from the energy put into the system by the stirrer and circulation pump was previously determined in a separate heating rate measurement in which the only source of energy was the pump and stirrer. The observed heating rates were 0.33 °C/min for the reactor at power and 0.013 °C/min for the reactor with only the stirrer and circulation pump on. From these values and the calculated system heat capacity a nuclear power of 82 kw was obtained. The estimated probable error in the nuclear power was ± 1.5%, due chiefly to lack of precision in the measurements of heating rate.

1133261

The output current for each chamber, determined from the magnitude of the deflection of the galvanometers during the nuclear heating cycle, was then obtained and the chamber calibration constants determined in terms of power per unit deflection and power per unit current. The estimated probable error in these chamber calibration constants was $\pm$ 2.5%.

Representative ion chamber constants ranged from 3.8 to 92 Mw/μa (the variation being due principally to the differences in the position of the chambers). The values of the output currents during power calibration ranged from about 0.5 μa for the least sensitive chambers to 3 μa for the most sensitive chambers. The number and arrangement of chambers chosen provided sufficient coverage for all values of the power levels obtained or anticipated during the transient test series.

In the transient test program, four ion chambers were used in each test to detect the relative neutron leakage from the core (proportional to the total power level). Amplification channels with three different sensitivity levels were used with each chamber, so that the full range of the power burst was detected with good sensitivity by the four chambers. In addition, the overall range setting of the chambers could be varied prior to each test, making possible the recording of a total of 10 decades of power level variation. It was required that the recorded power traces should include (with adequate sensitivity) both the initial exponential part of the burst, from which the asymptotic period was determined, and the region near the power peak where the reactivity shutdown processes were most effective.

1133262

V. TEMPERATURE AND PRESSURE MEASUREMENT

The two principal variables (other than reactor power) which were measured during the oxide core tests were the fuel-pin surface-temperature rise and the transient pressure. An attempt also was made to measure the fuel temperature in the interior of the fuel pins. These measured internal fuel temperatures were rather erratic, however, due to the difficulty in mounting the thermocouples within the fuel section of the pin [7,9]. For this reason, these data are not included in this report.

The pressures measured throughout the complete test series were very small (less than 10 psi). These data, therefore, have been omitted from the present report.

The temperature rise measured at the surface of the stainless steel cladding up to the time of peak power was only a few degrees, or less. This was due to the low heat conductivity of the UO_2 and the stainless steel. Further, since Doppler broadening of the U-238 resonances was the main contributor to the self-shutdown of this reactor, the fuel-pin surface-temperature data are of less importance in analyzing the excursion behavior of this system than for previous plate-type Spert reactors.

The scheme used to specify the location of the in-core instrumentation involved a three-dimensional coordinate system, as shown in Figure 1. The coordinate system consisted of dividing the core into four quadrants (north, south, east, and west) and using a rectangular grid in each quadrant. Each quadrant was treated as the first quadrant of a rectangular coordinate system with the center of the core at the origin and with each lattice position located at integral values of the X and Y coordinates. The reference for vertical placement of the transducers was the transverse midplane of the fuel pins. If a transducer were located below the midplane, the placement was denoted as negative; if above the midplane, the placement was positive. As an example, the thermocouple location specified as (W13:3-16) indicated that the thermocouple was mounted on the fuel pin located 13 pins from the origin (or core center) on the X-axis and 3 pins from the origin on the Y-axis. In Figure 1, the fuel pin which contains the thermocouple is designated by an open circle and the thermocouple is located 16 in. below the transverse midplane of the fuel pins.

The following is a brief description of the temperature and pressure measuring techniques used. The temperature-measuring devices were all

1133263

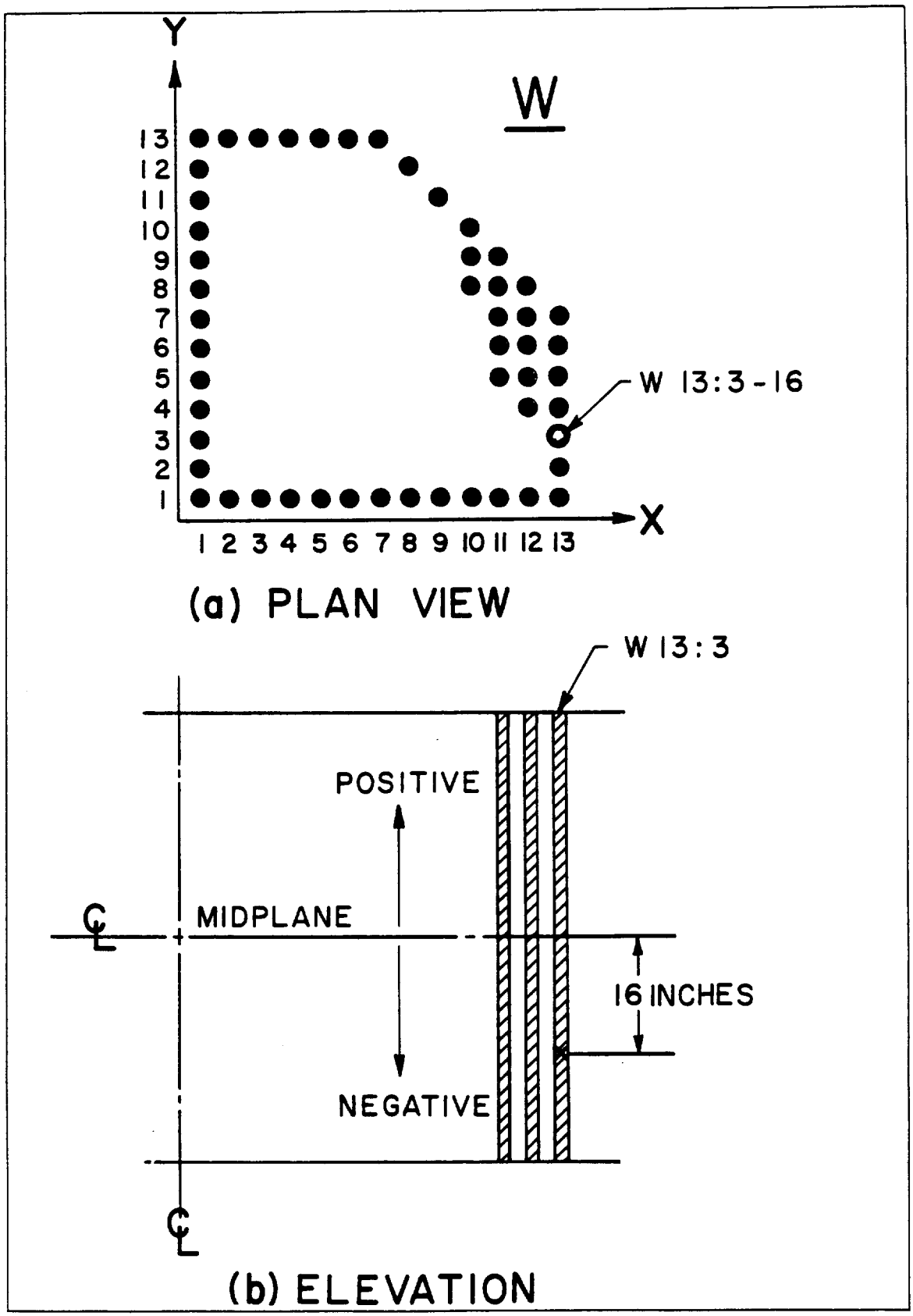

FIG. 1 SCHEME FOR SPECIFYING TRANSDUCERS LOCATION IN THE CORE.

1133264

5-mil chromel-alumel thermocouples. The surface thermocouples were spot-welded to the stainless steel cladding of the fuel pin. All of the thermocouples used had a frequency response of about 10 kc, and an absolute temperature error of $\pm$ 1°C.

The pressure transducers were strain-gage-type, diaphragm transducers having an overall resolution (including the effects of radiation sensitivity) of approximately 5% of full scale, and a frequency response of about 10 kc. (The resolution and frequency-response determinations were made in special tests carried out in the General Atomics TRIGA facility in San Diego, California [15]). One 0- to 25-psig transducer was located within the core (W13:7-18). In addition, one 0- to 50-psig transducer was located in the reflector at the edge of the core (53 in. below the upper core hold-down grid). During the later parts of the test series, when the shorter-period transient tests were performed, two additional pressure transducers were placed around the periphery of the core. These consisted of one 1000-psig transducer and one 500-psig transducer, and were intended primarily as backup in case the 50- and 25-psig transducers were saturated by a strong pressure burst occurring at the shorter periods.

1133265

VI. PHOTOGRAPHIC MEASUREMENTS OF FUEL ROD MOVEMENT

High-speed, in-core motion pictures were taken during some of the unconstrained and constrained core tests. These pictures gave the first direct evidence of significant rod movement during the tests in the unconstrained core. The pictures indicated that a small but systematic bowing of the fuel rods occurred during the power burst, and that a more violent and random type of movement occurred after the power burst had subsided (presumably due to thermal and hydraulic forces following transfer of heat from the fuel rods to the water).

The motion pictures were obtained by viewing though a heavy glass port in the side of the reactor vessel roughly at the level of the midplane of the core. To protect the film from possible radiation damage during the test, a pair of large plane mirrors were used to transmit the image from the level of the glass port to the floor level of the reactor building. The concrete floor of the reactor building provided sufficient radiation shielding for the film. The pictures were taken at approximately 400 frames/sec which, on projection at normal speed, effectively slowed down the rod motion sufficiently to allow analysis of the motion of the individual rods observed. Figure 2 presents a set of prints made from these motion pictures showing fuel pin motion.

A more detailed discussion of the nature and effect of the rod motion was given by Spano [12].

1133266

FIG. 2 TIME-SEQUENCE PHOTOGRAPHS SHOWING POST-BURST RANDOM MOVEMENT OF FUEL RODS.

1133267

VII. DATA-PROCESSING PROCEDURES

The primary data-collecting method used at Spert until the recent introduction of magnetic tape techniques involved high-speed optical recording galvanometers; ie, oscillographs. In the system used in the oxide core tests, signals from the transducers at the reactor area (neutron-detecting ion chambers, pressure transducers, thermocouples, etc) were amplified and transmitted to oscillograph recorders located in the control center one-half mile away. Data from 52 different channels were recorded on the oscillographs in analog format.

The analog data recorded on the oscillograph records were processed through an analog-to-digital conversion system. The conversion system consisted of a manually operated analog curve follower with variable coordinates, and a digital converter with tabulated and punched card outputs. The digital reduced data was made available not only in arbitrary units, but also in the desired engineering units. These reduced data were then plotted on a digital X-Y plotter to obtain individual curves representing the time variation of each of the test variables.

The errors introduced by the data processing procedures were as follows: The analog curve follower introduced an estimated error of ± 1/2 mm (or about 0.7% of the full scale deflection of 76 mm) due to the parallax encountered by the operator in attempting to position the movable index precisely on a point of the analog curve being reduced. The estimated error introduced in the analog-to-digital conversion was ± 1 unit in the least significant digit of the converter's output. This was equivalent to an error of from 0.1 to 1.0% in the processed data, depending upon the full-scale digital setting of the converter. The estimated error introduced in setting the scale factors for the digital plotter was ± 0.02 in. (0.2% of the full-scale deflection of 10 in. on the digital plotter). There was also an inherent error of ± 0.015 in. (0.15% of full scale) contributed by the servo-plotting mechanisms which locate the data points on the graph paper. A small additional error was contributed by nonlinearities in the commercial graph paper used.

The normal range of deflection of the galvanometer traces was from 10 to 70 mm. For deflections of 35 mm or greater, the combined error from the errors sources discussed above was 3% or less.

1133268

VIII. TEST DATA

The transient test data from the Spert I oxide core tests are presented in graphical and tabular form in Appendices A, B, C, and D.

Appendices A and B consist of graphs of data taken during the unconstrained and the constrained core transient tests, respectively. Data from each test are presented in two figures, in sequence, indexed according to the transient run number and the initial asymptotic reactor period. The first (odd-numbered) figure consists of curves showing a comparison between the time history of the reactor power and that of the hottest fuel-pin surface temperature (ie, the hottest-reading fuel pin surface thermocouple for each transient; usually the thermocouple in location E1:1-20). The curves give a graphical demonstration of the delay between the time of peak power and the time of peak fuel pin surface temperature due to the low thermal conductivity of the fuel. Also indicated in the odd-numbered figures are error limits which represent the square root of the sum of the squares of the estimated data-processing errors. The error limits are indicated at the maxima of both the power and temperature curves.

The second (even-numbered) figure for each test consists of curves showing a comparison of the time histories of the power, the energy, and the compensated reactivity. The compensated reactivity was calculated from the experimental power data by solving the one-energy group, space-independent, reactor kinetic equations. (This method is similar to the method used by Miller [16].) For this calculation, a set of delayed neutron parameters was derived [1] from the values measured by Keepin and Wimmett [17] for fast fission of U-235 and U-238, and from the relative effectiveness factors γ_i for the different delayed groups as plotted by Henry [18]. A value of 3.57 msec was used for the reduced prompt neutron lifetime, ℓ/β_{eff}, as determined from the step-transient measurements [1].

The time origins in the figures presented in Appendices A and B are arbitrary. The time interval from ejection of the transient rod to the time of peak power for each run is listed in the tables presented in Appendix D, as discussed below.

Appendix C contains a set of correlative plots giving the variation with the inverse asymptotic period, α, of the values at the time of peak power of (a) the power, (b) the energy released, and (c) the compensated reactivity. Also

1133269

included are two plots (for the unconstrained and constrained cores, respectively) showing the variation in power burst shape as a function of the initial asymptotic period.

Appendix D is a tabulation of test data taken from the plots and operational records. Tables II and III for the unconstrained and constrained cores, respectively, are included as a ready source for comparison and reference of the experimental data. The tables include the figure number, the run number, the initial asymptotic reactor period, the inverse period, the peak power, the energy at time of peak power, the maximum pin-surface temperature, the pin-surface temperature at time of peak power, the location of the thermocouple used to measure the pin-surface temperatures, the time interval between the ejection of the transient rod and the time of peak power, the initial reactivity inserted, and the compensated reactivity at time of peak power.

1133270

IX. REFERENCES

1. A. H. Spano et al, Self-Limiting Power Excursion Tests of a Water-Moderated Low-Enrichment UO_2 Core in Spert I, IDO-16751 (February 28, 1962).
2. Quarterly Technical Report, Spert Project, 4th Qtr 1960, IDO-16687, pp 3, 4 (1961).
3. Quarterly Technical Report, Spert Project, 1st Qtr 1961, IDO-16693, pp 3-6 (1961).
4. Quarterly Technical Report, Spert Project, 2nd Qtr 1961, IDO-16716, pp 3-13 (1961).
5. Quarterly Technical Report, Spert Project, 3rd Qtr 1961, IDO-16726, pp 4-11 (1961).
6. Quarterly Technical Report, Spert Project, 4th Qtr 1961, IDO-16750, pp 1-4 (1962).
7. T. M. Quigley et al, "Spert I Power Excursion Test of a 4%-Enriched UO_2 Fuel Rod", Trans. Am. Nucl. Soc., 4, No. 1, pp 39, 40 (June 1961).
8. A. H. Spano, L. A. Stephan, "Experimental Investigation of the Kinetic Behavior of a 4%-Enriched UO_2 Reactor in Spert I", Trans. Am. Nucl. Soc., 4, No. 2, pp 312, 313 (November 1961).
9. J. E. Houghtaling et al, Calculation and Measurement of the Transient Temperature in a Low-Enrichment UO_2 Fuel Rod During Large Power Excursions, IDO-16773 (May 18, 1962).
10. A. H. Spano, W. K. Ergen, "Direct Measurement of the Dynamic Doppler Coefficient by Self-Limiting Power Excursion Tests", Trans. Am. Nucl. Soc., 5, No. 1, pp 157, 158 (June 1962).
11. W. K. Ergen, A. H. Spano, "Effect of Fuel-Rod Bowing During Self-Limiting Power Excursions in the Spert I Oxide Core", Trans. Am. Nucl. Soc., 5, No. 1, p 172 (June 1962).
12. A. H. Spano, "Self-Limiting Power Excursion Tests of a Water-Moderated Low-Enrichment UO_2 Core", Nucl. Sci. and Eng., 15, pp 37-51 (January 1963).
13. J. C. Haire, Subcooled Transient Tests in the Spert I Reactor - Experimental Data, IDO-16342, pp 14-17 (July 1, 1958).
14. H. H. Hausner, R. G. Mills, "Uranium Dioxide for Fuel Elements", Nucleonics, 15, No. 7 pp 94-103 (July 1957).
15. S. D. Anderson, private communication, Phillips Petroleum Co., Idaho Falls, Idaho (June 1962).

1133271

16. R. W. Miller, Calculations of Reactivity Behavior During Spert I Transients, IDO-16317 (June 1, 1957).

17. G. R. Keepin, T. F. Wimett, "Reactor Kinetic Functions: A New Evaluation", Nucleonics, 16, No. 10, pp 86-90 (October 1958).

18. A. F. Henry, Computation of Parameters Appearing in the Reactor Kinetics Equations, WAPD-142 (December 1955).

1133272

INTENTIONAL BLANK PAGE NO. 18

1133273

APPENDIX A

PLOTS OF SURFACE TEMPERATURE, POWER, ENERGY, AND COMPENSATED REACTIVITY VS TIME, FOR UNCONSTRAINED SPERT I OXIDE CORE

1133274

INTENTIONAL BLANK PAGE NO. 20

1133275

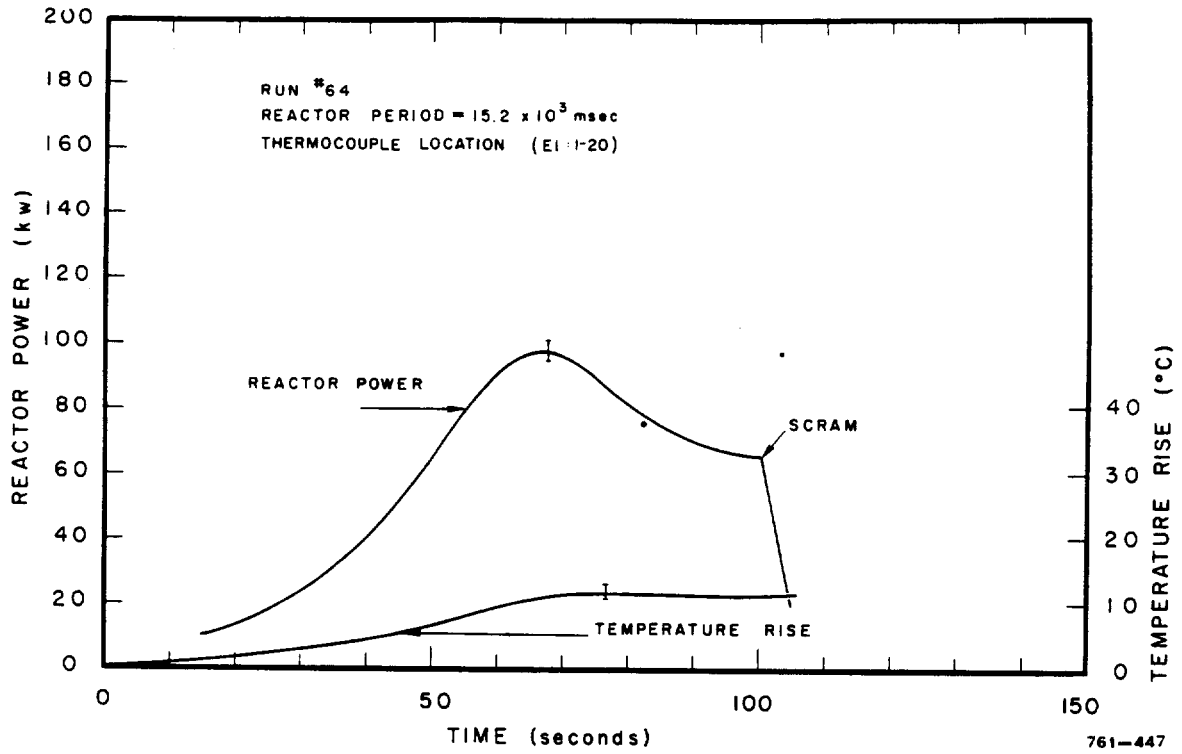

FIG. A-1 RUN 64 – 15.2-SEC-PERIOD TEST.

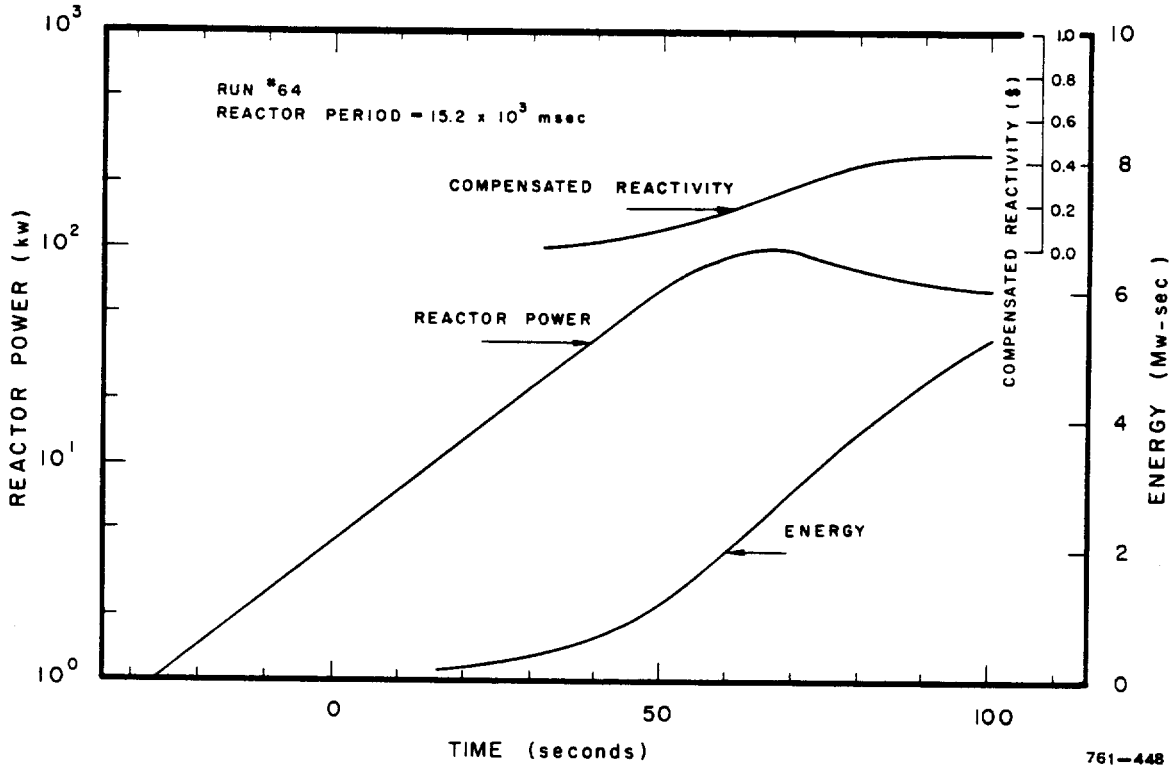

FIG. A-2 RUN 64 – 15.2-SEC-PERIOD TEST.

1133276

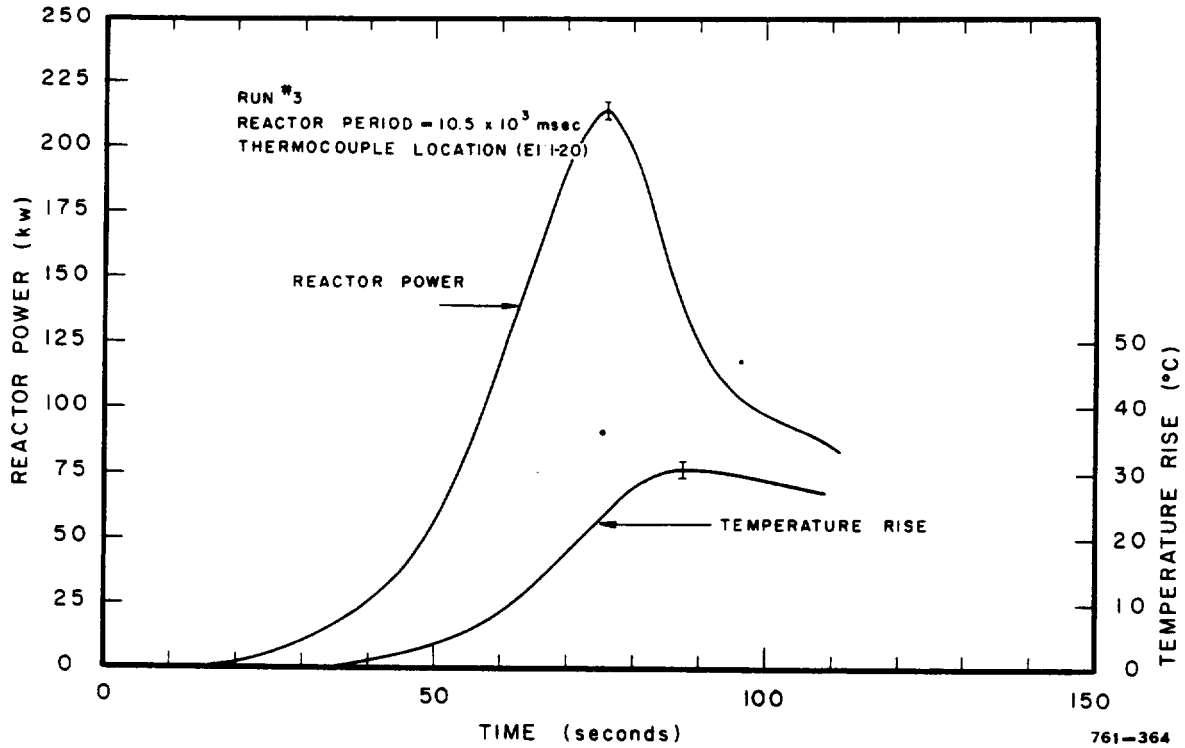

FIG. A-3 RUN 3 – 10.5-SEC-PERIOD TEST.

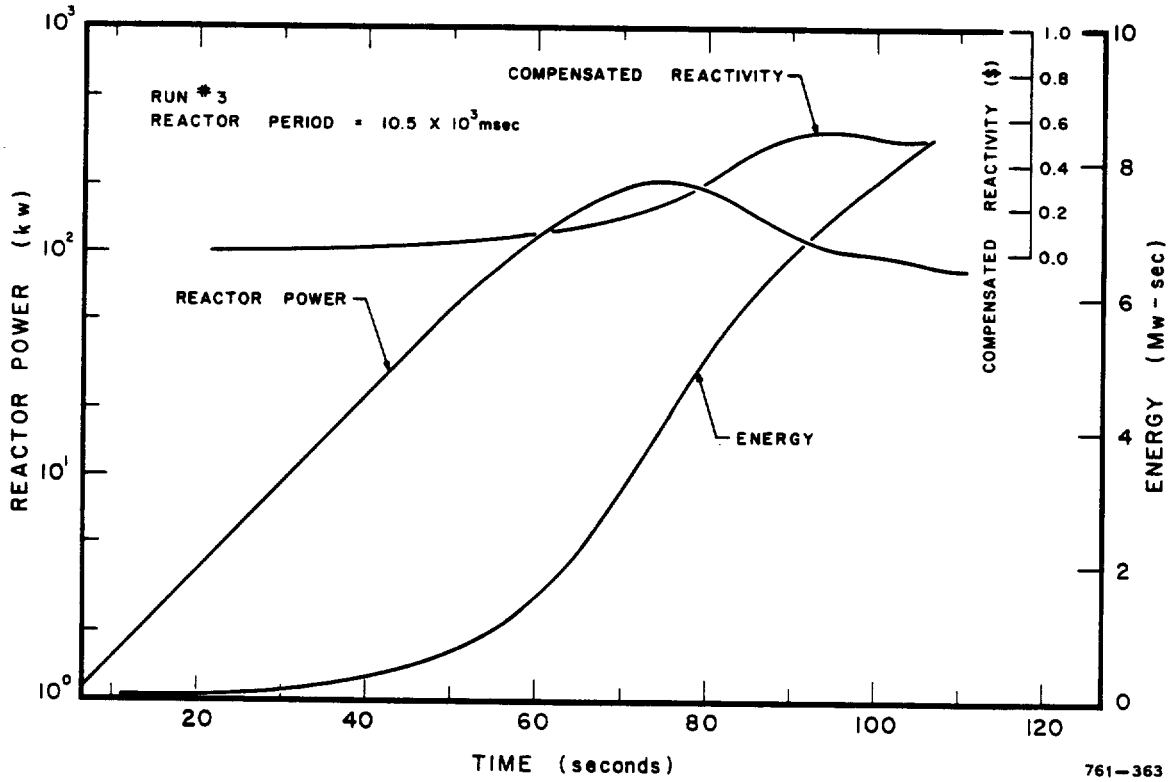

FIG. A-4 RUN 3 – 10.5-SEC-PERIOD TEST.

1133277

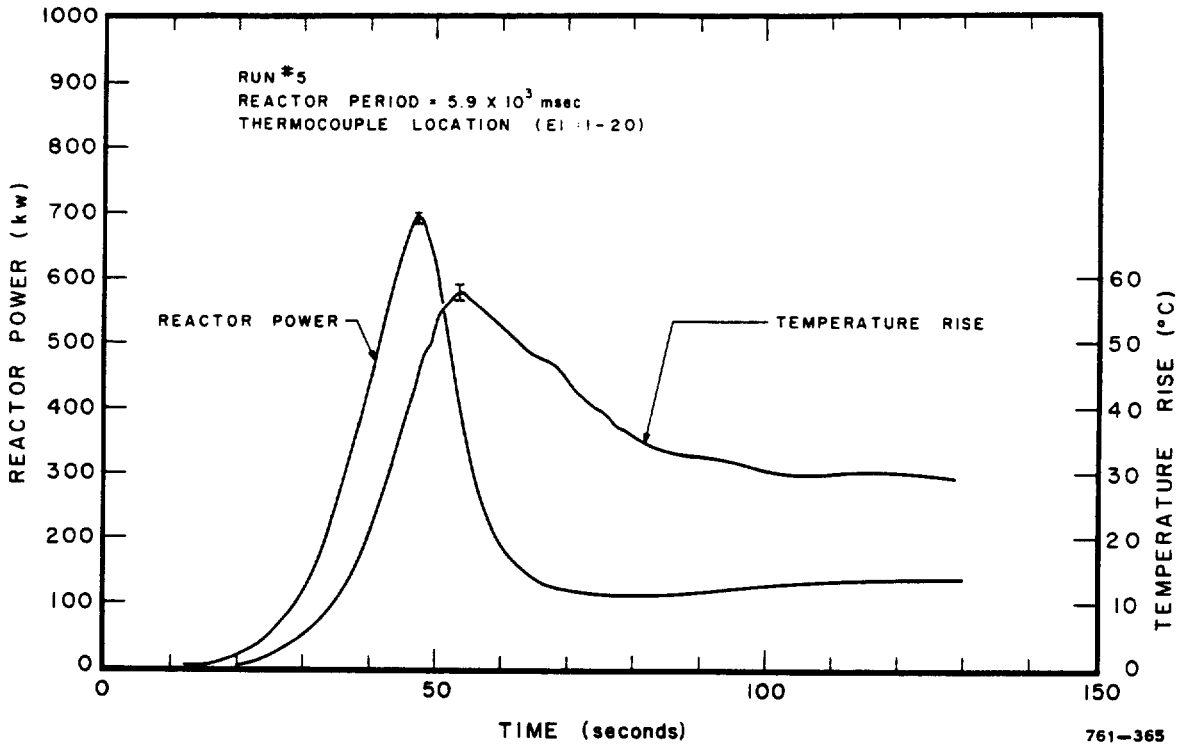

FIG. A-5 RUN 5 – 5.9-SEC-PERIOD TEST.

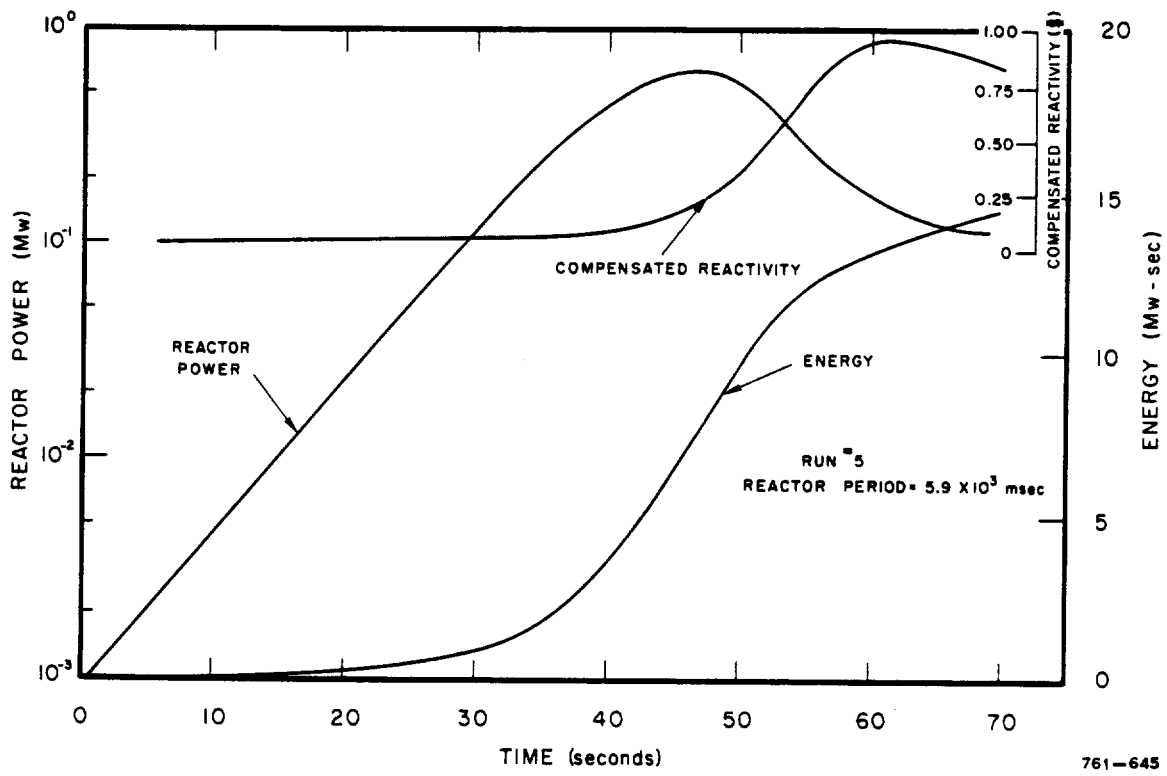

FIG. A-6 RUN 5 – 5.9-SEC-PERIOD TEST.

1133278

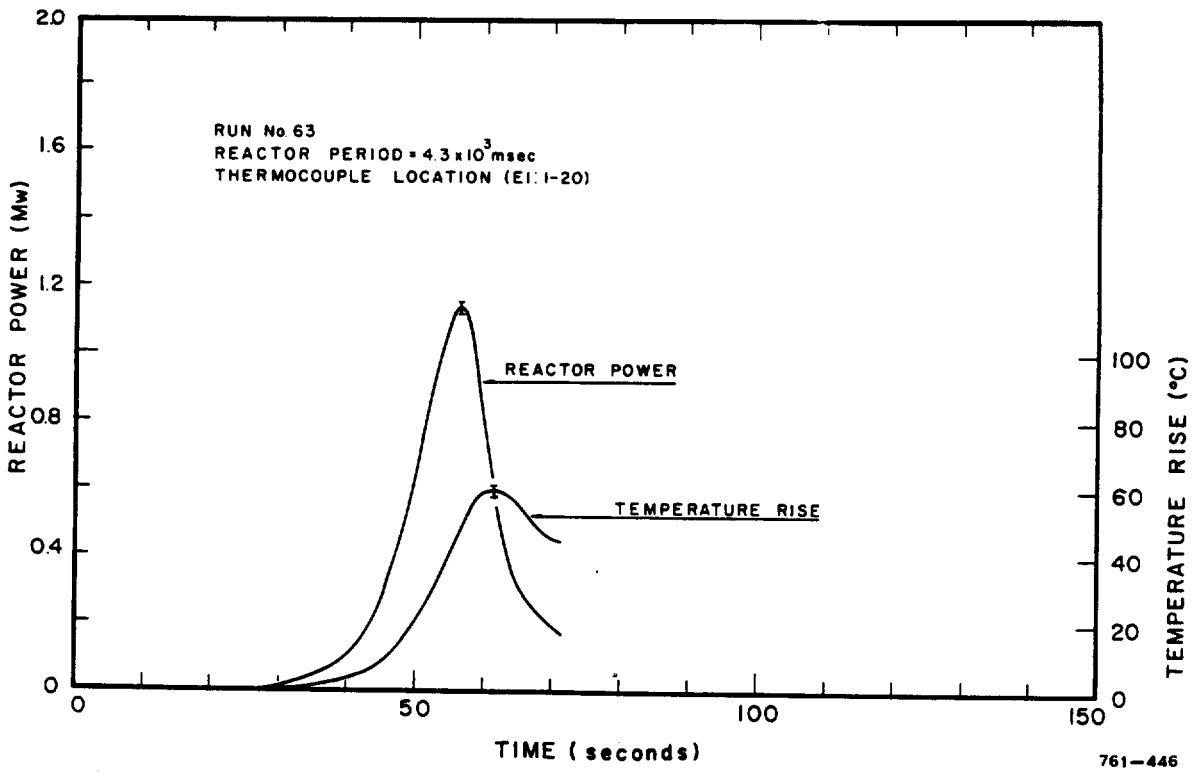

FIG. A-7 RUN 63 – 4.3-SEC-PERIOD TEST.

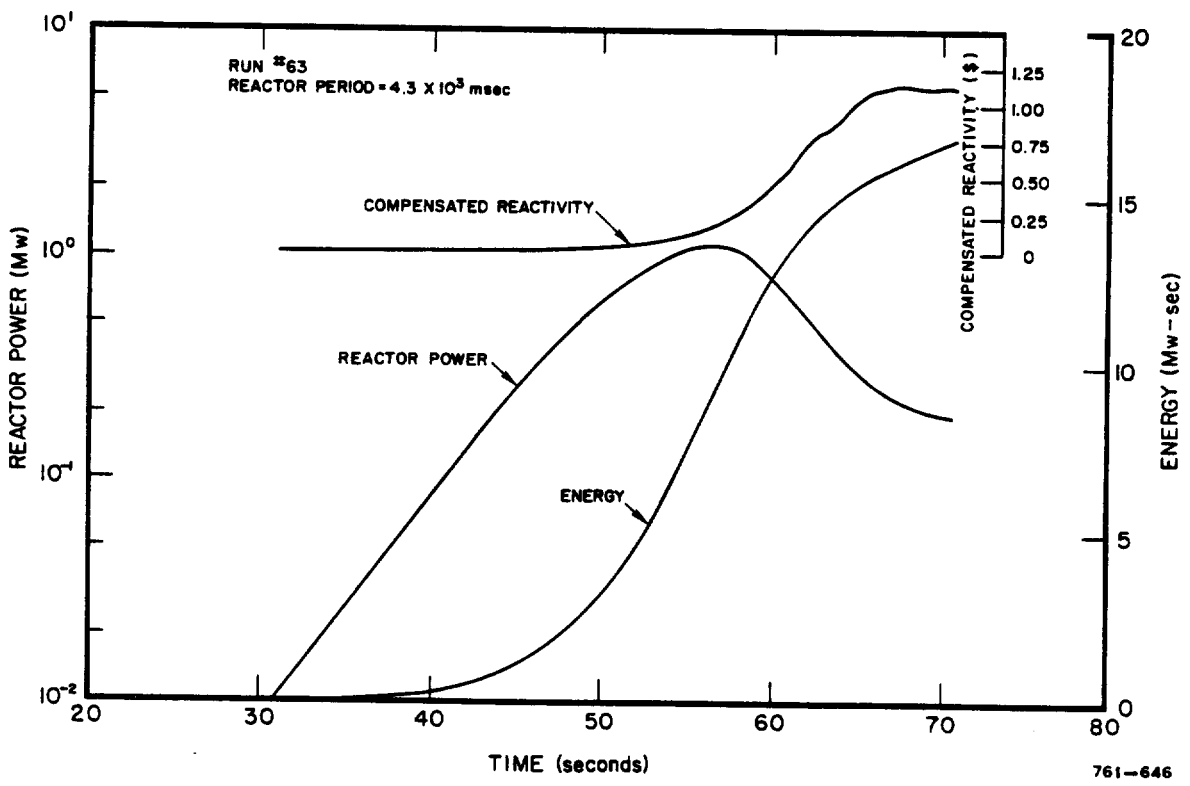

FIG. A-8 RUN 63 – 4.3-SEC-PERIOD TEST.

1133279

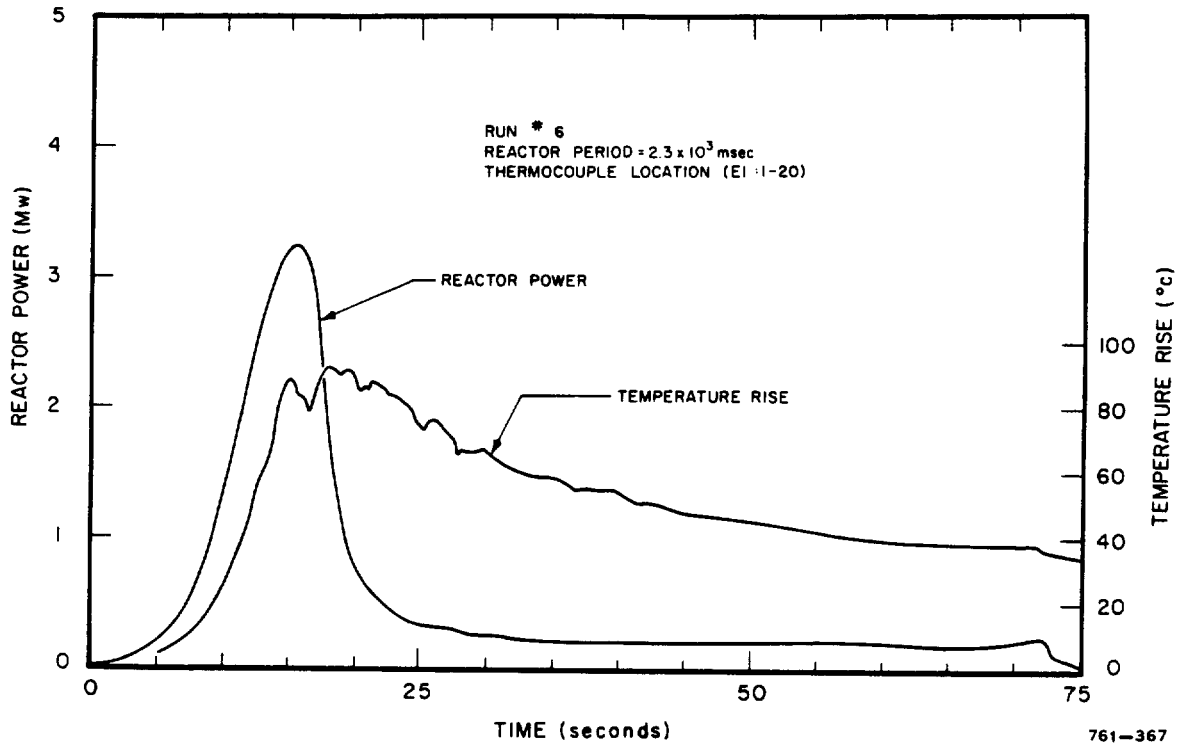

FIG. A-9 RUN 6 – 2.3-SEC-PERIOD TEST.

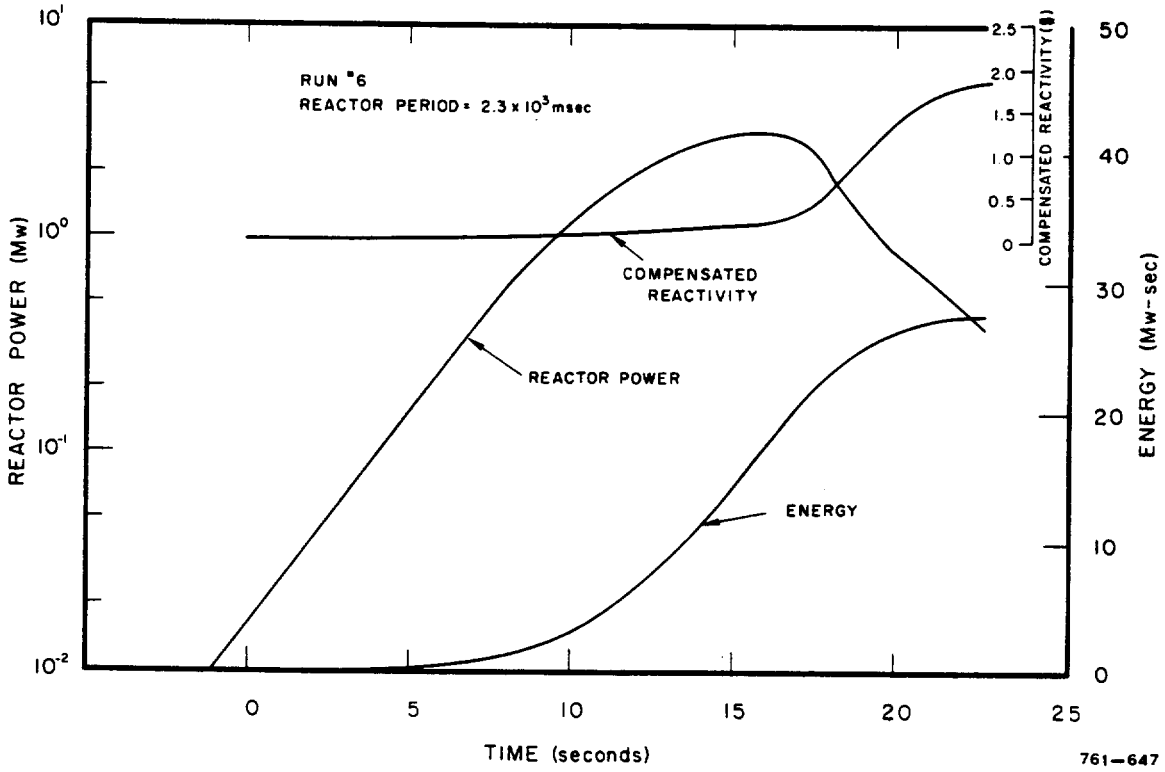

FIG. A-10 RUN 6 – 2.3-SEC-PERIOD TEST.

1133280

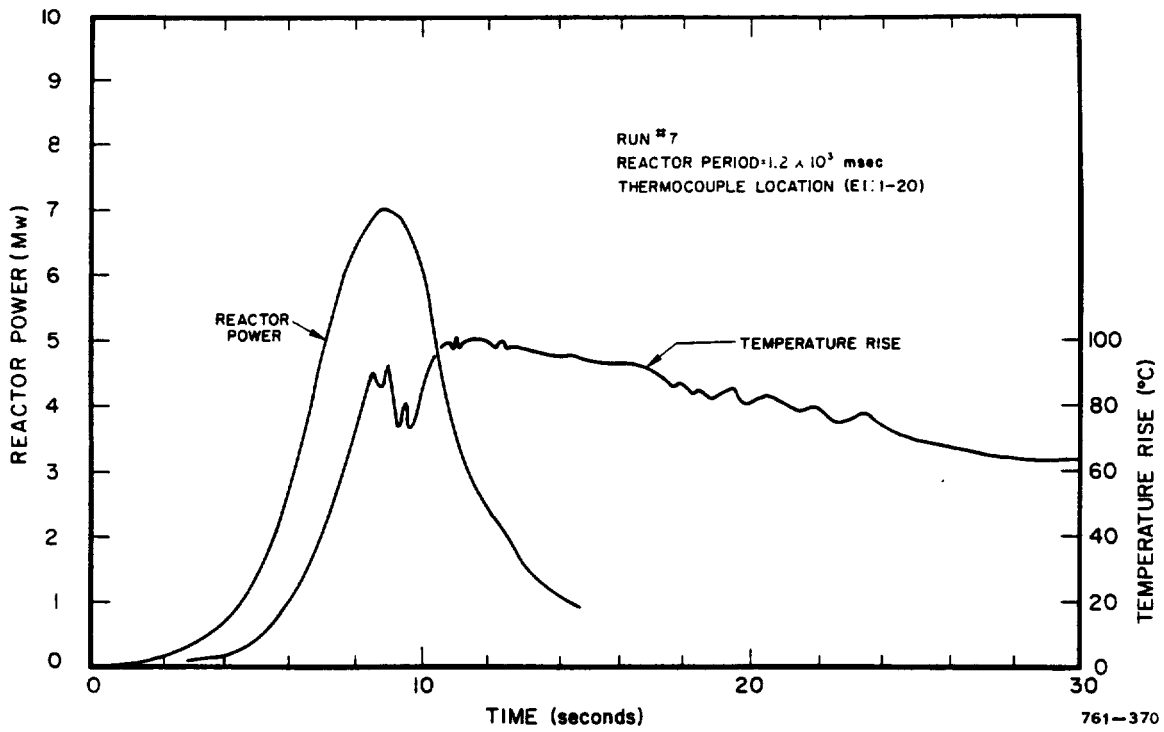

FIG. A-11 RUN 7 – 1.2-SEC-PERIOD TEST.

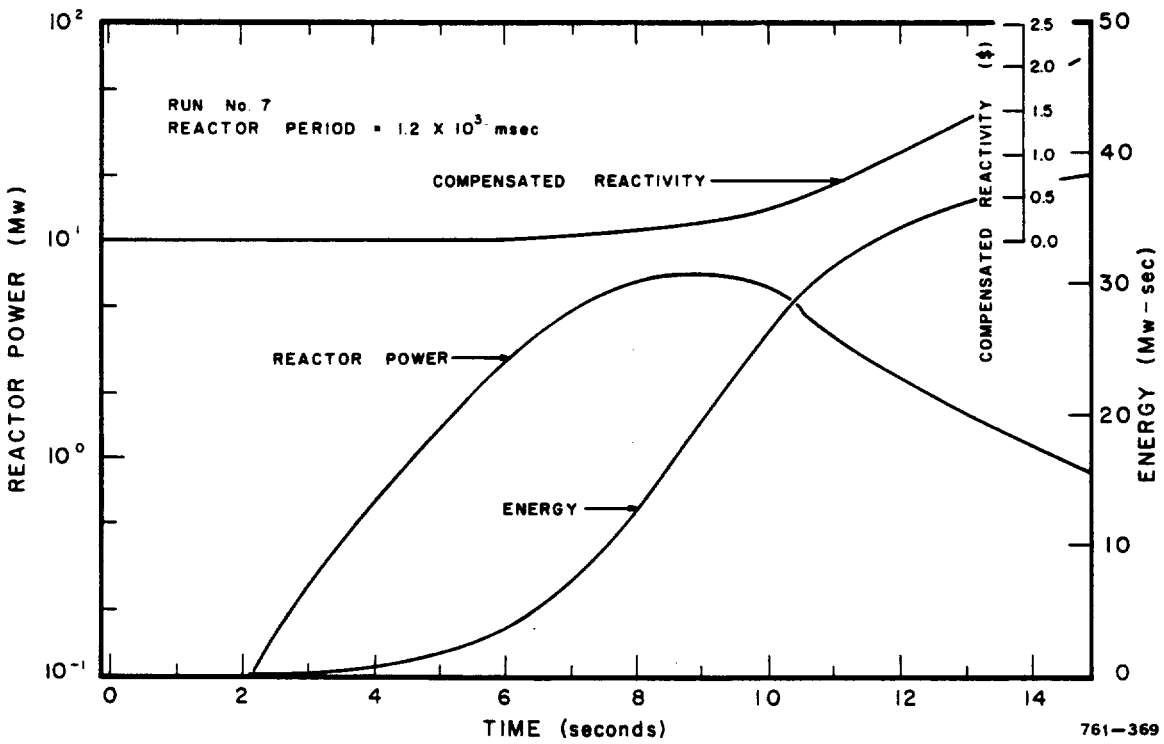

FIG. A-12 RUN 7 – 1.2-SEC-PERIOD TEST.

1133281

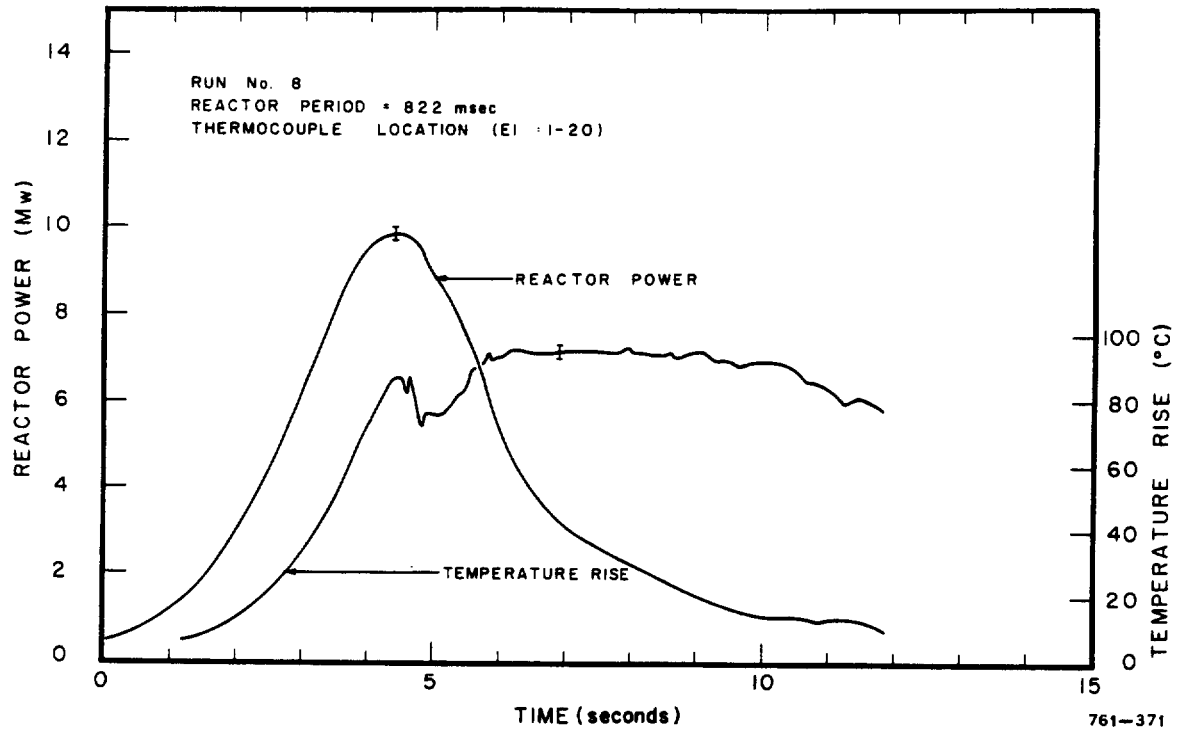

FIG. A-13 RUN 8 – 822-MSEC-PERIOD TEST.

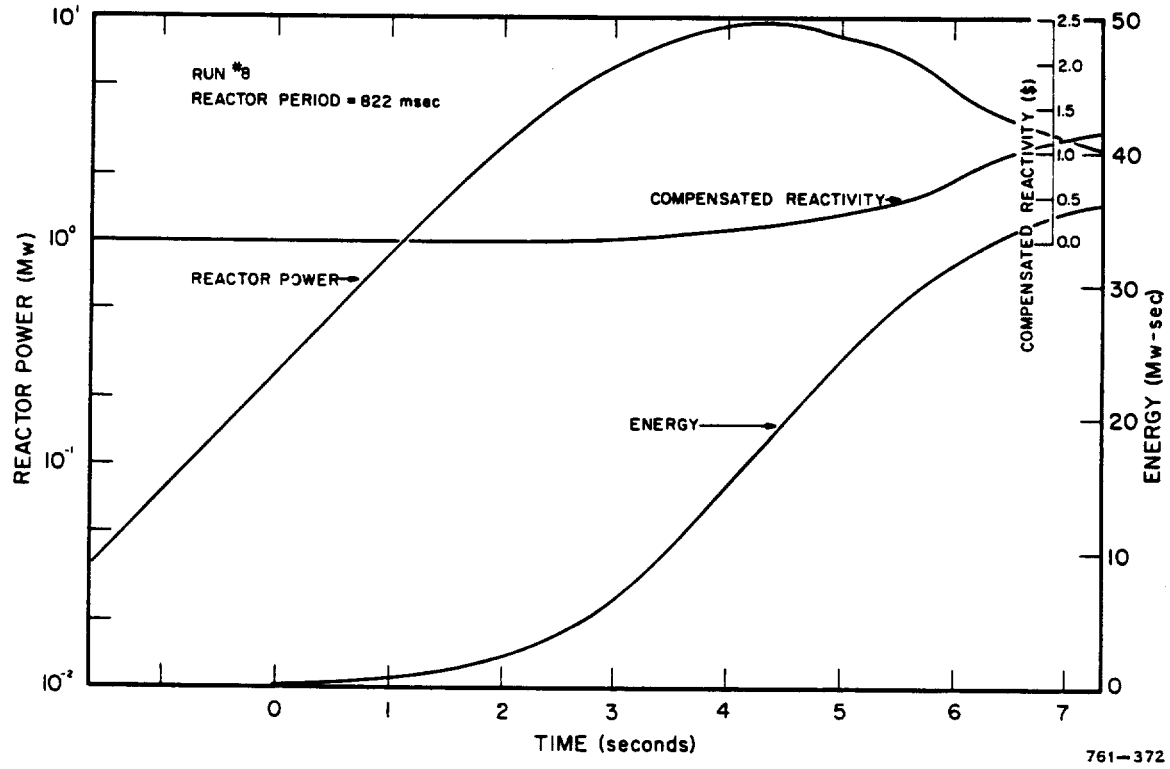

FIG. A-14 RUN 8 – 822-MSEC-PERIOD TEST.

1133282

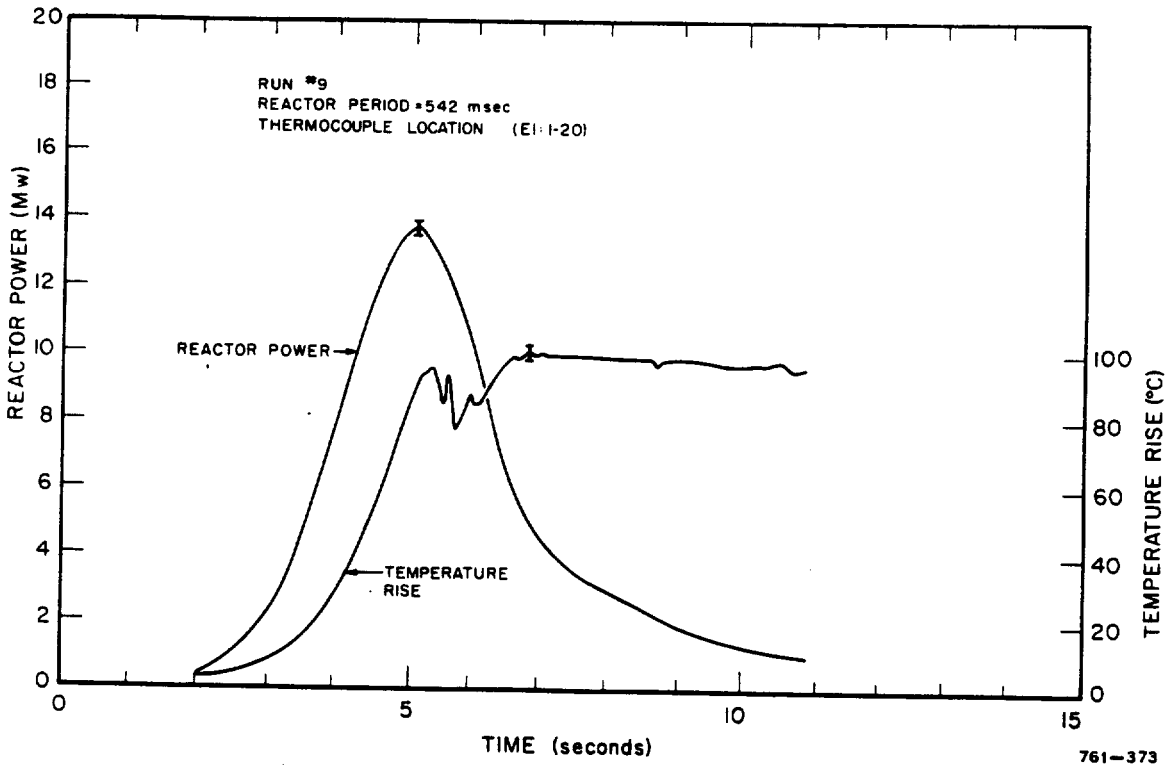

FIG. A-15 RUN 9 – 542-MSEC-PERIOD TEST.

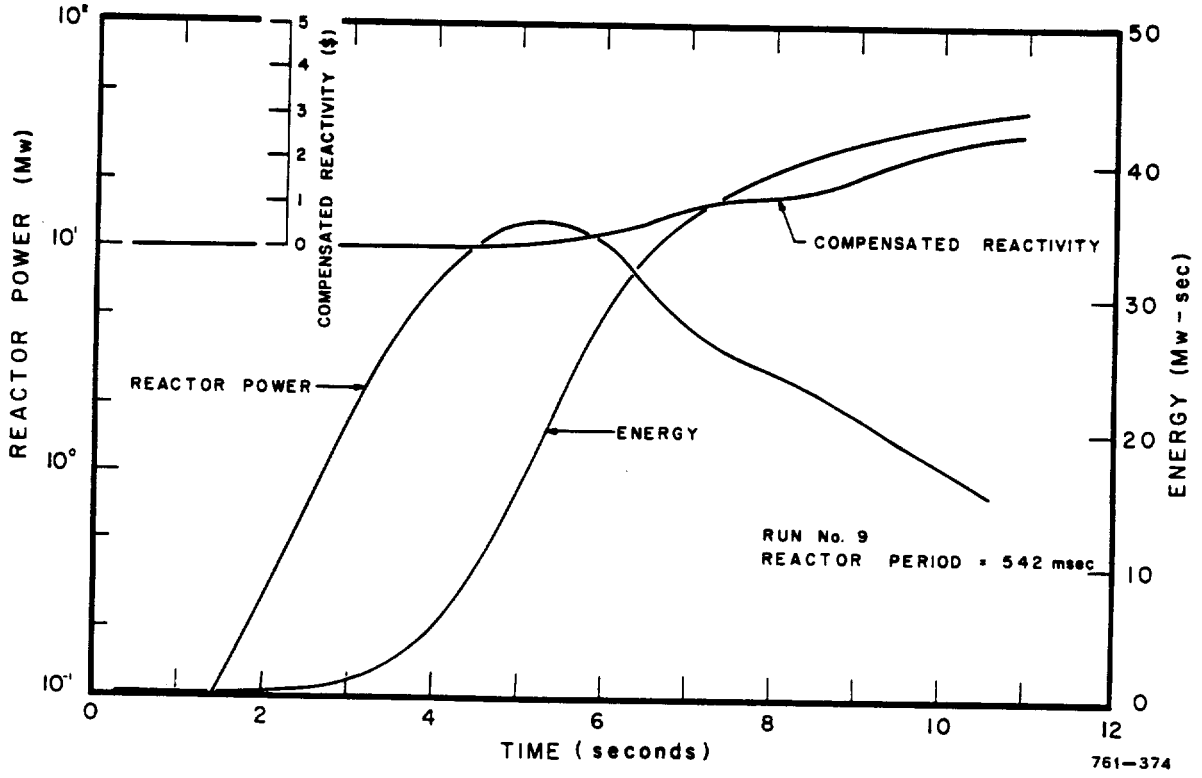

FIG. A-16 RUN 9 – 542-MSEC-PERIOD TEST.

1133283

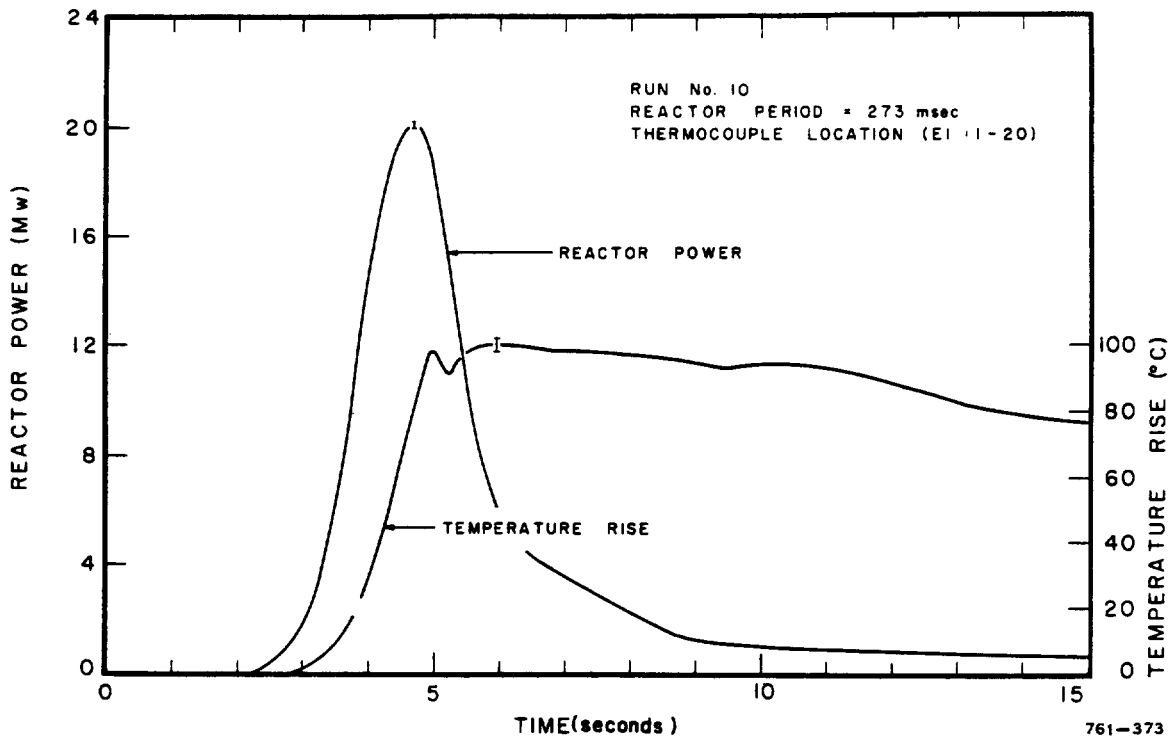

FIG. A-17 RUN 10 – 273-MSEC-PERIOD TEST.

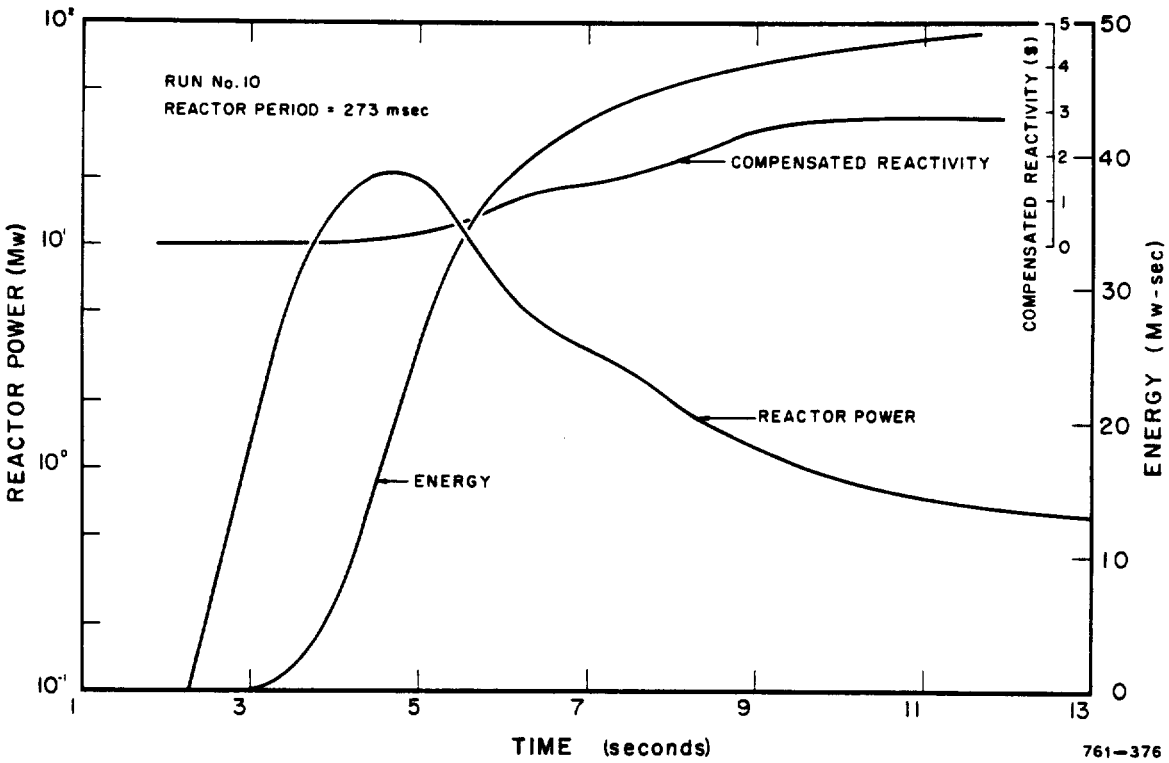

FIG. A-18 RUN 10 – 273-MSEC-PERIOD TEST.

1133284

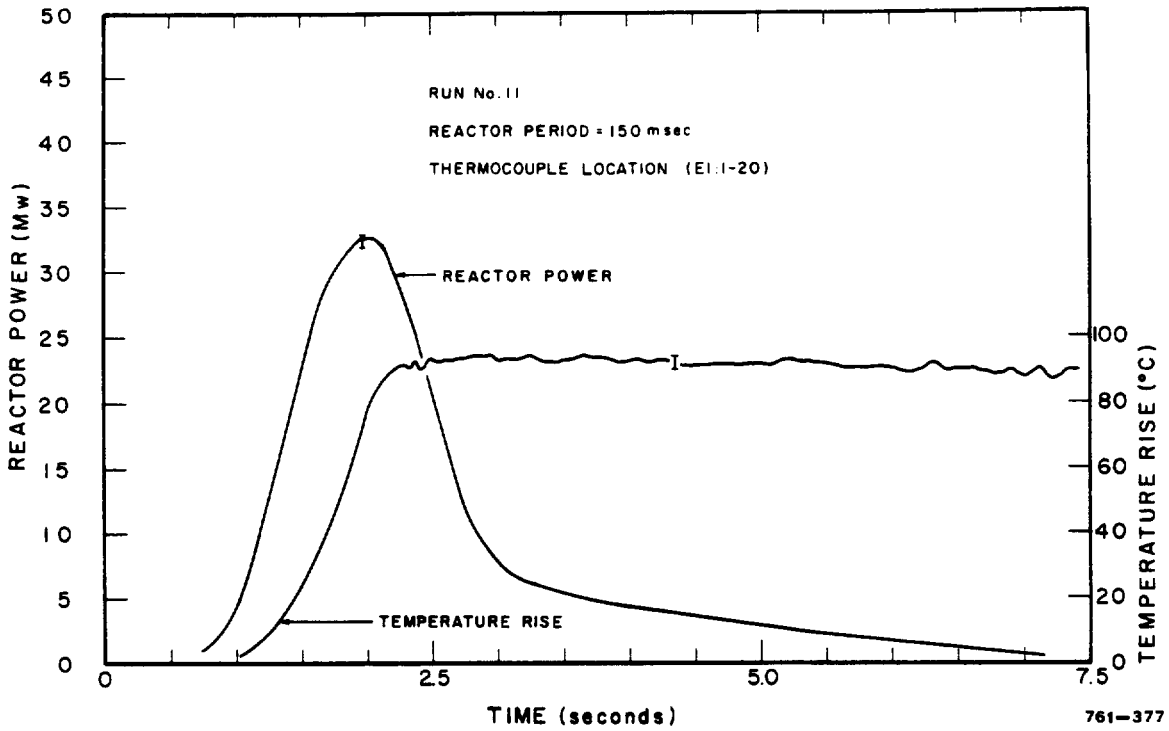

FIG. A-19 RUN 11 – 150-MSEC-PERIOD TEST.

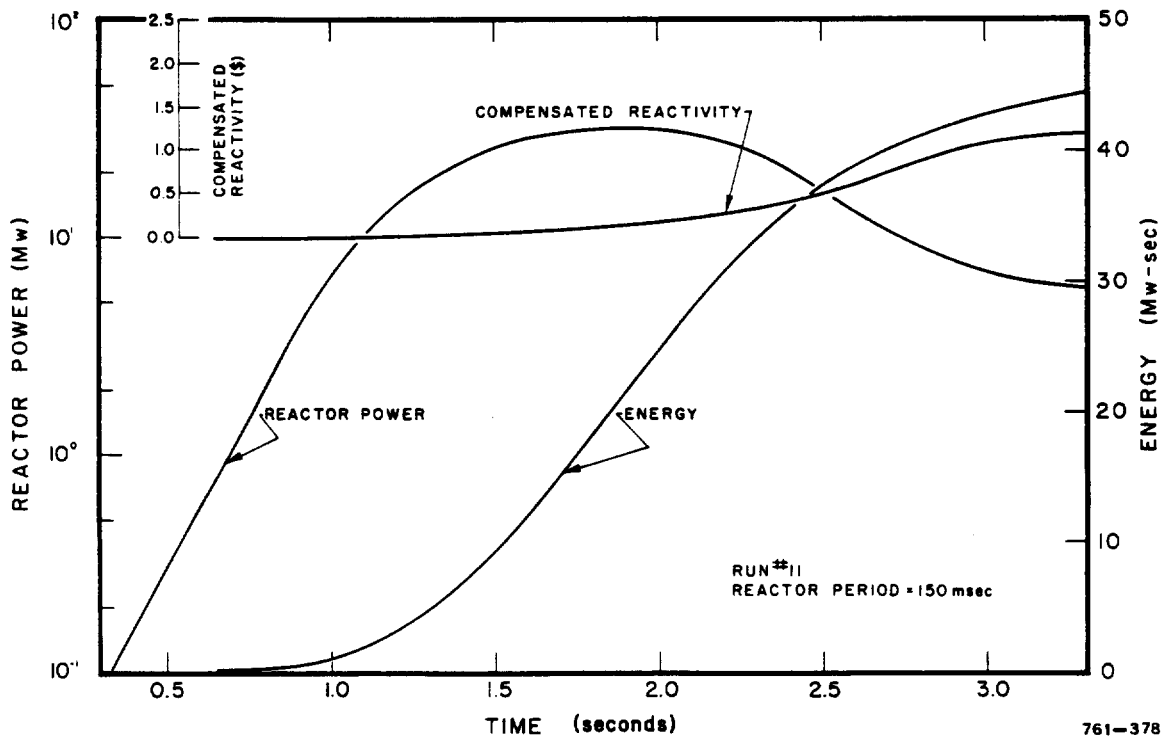

FIG. A-20 RUN 11 – 150-MSEC-PERIOD TEST.

1133285

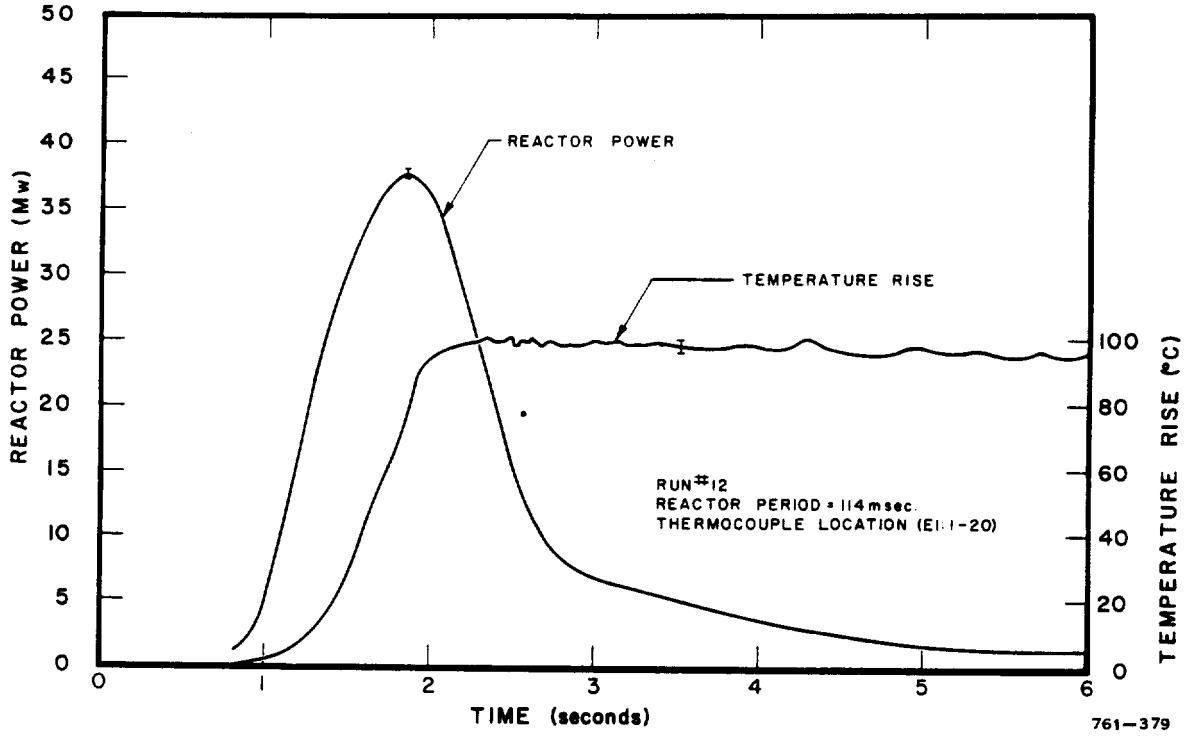

FIG. A-21 RUN 12 - 114-MSEC-PERIOD TEST.

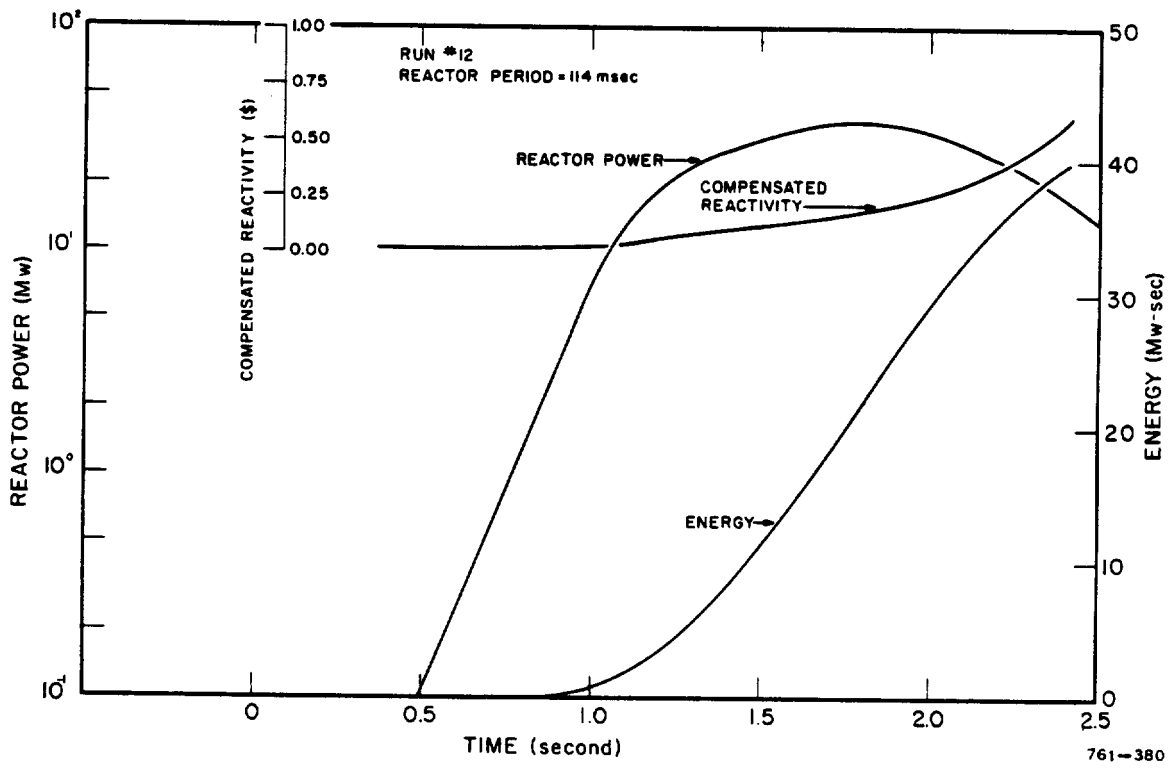

FIG. A-22 RUN 12 - 114-MSEC-PERIOD TEST.

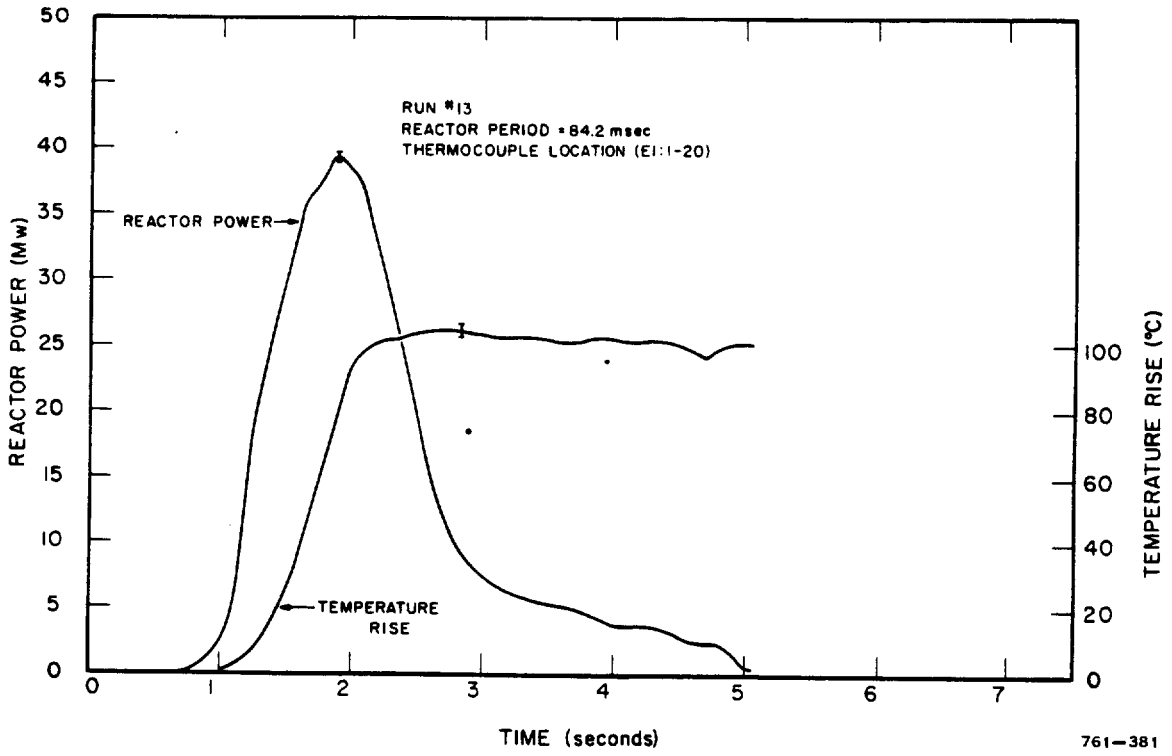

FIG. A-23 RUN 13 – 84.2-MSEC-PERIOD TEST.

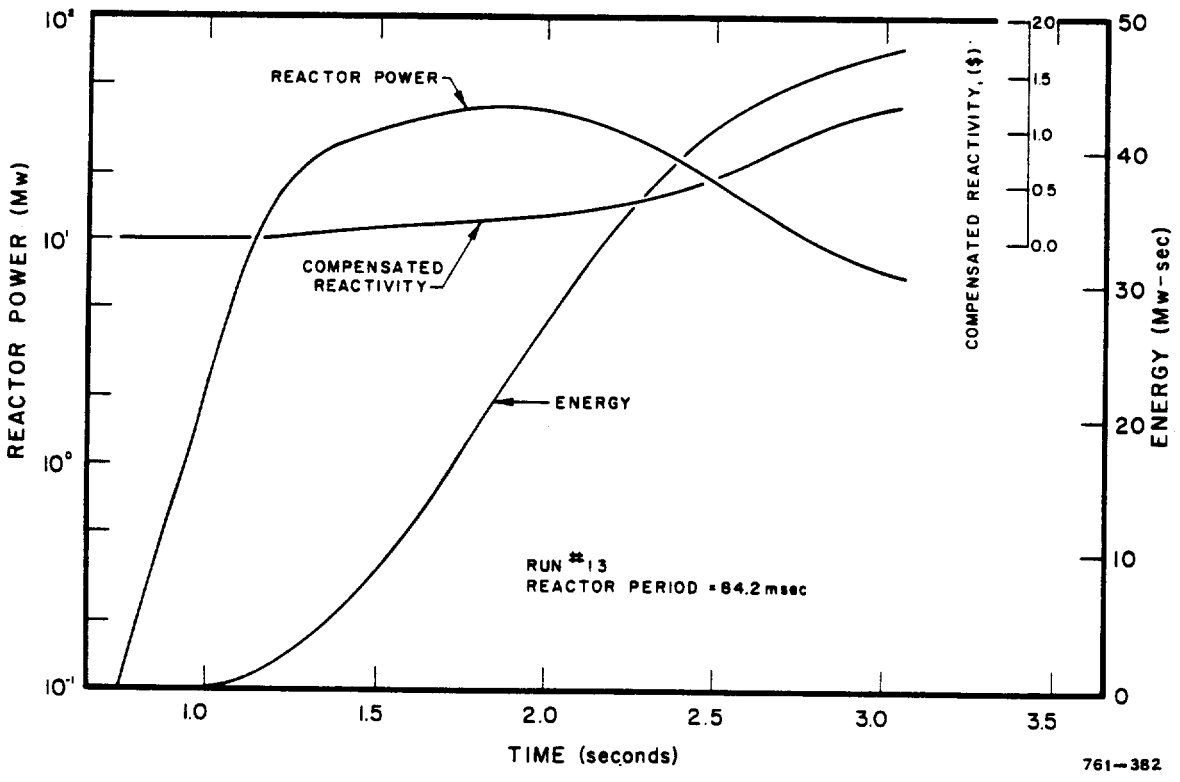

FIG. A-24 RUN 13 – 84.2-MSEC-PERIOD TEST.

1133287

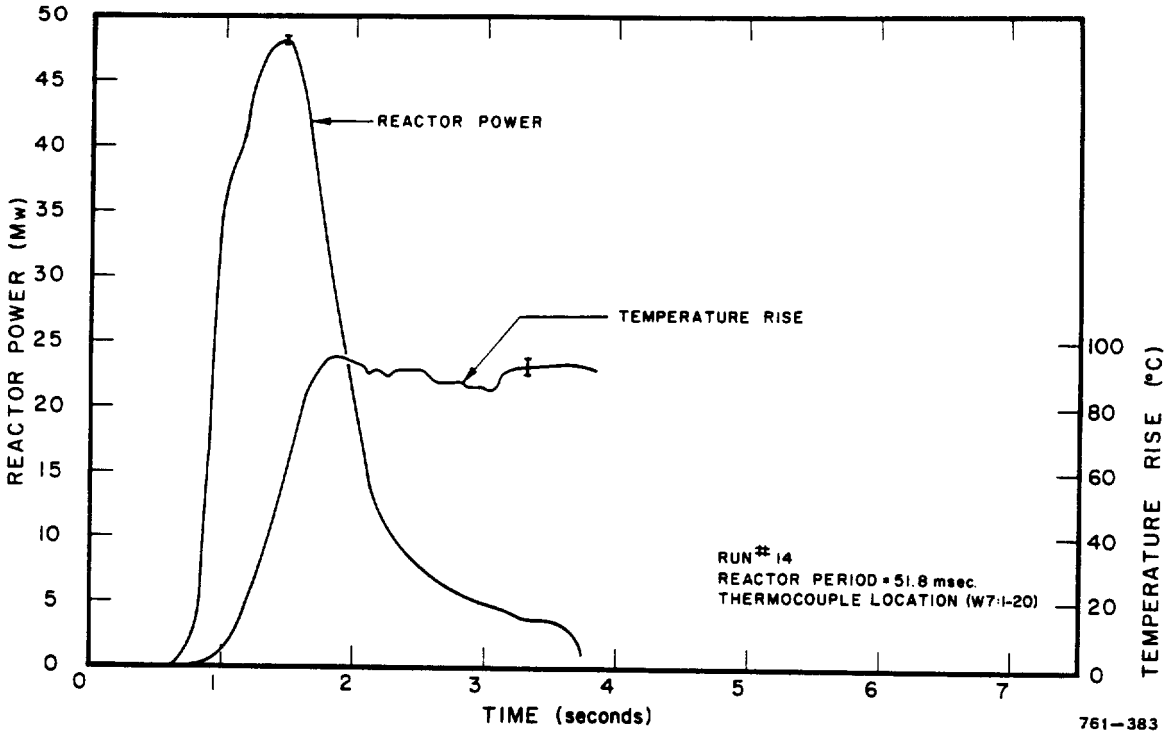

FIG. A-25 RUN 14 – 51.8-MSEC-PERIOD TEST.

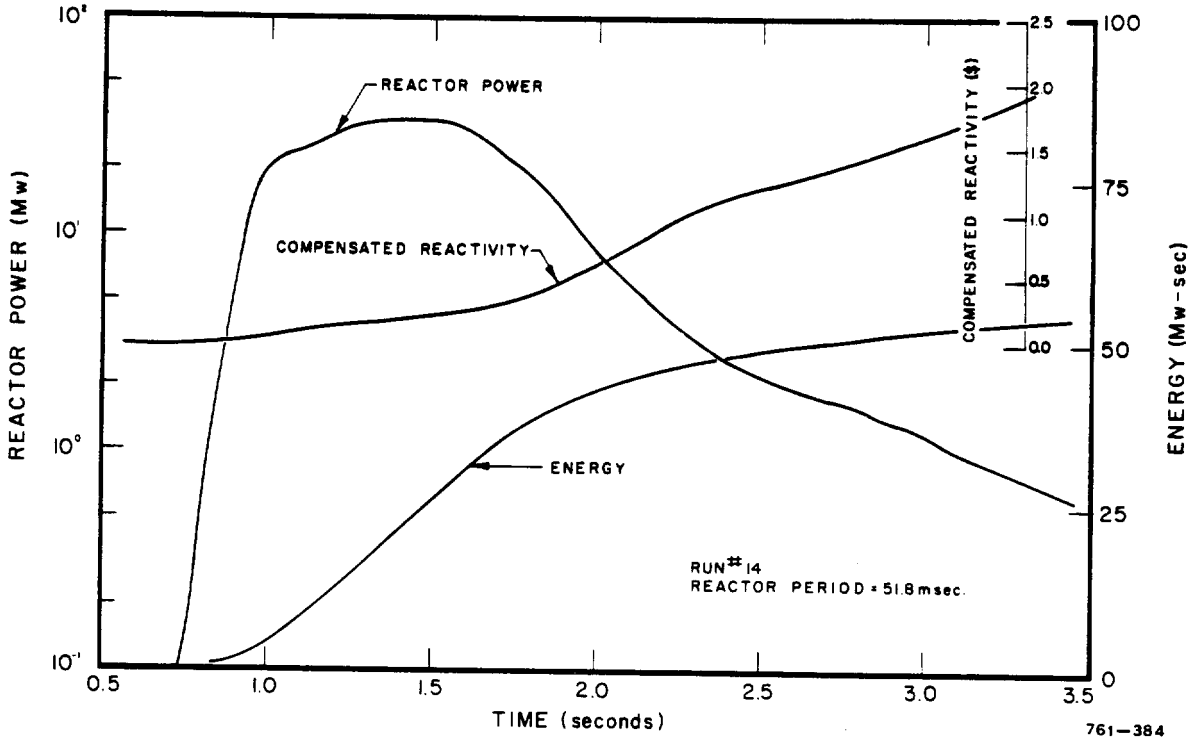

FIG. A-26 RUN 14 – 51.8-MSEC-PERIOD TEST.

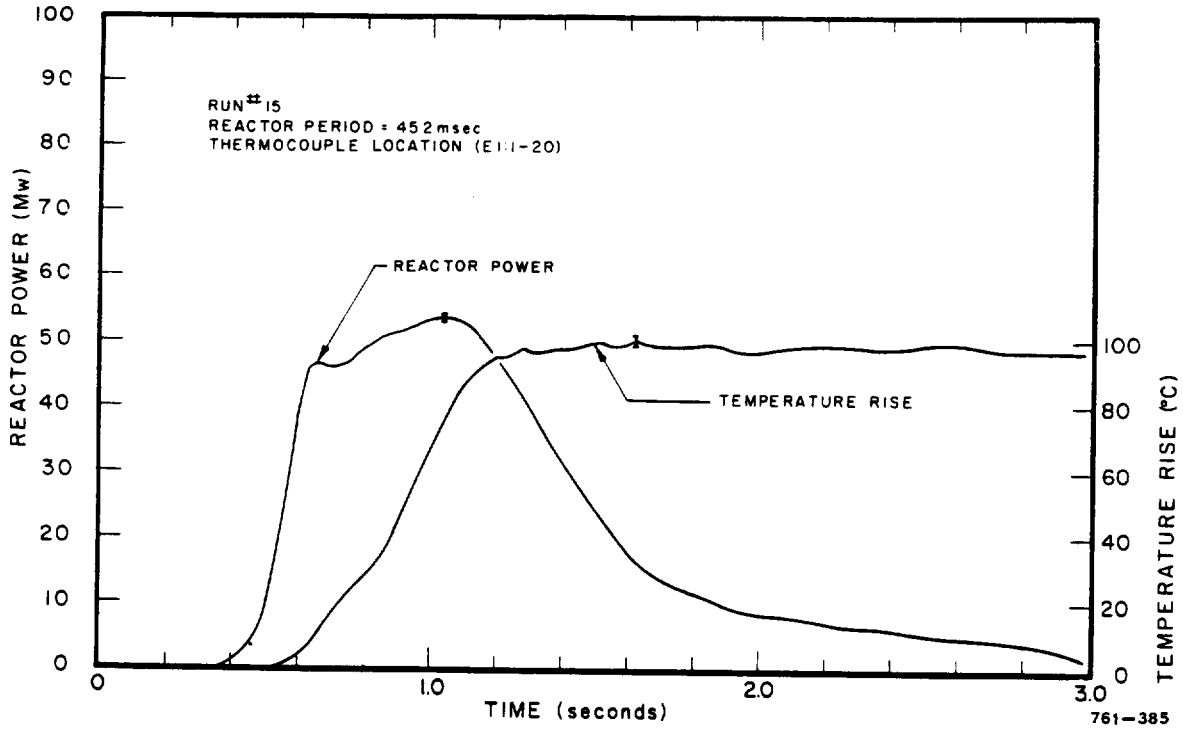

FIG. A-27 RUN 15 – 45.2-MSEC-PERIOD TEST.

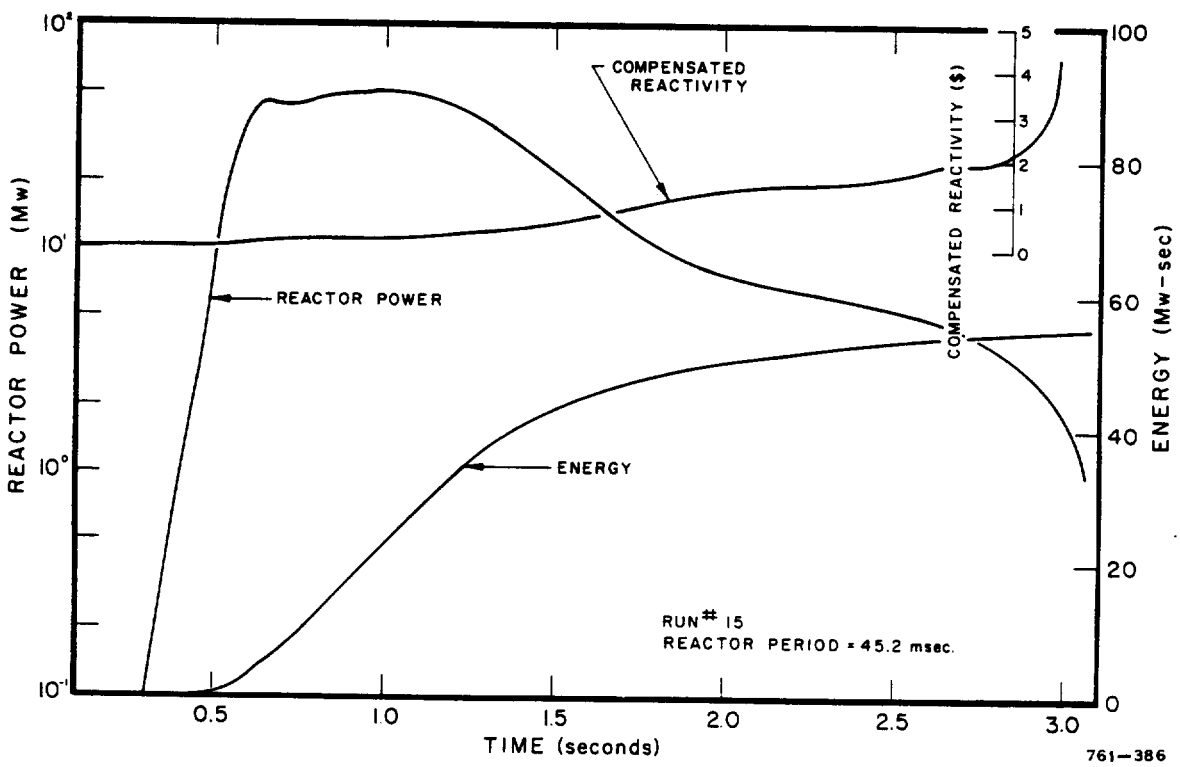

FIG. A-28 RUN 15 – 45.2-MSEC-PERIOD TEST.

1133289

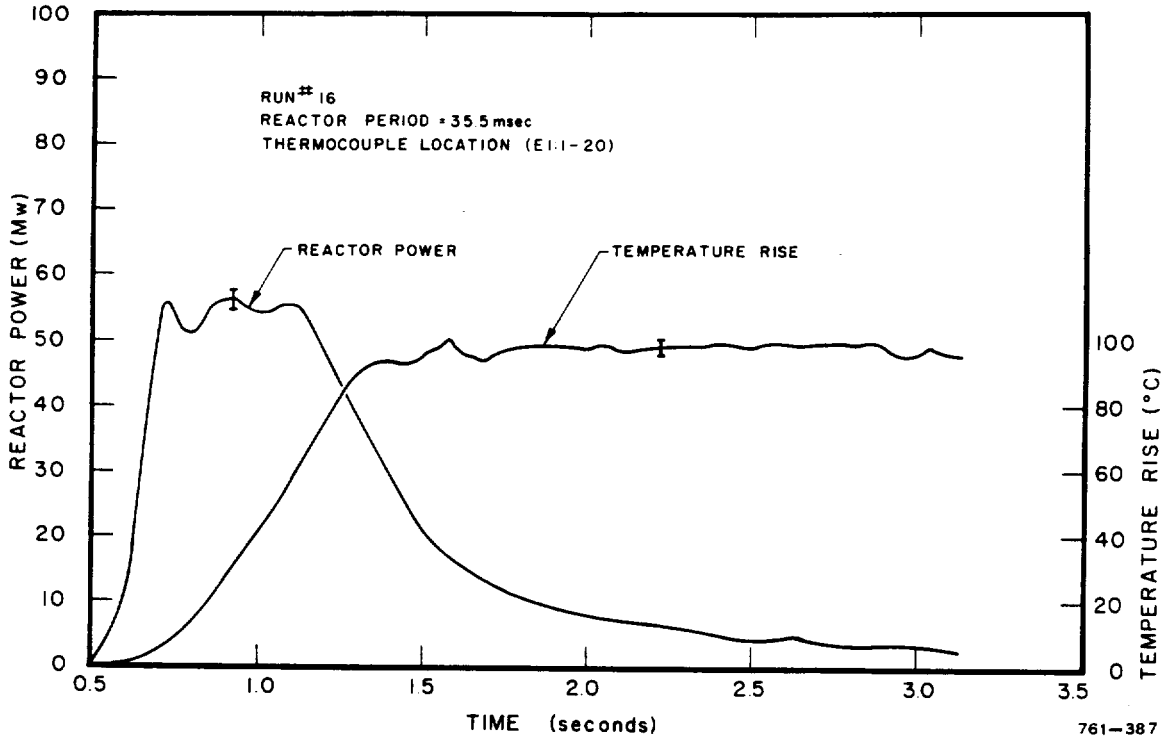

FIG. A-29 RUN 16 – 35.5-MSEC-PERIOD TEST.

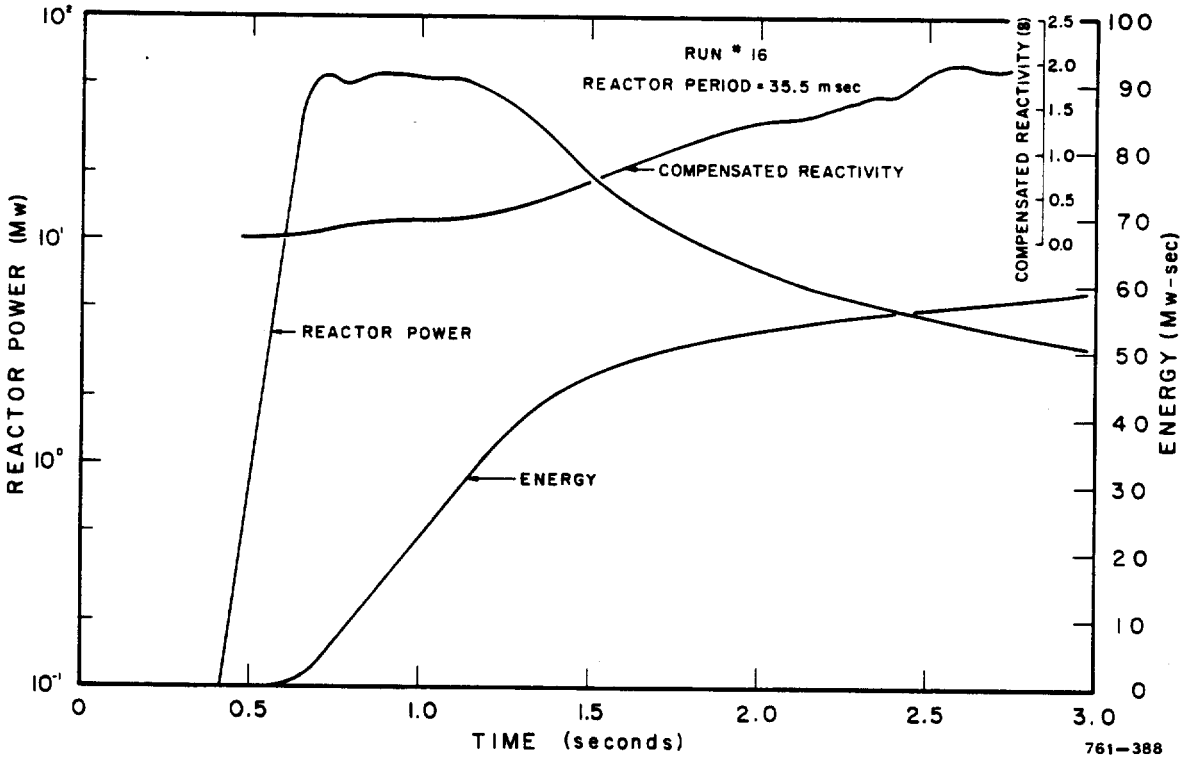

FIG. A-30 RUN 16 – 35.5-MSEC-PERIOD TEST.

1133290

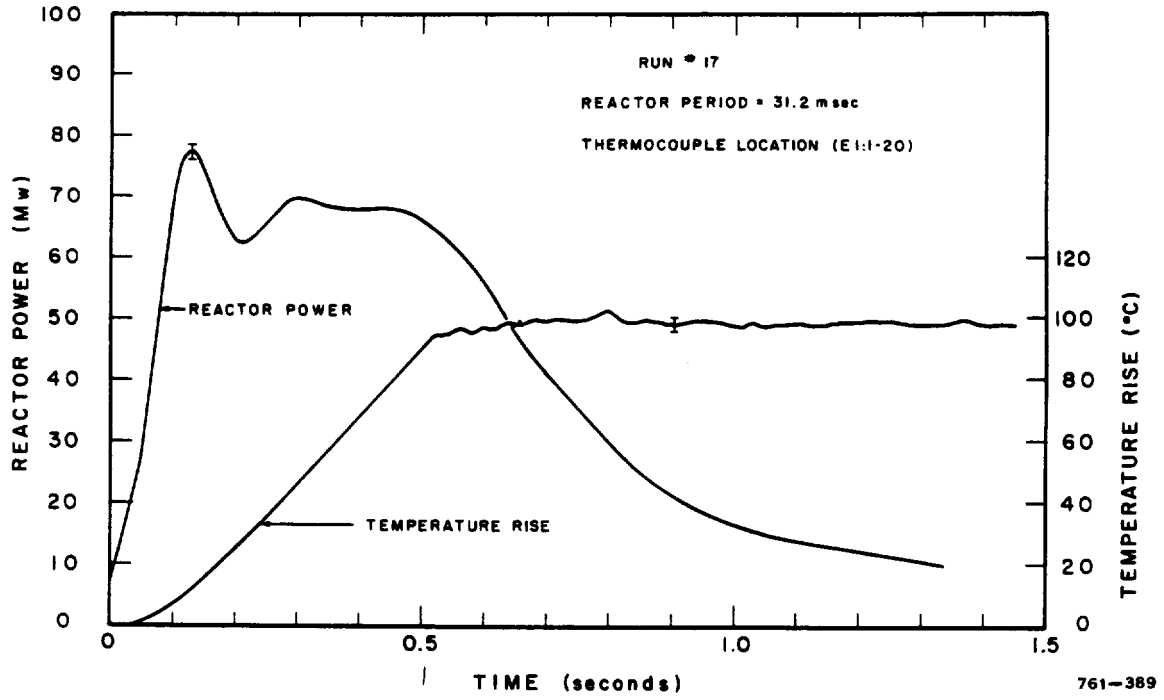

FIG. A-31 RUN 17 – 31.2-MSEC-PERIOD TEST.

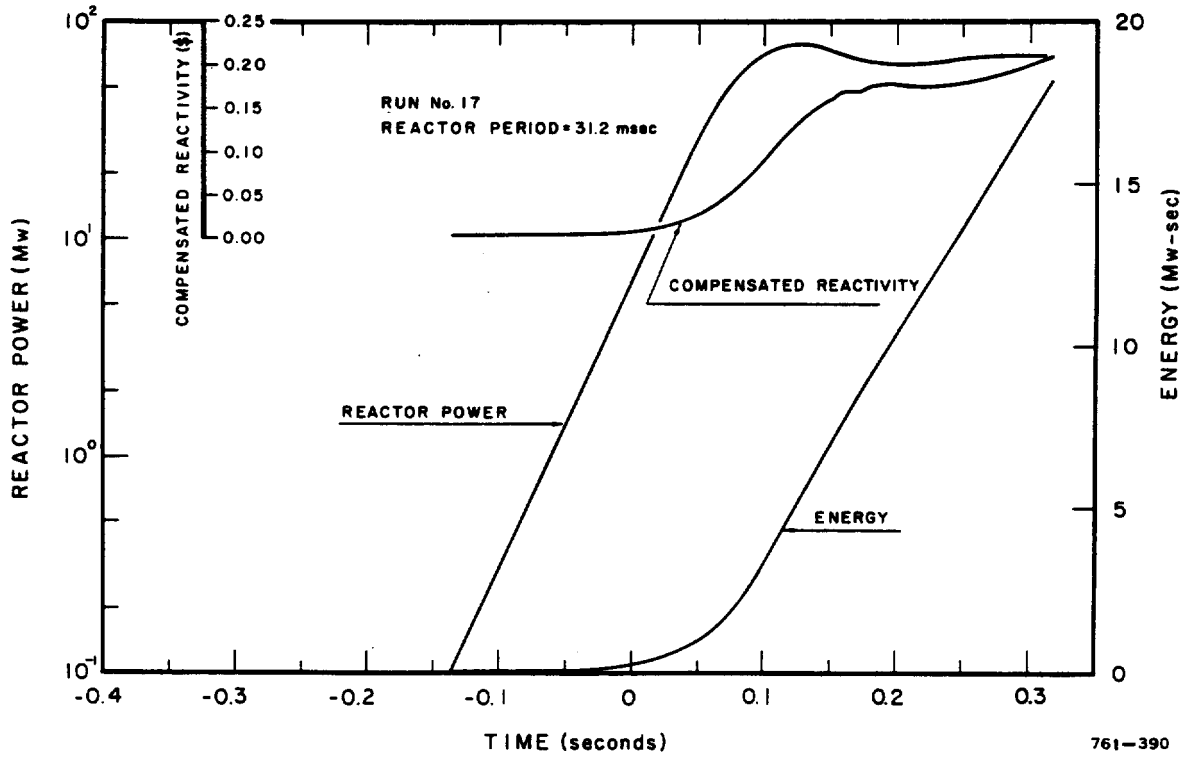

FIG. A-32 RUN 17 – 31.2-MSEC-PERIOD TEST.

1133291

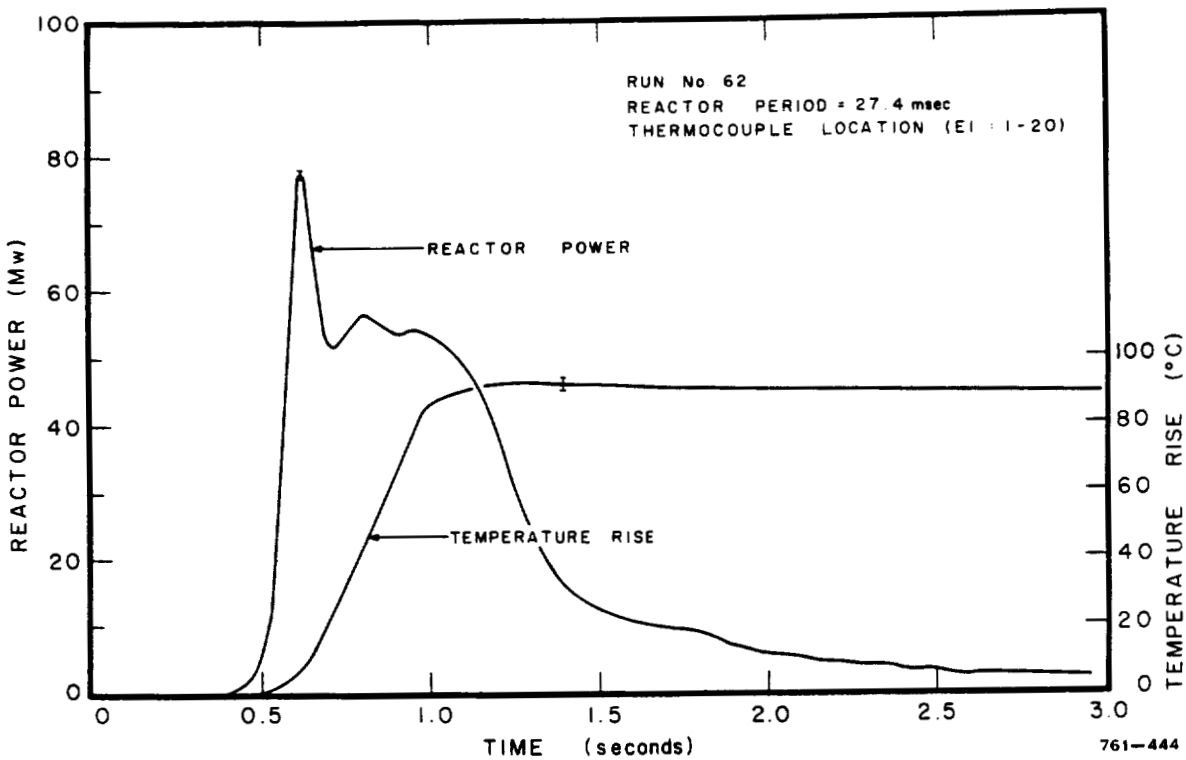

FIG. A-33 RUN 62 – 27.4-MSEC-PERIOD TEST.

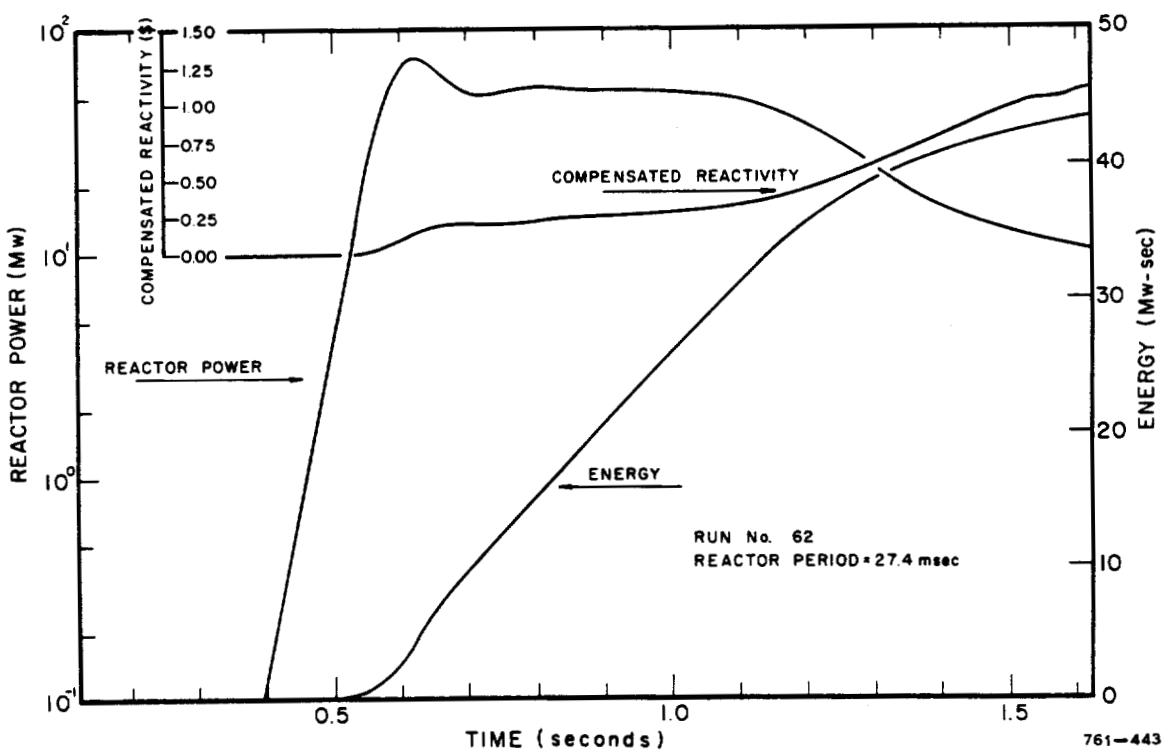

FIG. A-34 RUN 62 – 27.4-MSEC-PERIOD TEST.

1133292

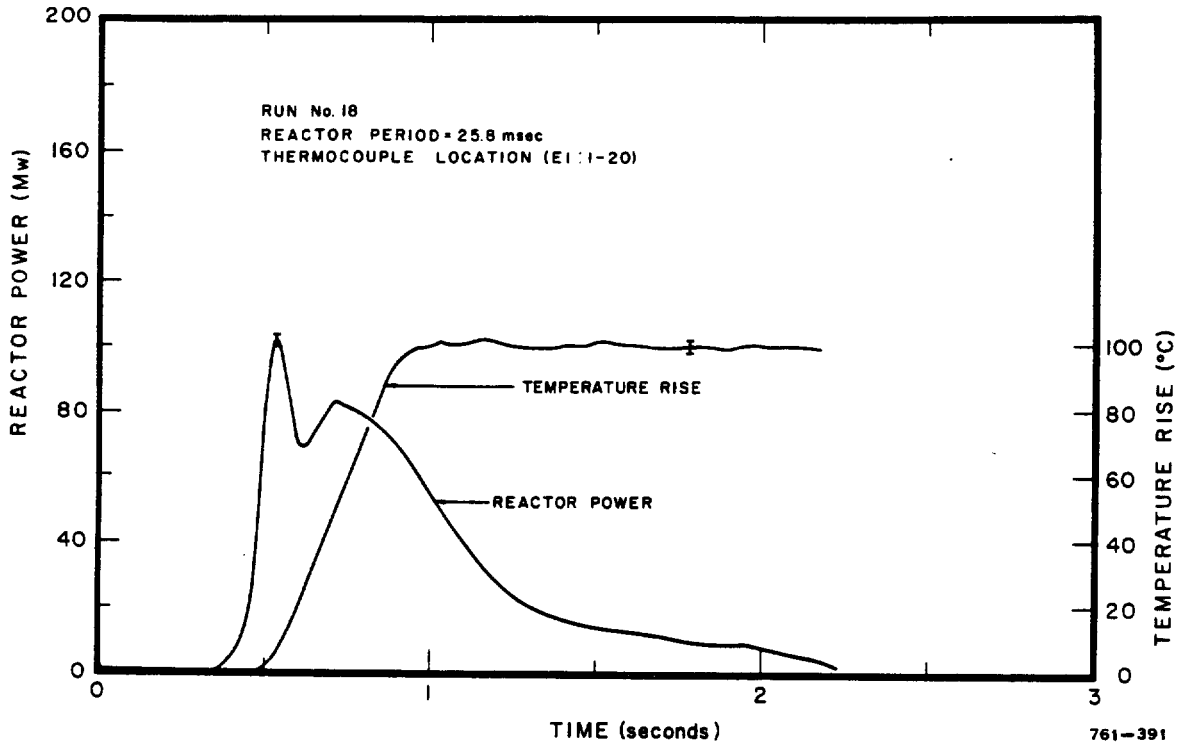

FIG. A-35 RUN 18 – 25.8-MSEC-PERIOD TEST.

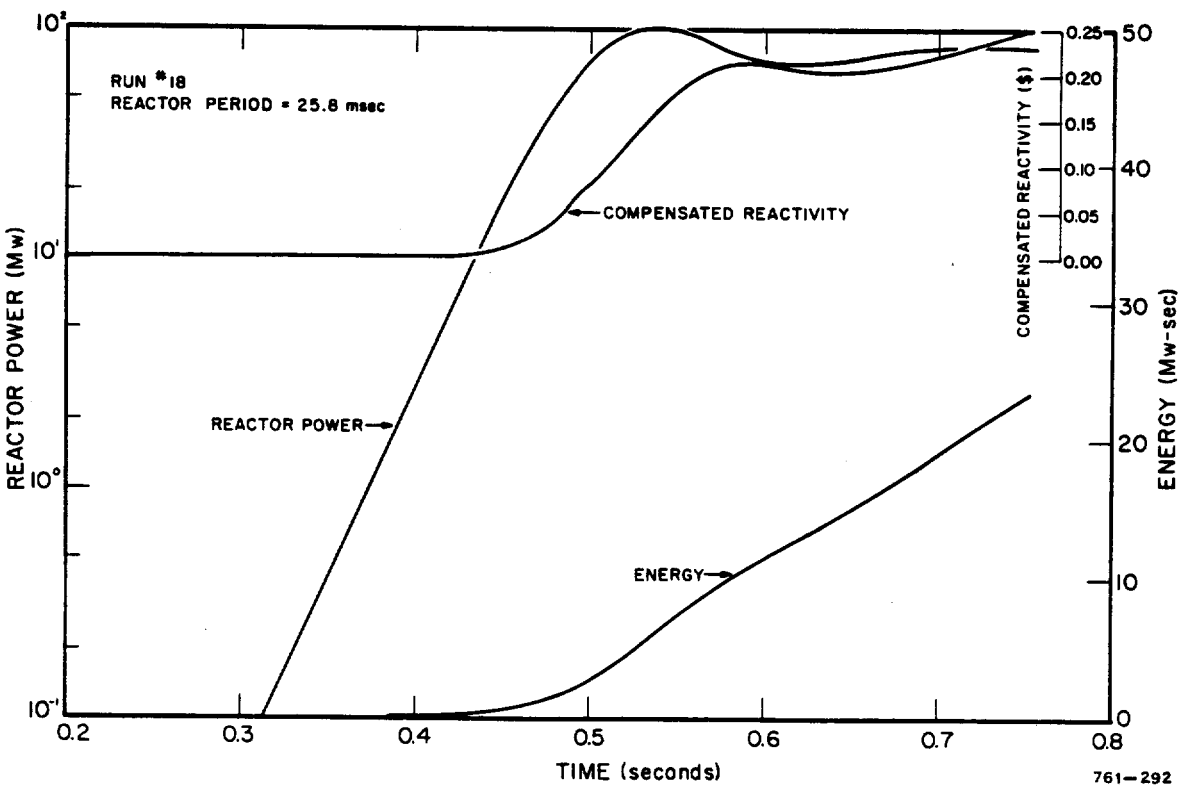

FIG. A-36 RUN 18 – 25.8-MSEC-PERIOD TEST.

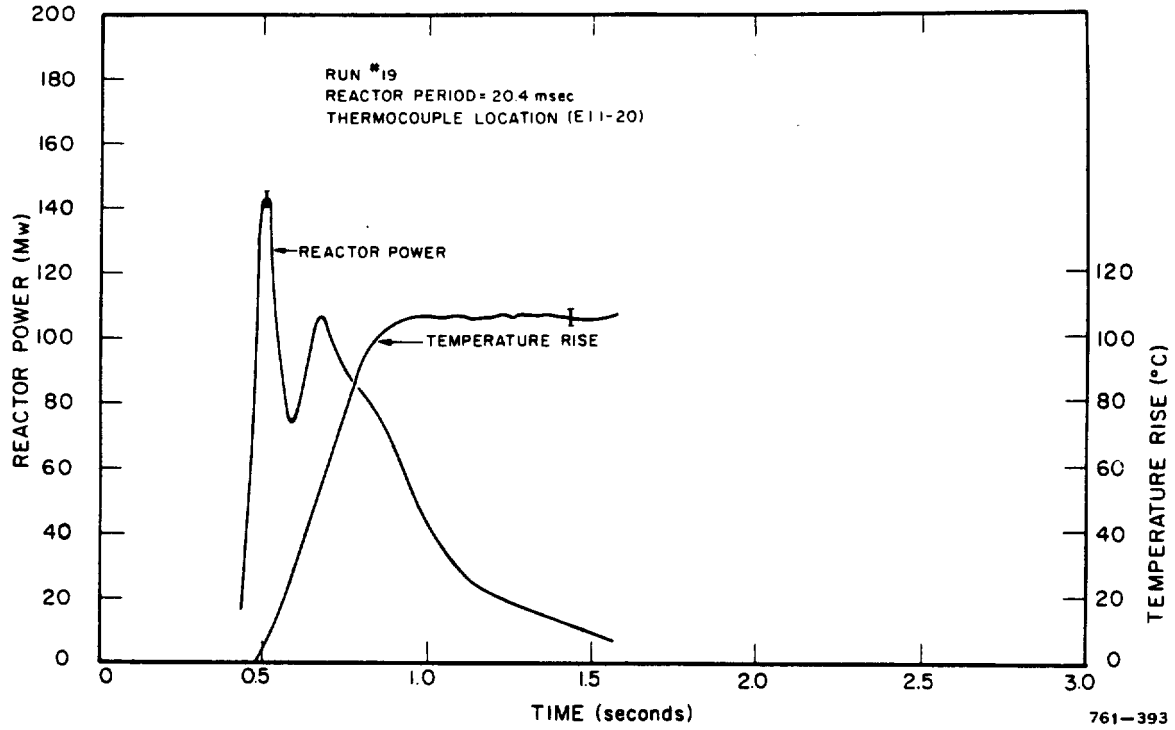

FIG. A-37 RUN 19 – 20.4-MSEC-PERIOD TEST.

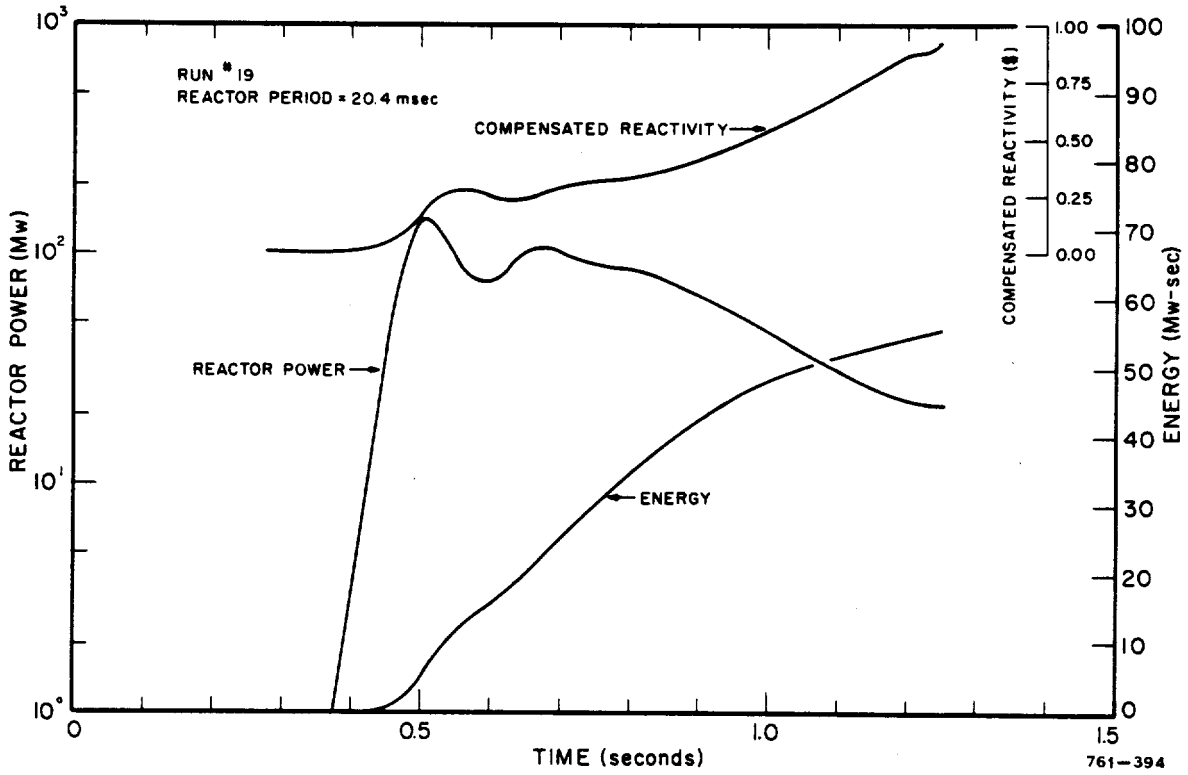

FIG. A-38 RUN 19 – 20.4-MSEC-PERIOD TEST.

1133294

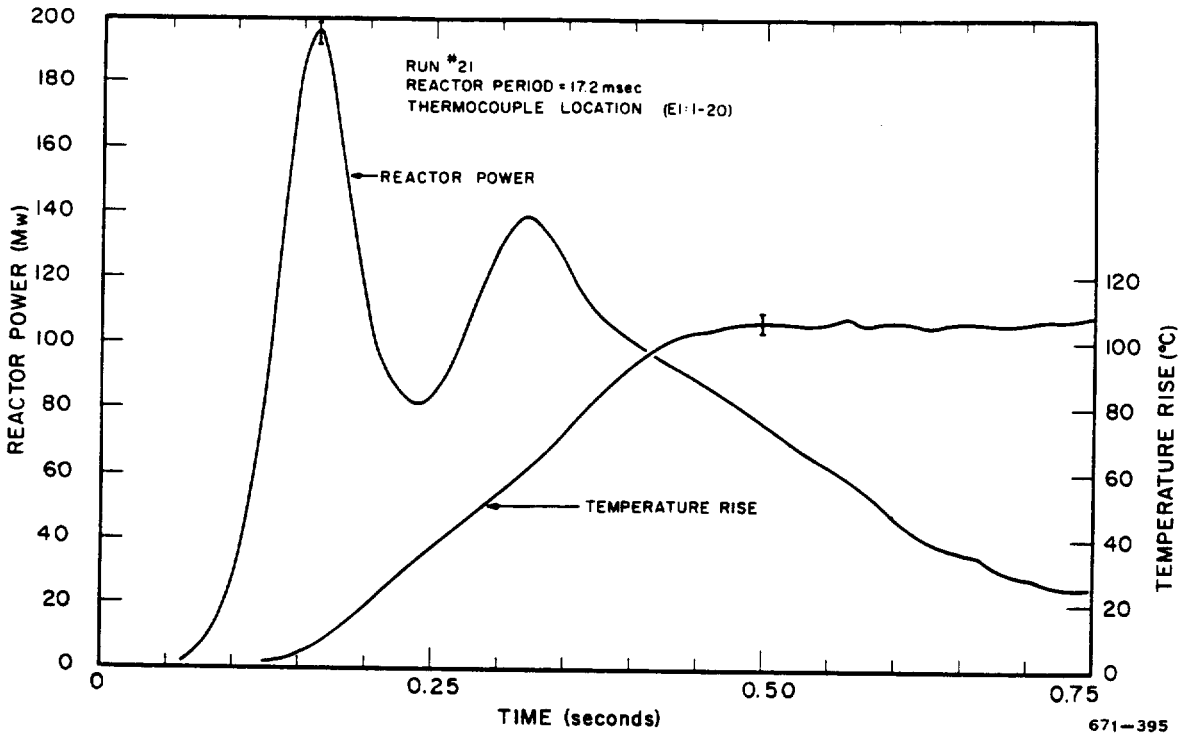

FIG. A-39 RUN 21 – 17.2-MSEC-PERIOD TEST.

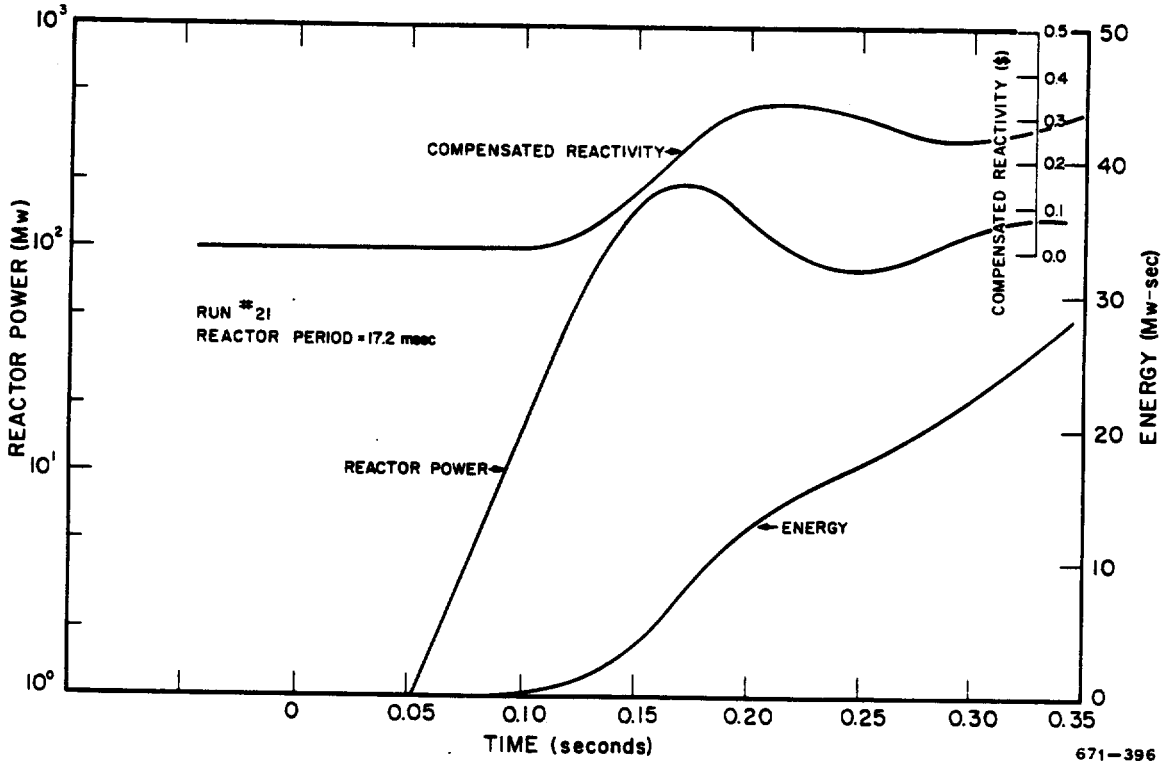

FIG. A-40 RUN 21 – 17.2-MSEC-PERIOD TEST.

1133295

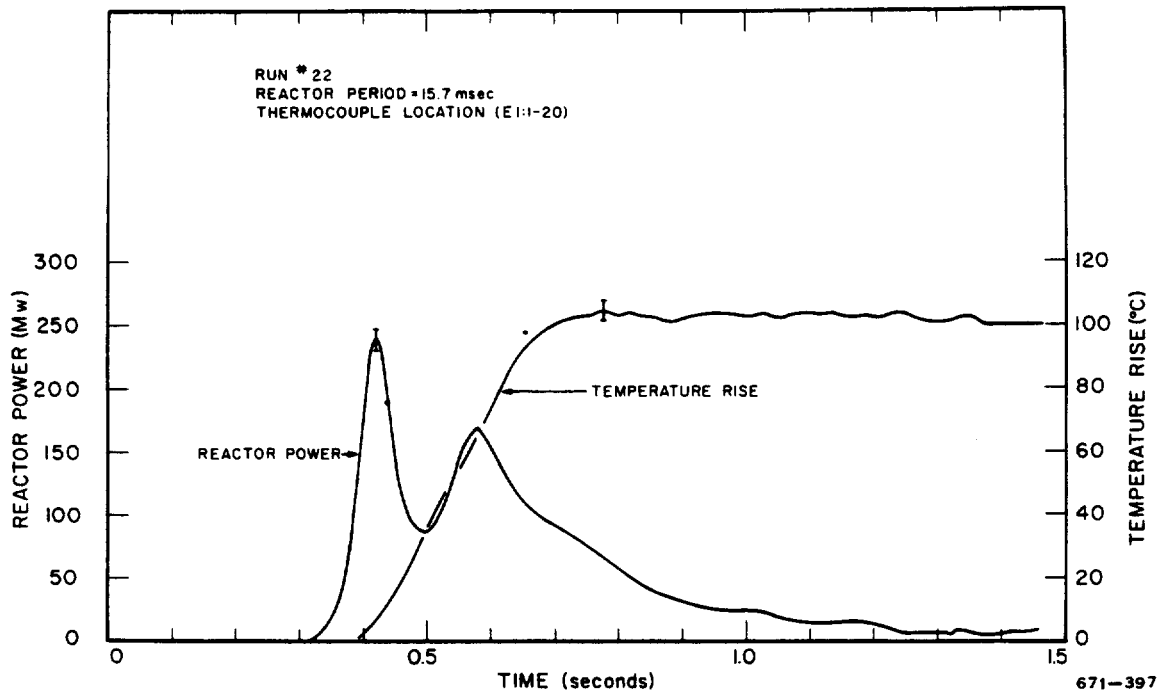

FIG. A-41 RUN 22 – 15.7-MSEC-PERIOD TEST.

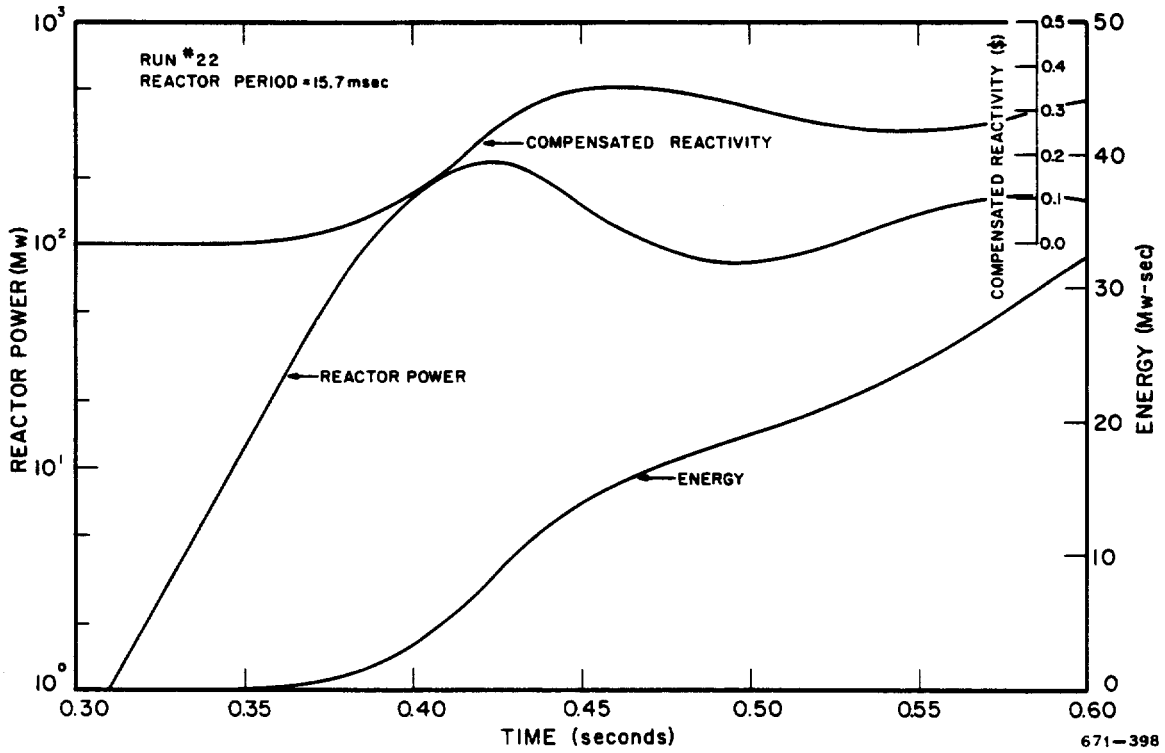

FIG. A-42 RUN 22 – 15.7-MSEC-PERIOD TEST.

1133296

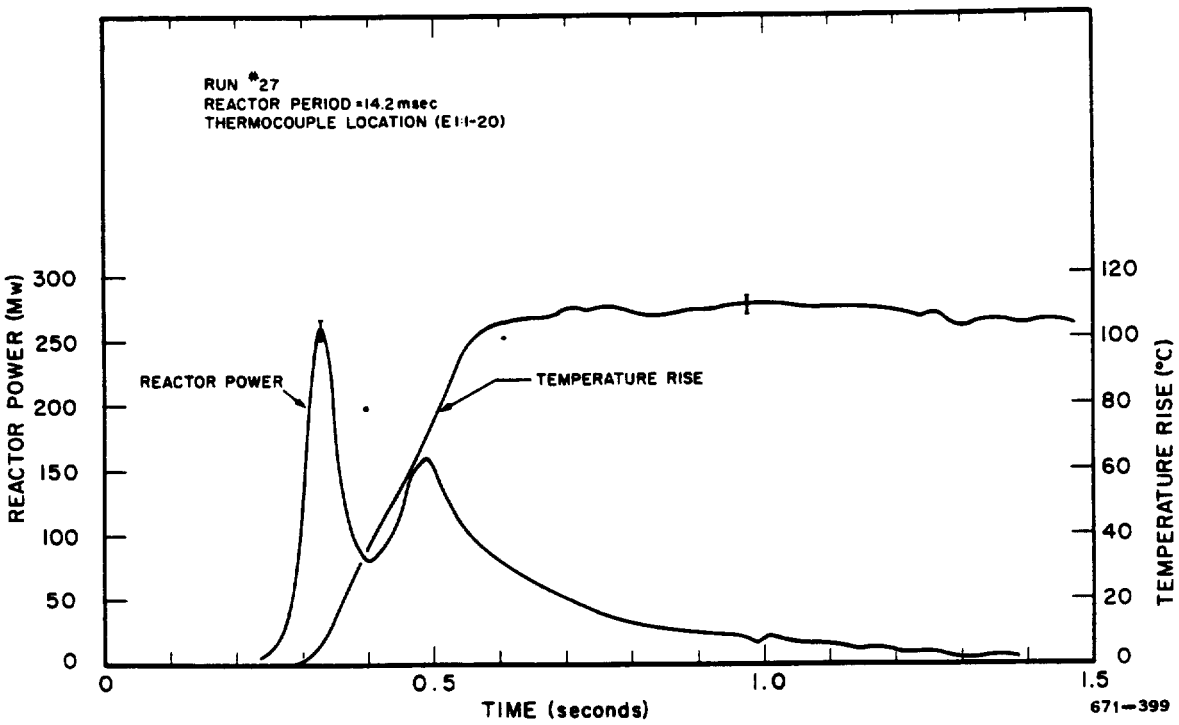

FIG. A-43 RUN 27 – 14.2-MSEC-PERIOD TEST.

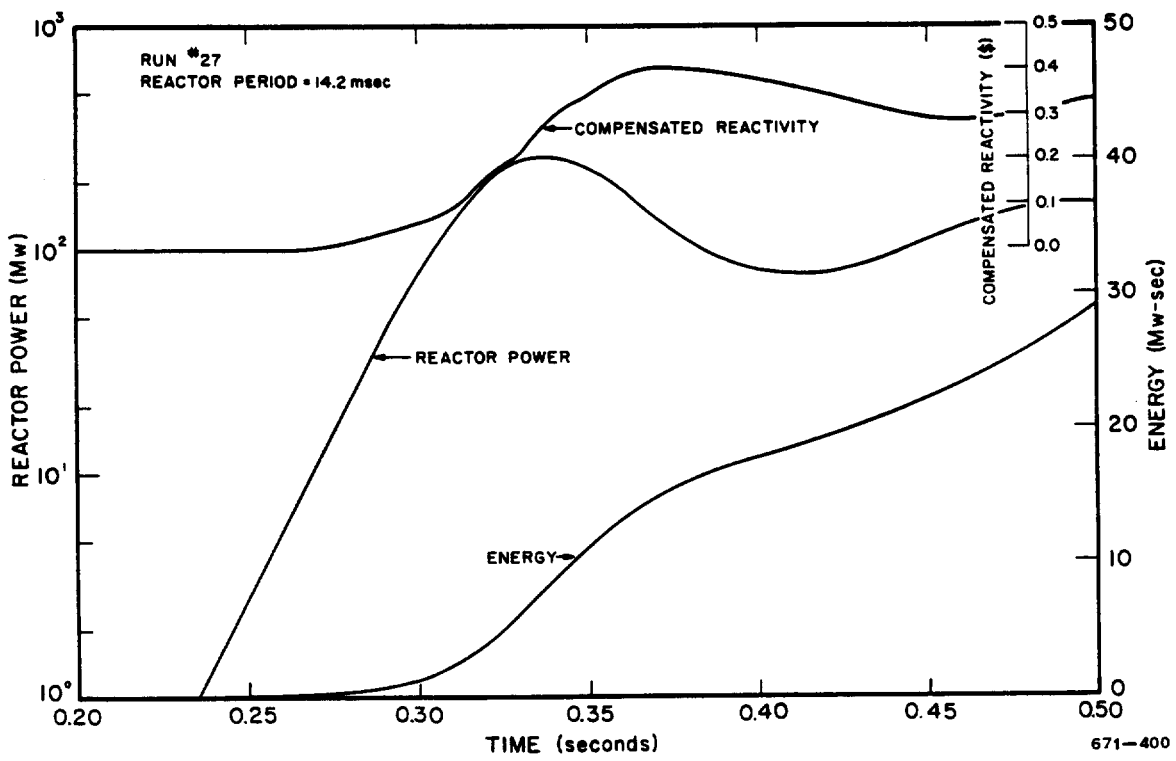

FIG. A-44 RUN 27 – 14.2-MSEC-PERIOD TEST.

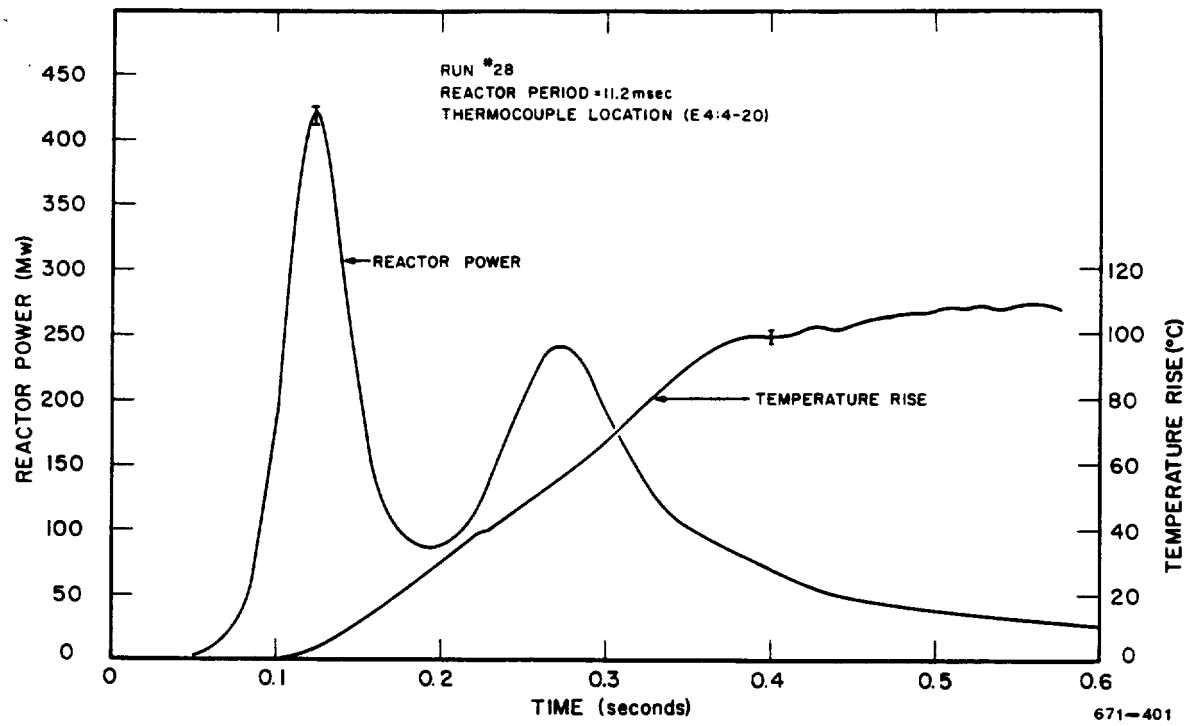

FIG. A-45 RUN 28 – 11.2-MSEC-PERIOD TEST.

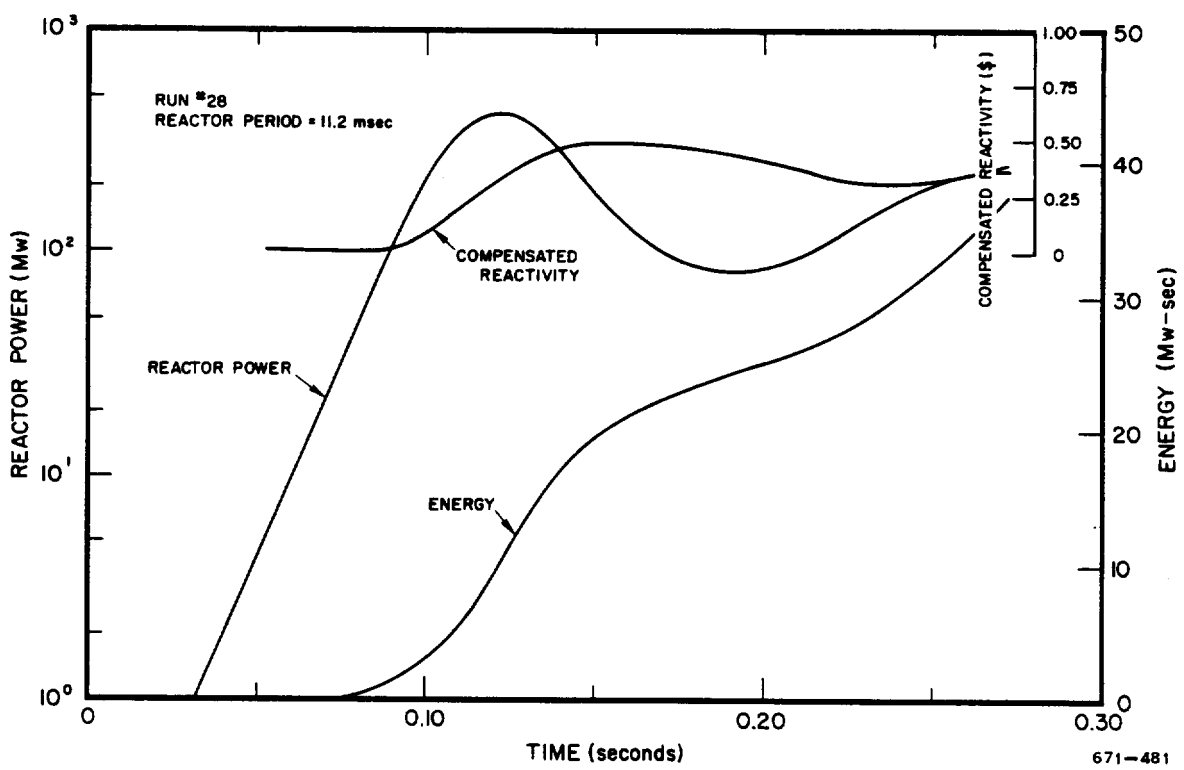

FIG. A-46 RUN 28 – 11.2-MSEC-PERIOD TEST.

1133298

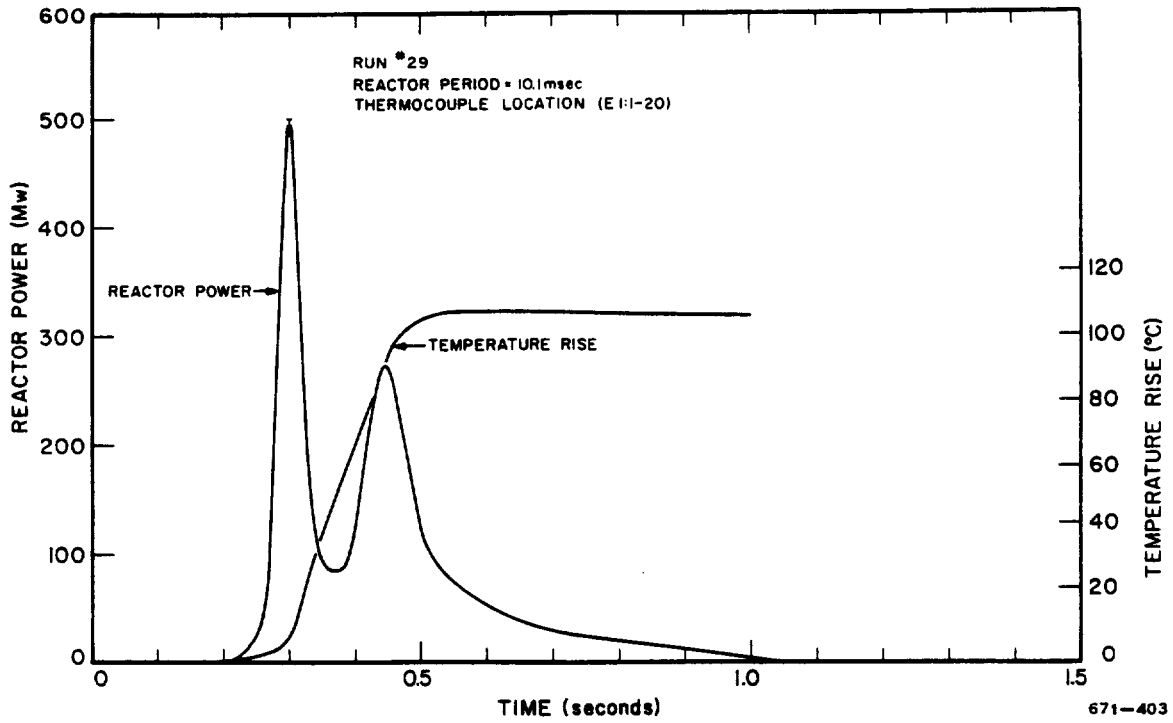

FIG. A-47 RUN 29 – 10.1-MSEC-PERIOD TEST.

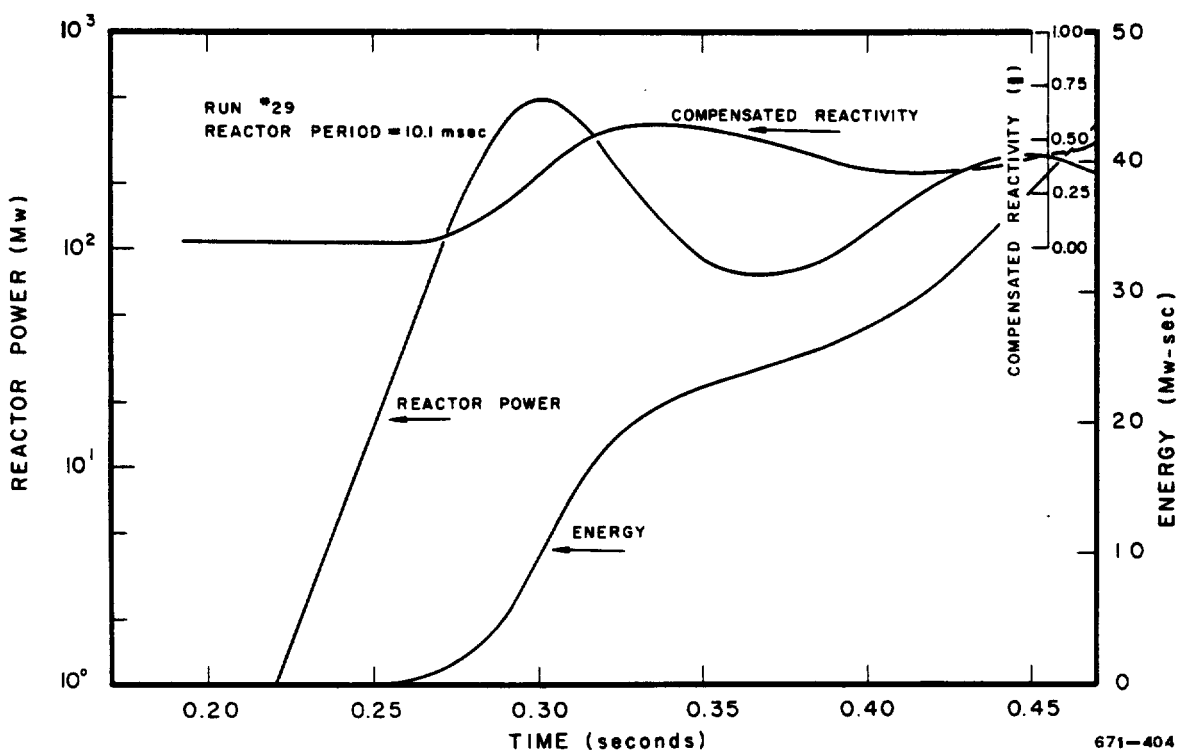

FIG. A-48 RUN 29 – 10.1-MSEC-PERIOD TEST.

1133299

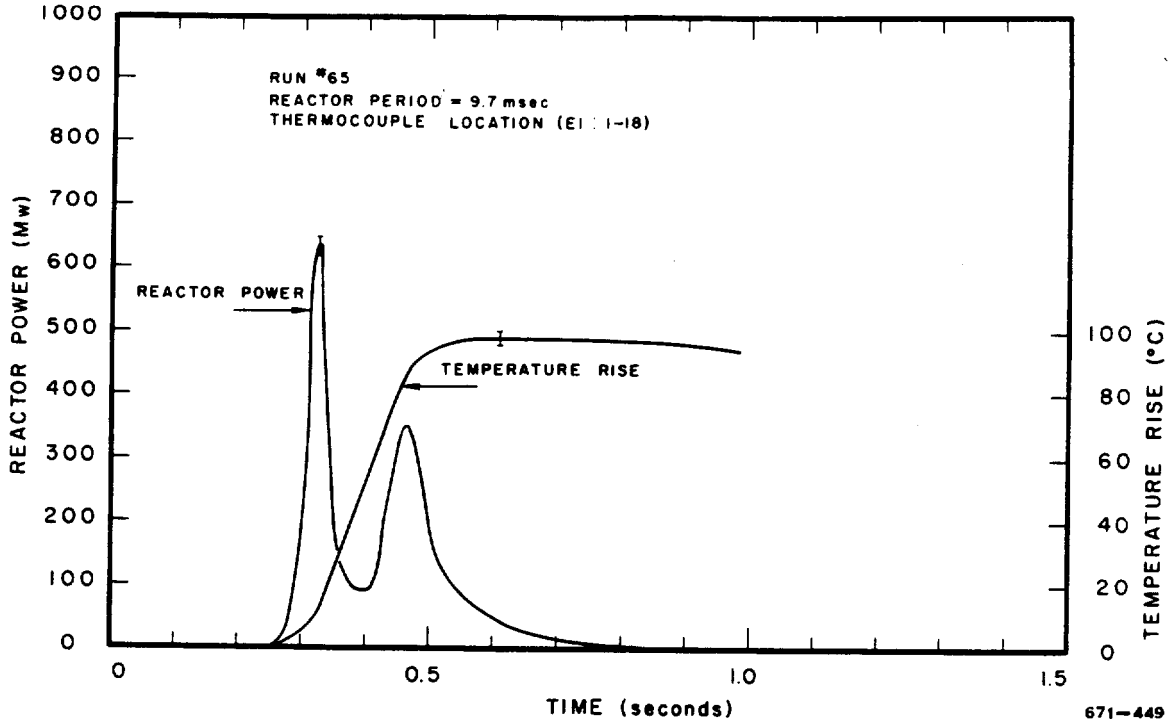

FIG. A-49 RUN 65 – 9.7-MSEC-PERIOD TEST.

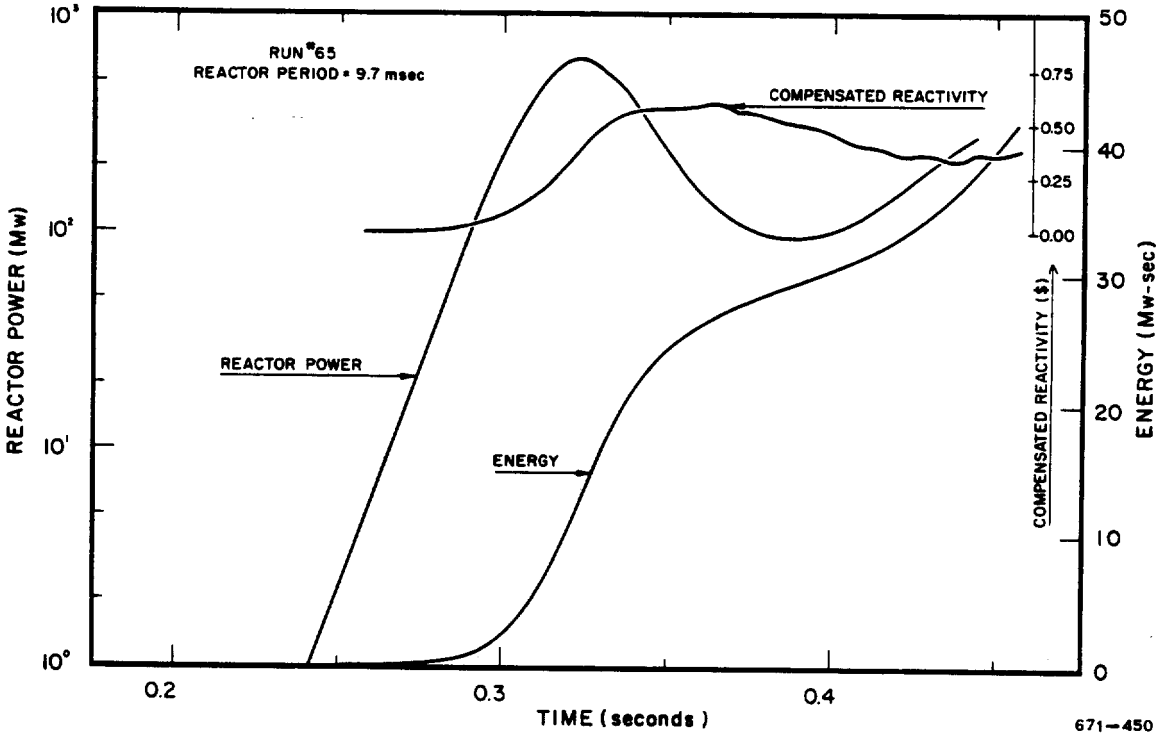

FIG. A-50 RUN 65 – 9.7-MSEC-PERIOD TEST.

1133300

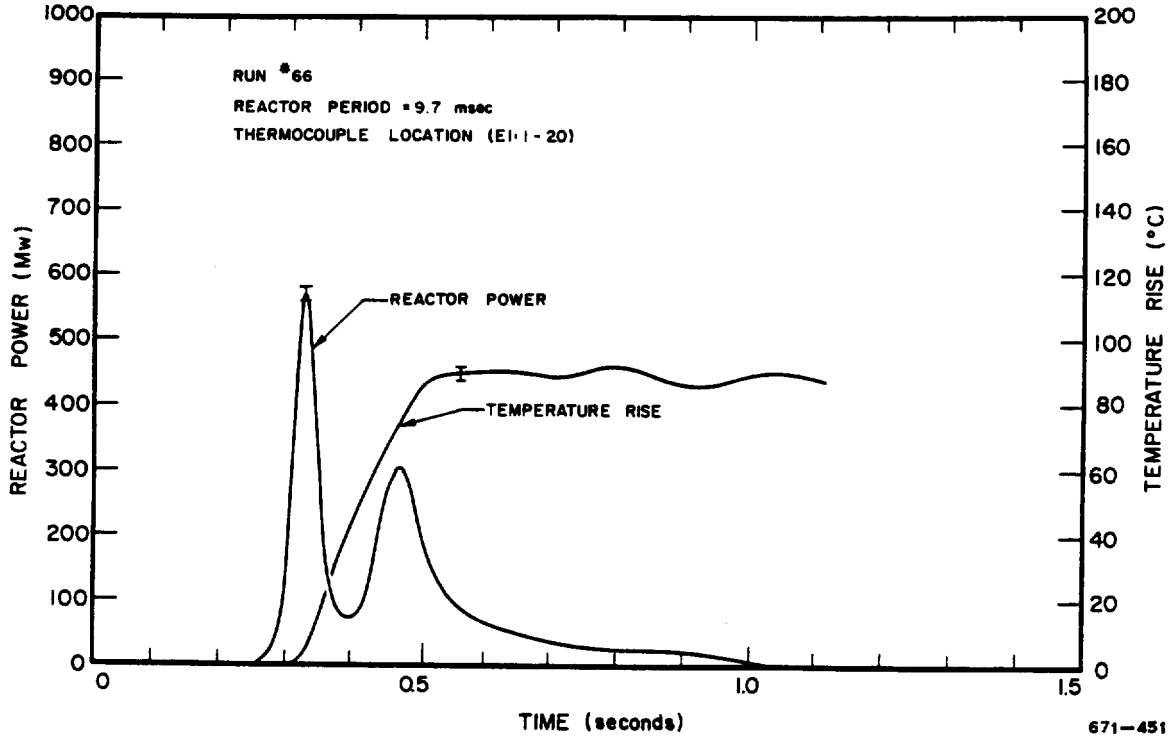

FIG. A-51 RUN 66 – 9.7-MSEC-PERIOD TEST.

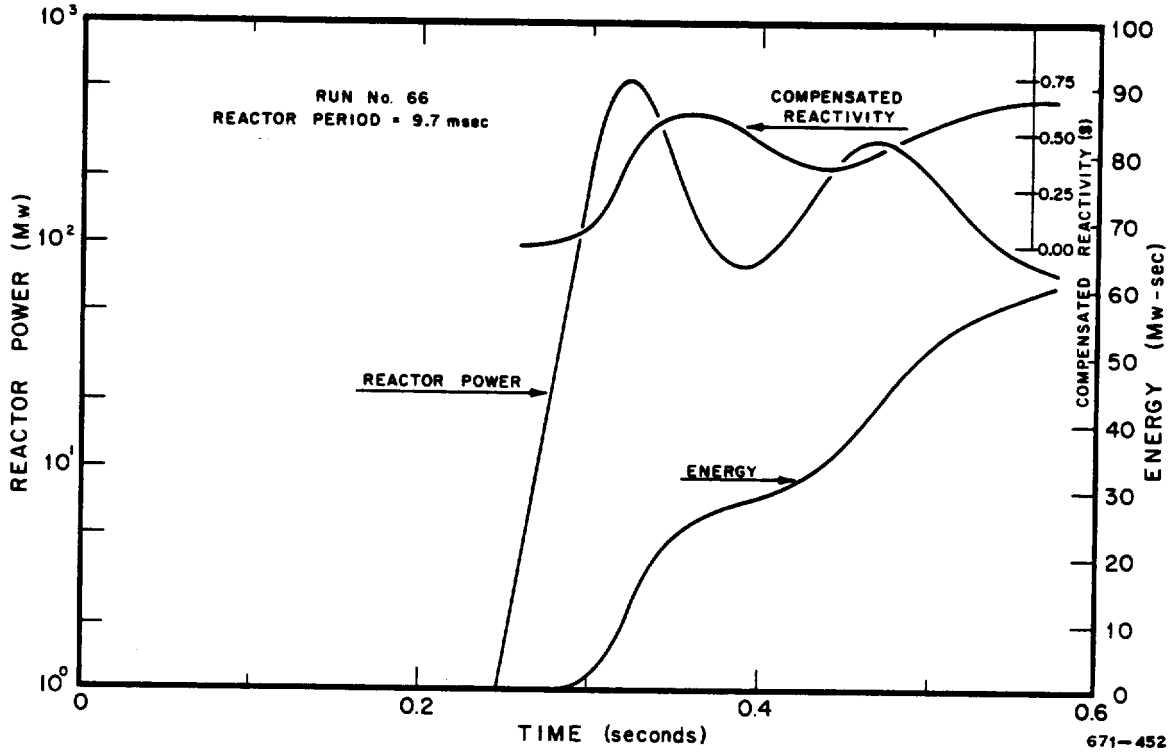

FIG. A-52 RUN 66 – 9.7-MSEC-PERIOD TEST.

1133301

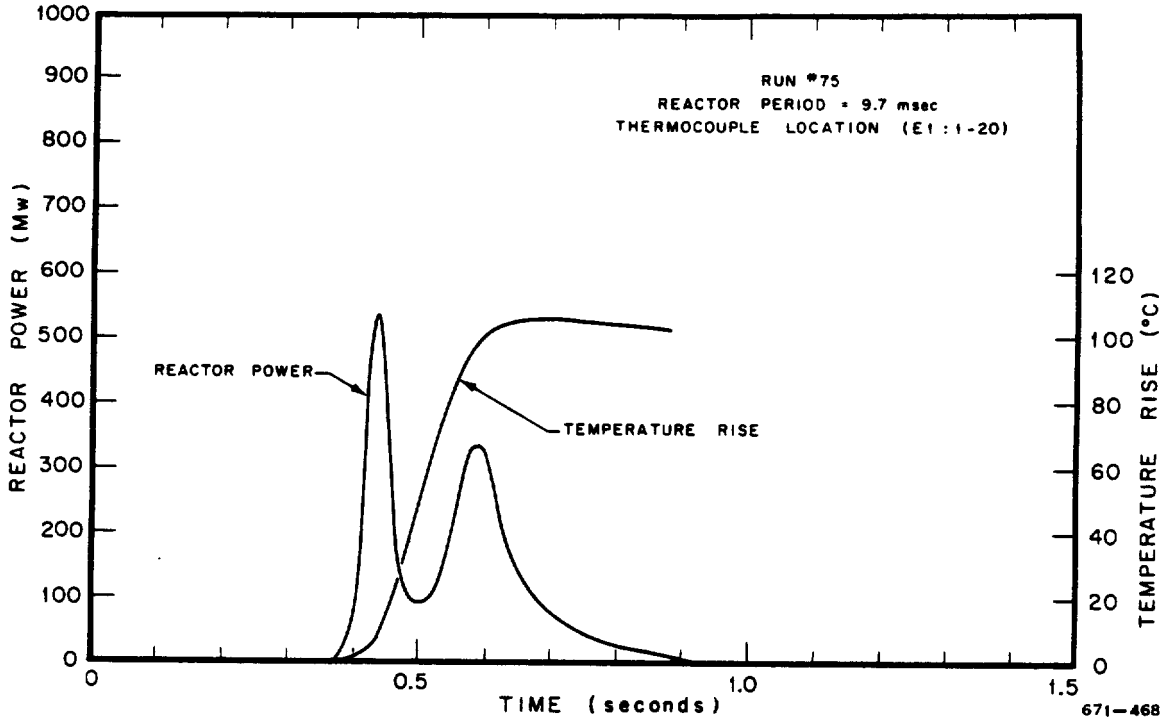

FIG. A-53 RUN 75 – 9.7-MSEC-PERIOD TEST.

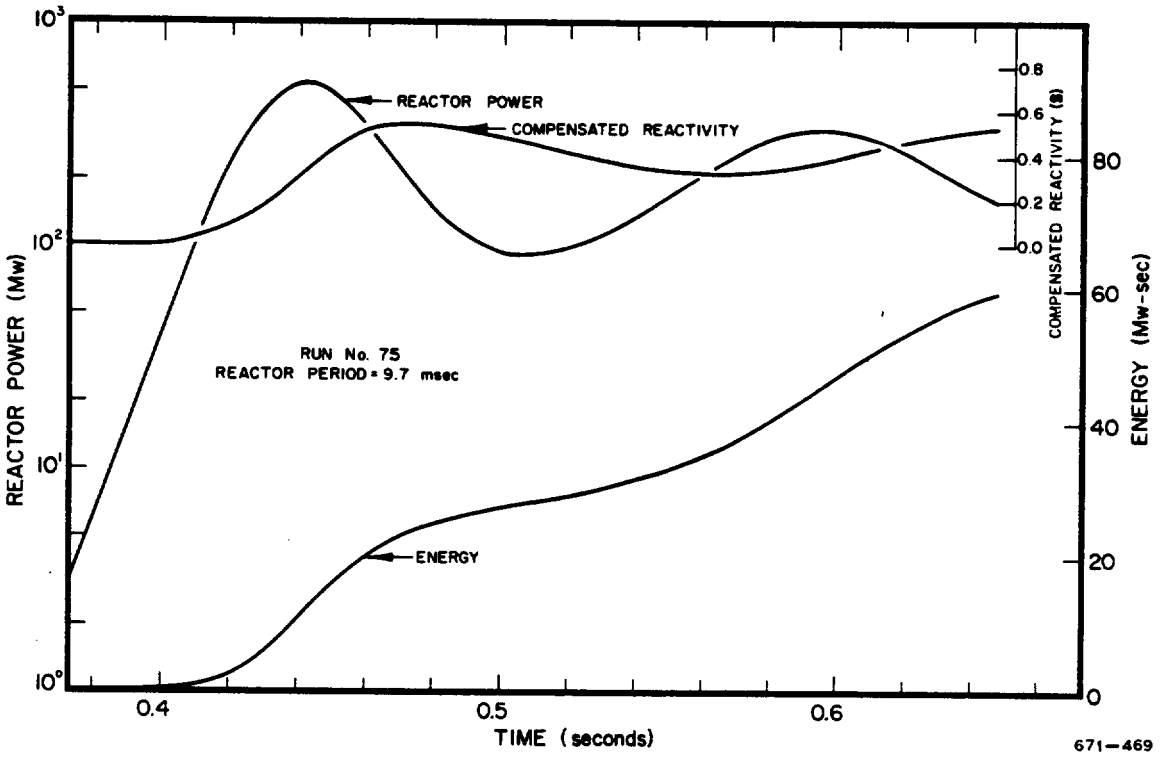

FIG. A-54 RUN 75 – 9.7-MSEC-PERIOD TEST.

1133302

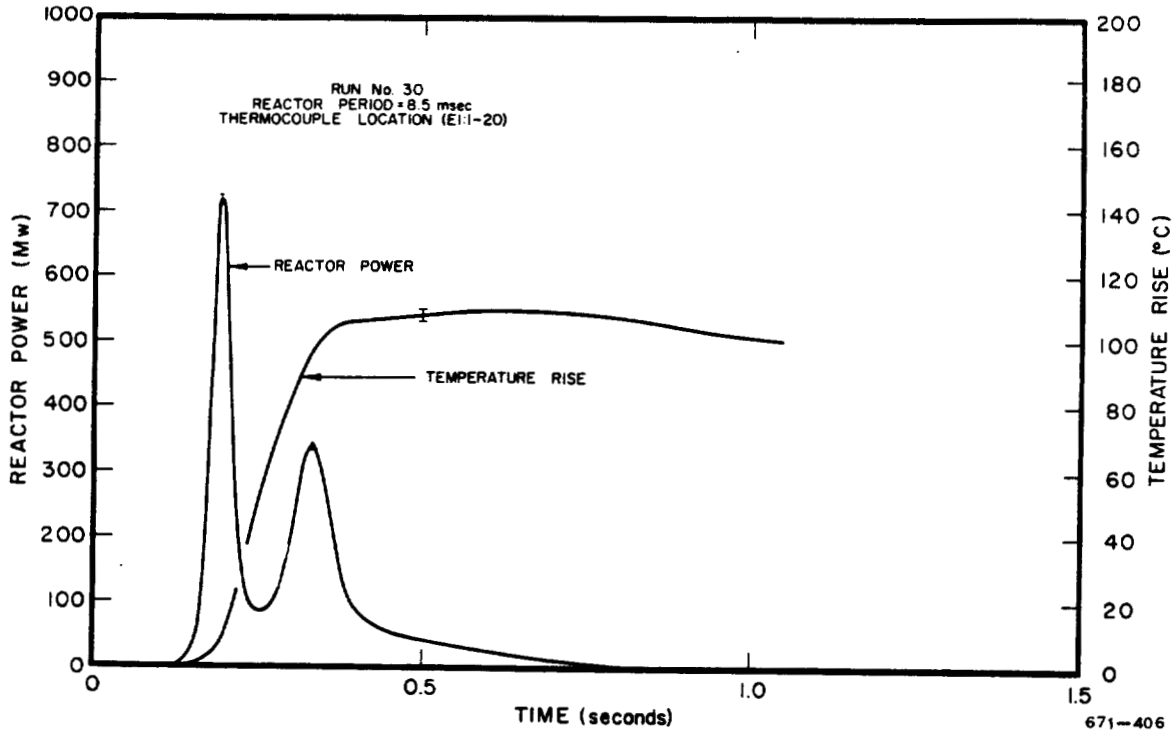

FIG. A-55 RUN 30 – 8.5-MSEC-PERIOD TEST.

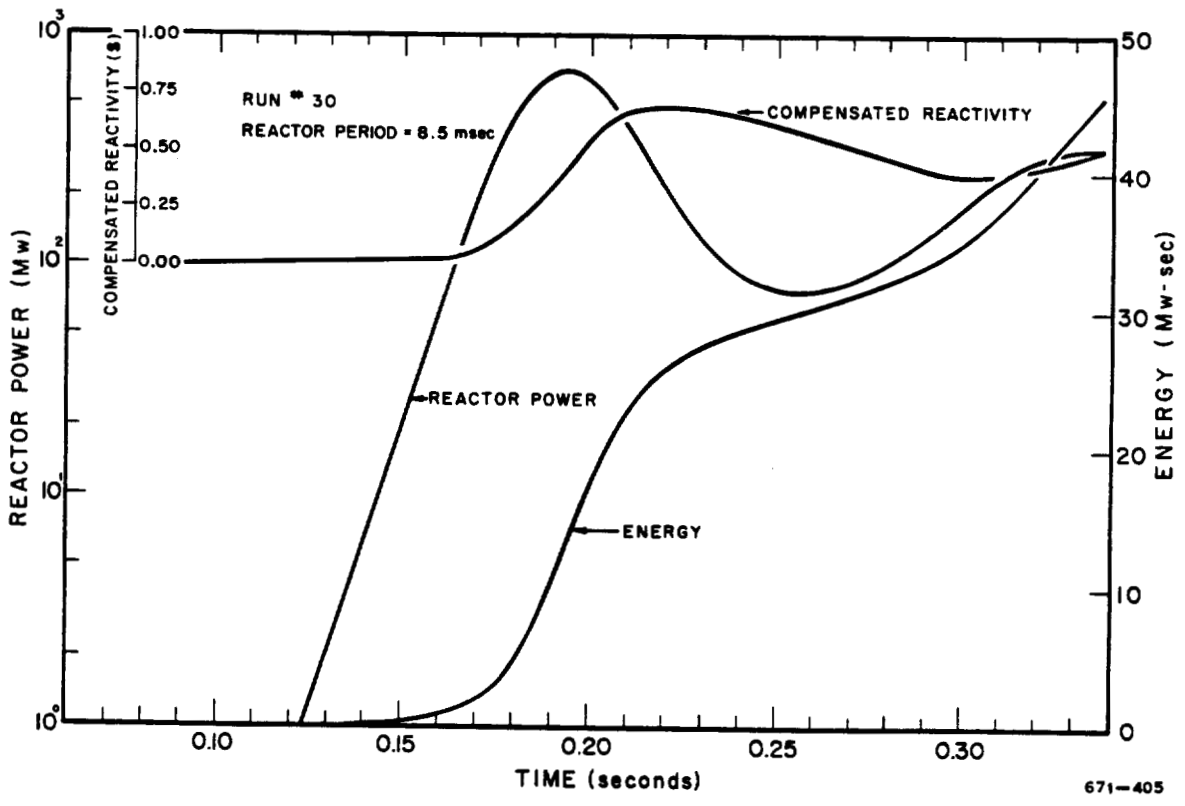

FIG. A-56 RUN 30 – 8.5-MSEC-PERIOD TEST.

1133303

APPENDIX B

PLOTS OF SURFACE TEMPERATURE, POWER, ENERGY, AND COMPENSATED REACTIVITY VS TIME, FOR CONSTRAINED SPERT I OXIDE CORE

1133304

INTENTIONAL BLANK PAGE NO. 50

1133305

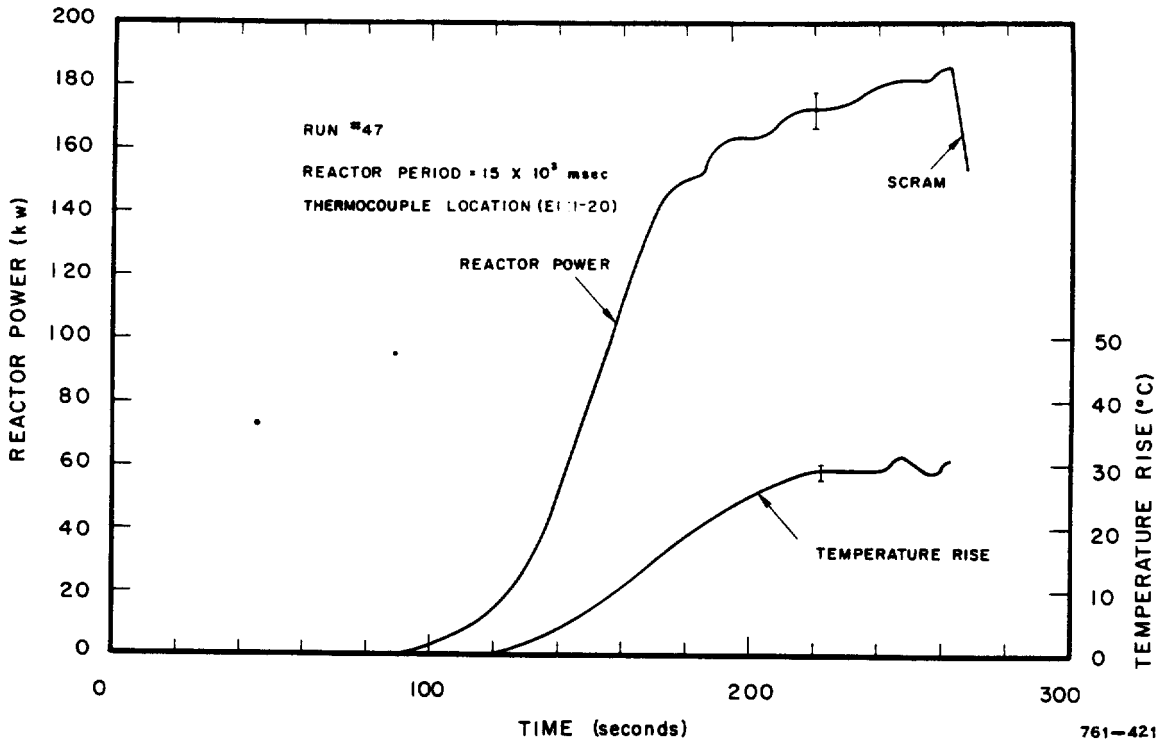

FIG. B-1 RUN 47 – 15.0-SEC-PERIOD TEST.

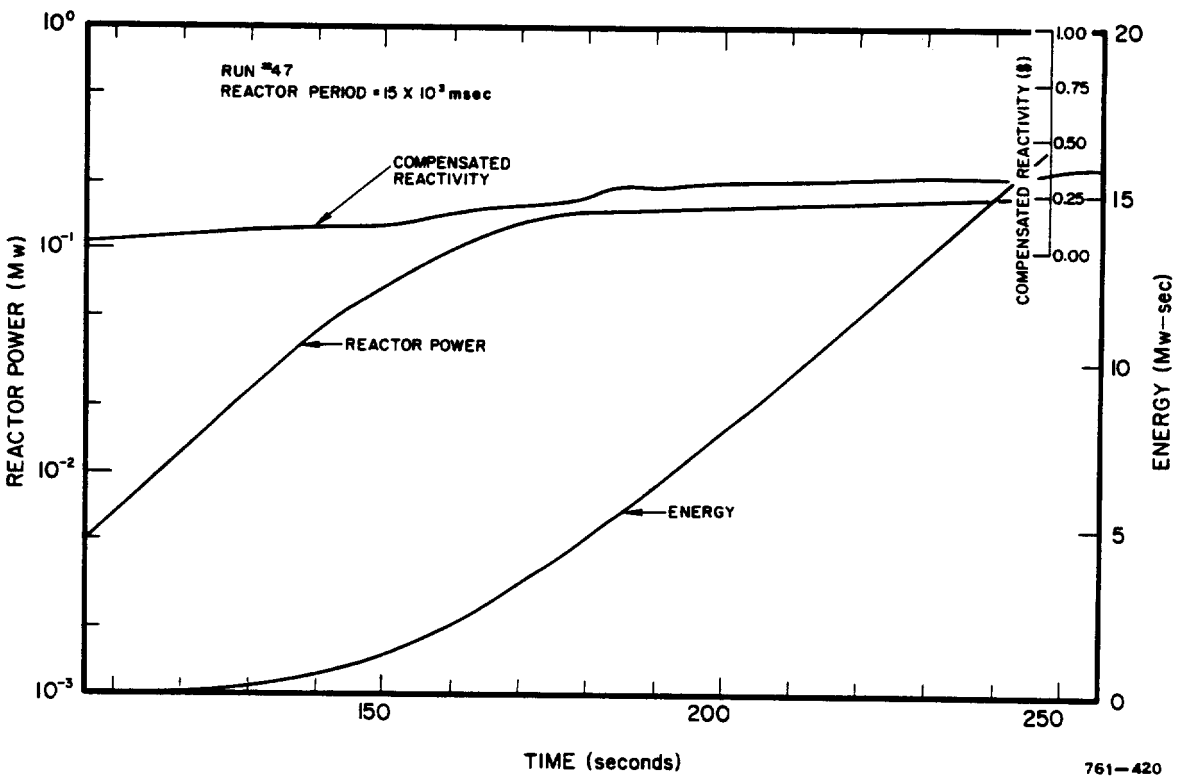

FIG. B-2 RUN 47 – 15.0-SEC-PERIOD TEST.

1133306

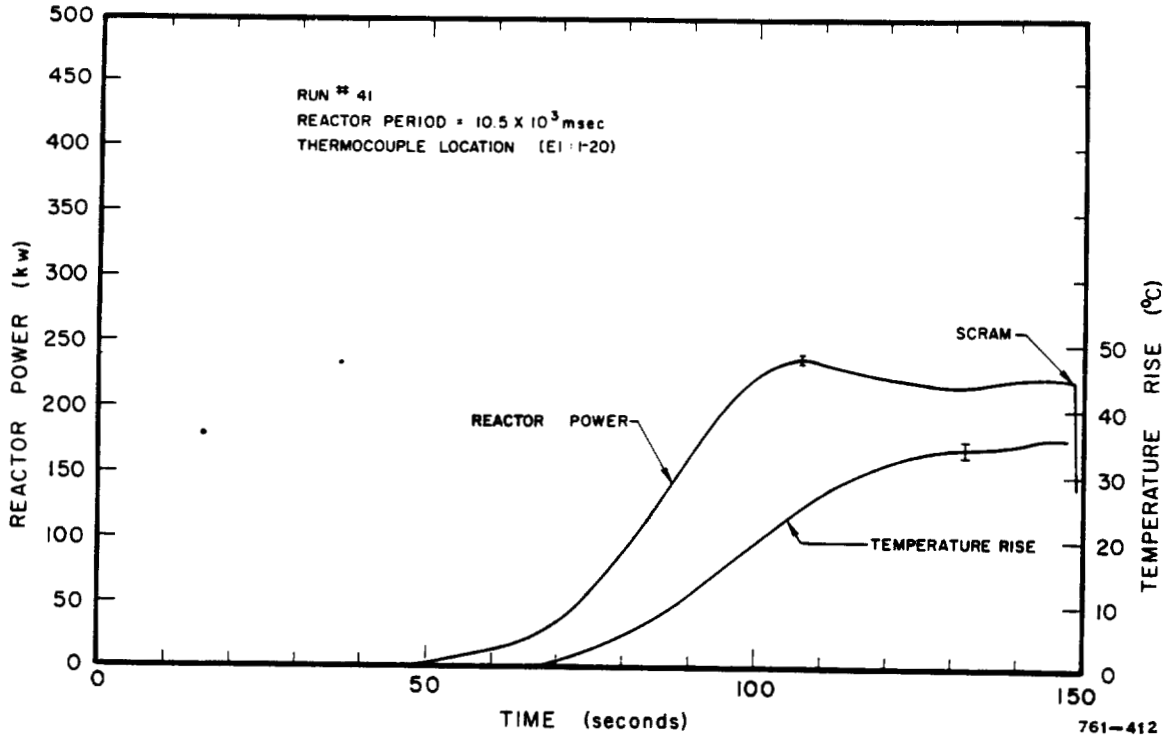

FIG. B-3 RUN 41 – 10.5-SEC-PERIOD TEST.

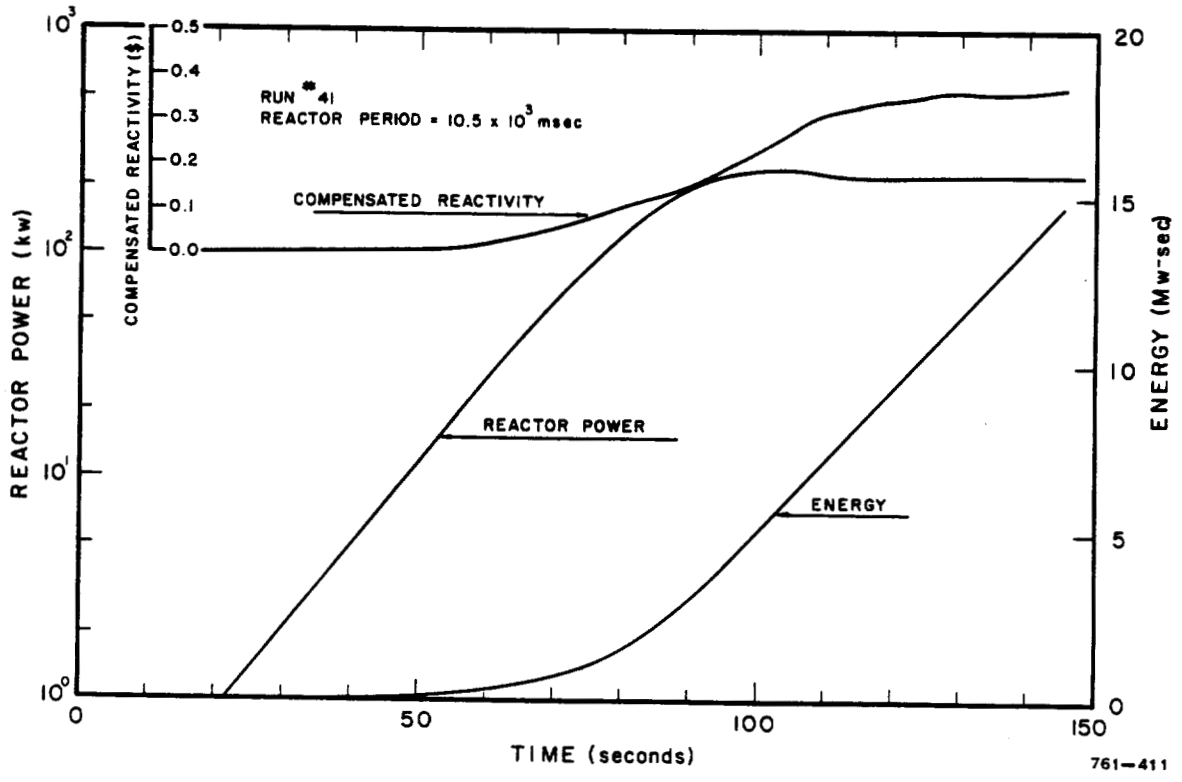

FIG. B-4 RUN 41 – 10.5-SEC-PERIOD TEST.

1133307

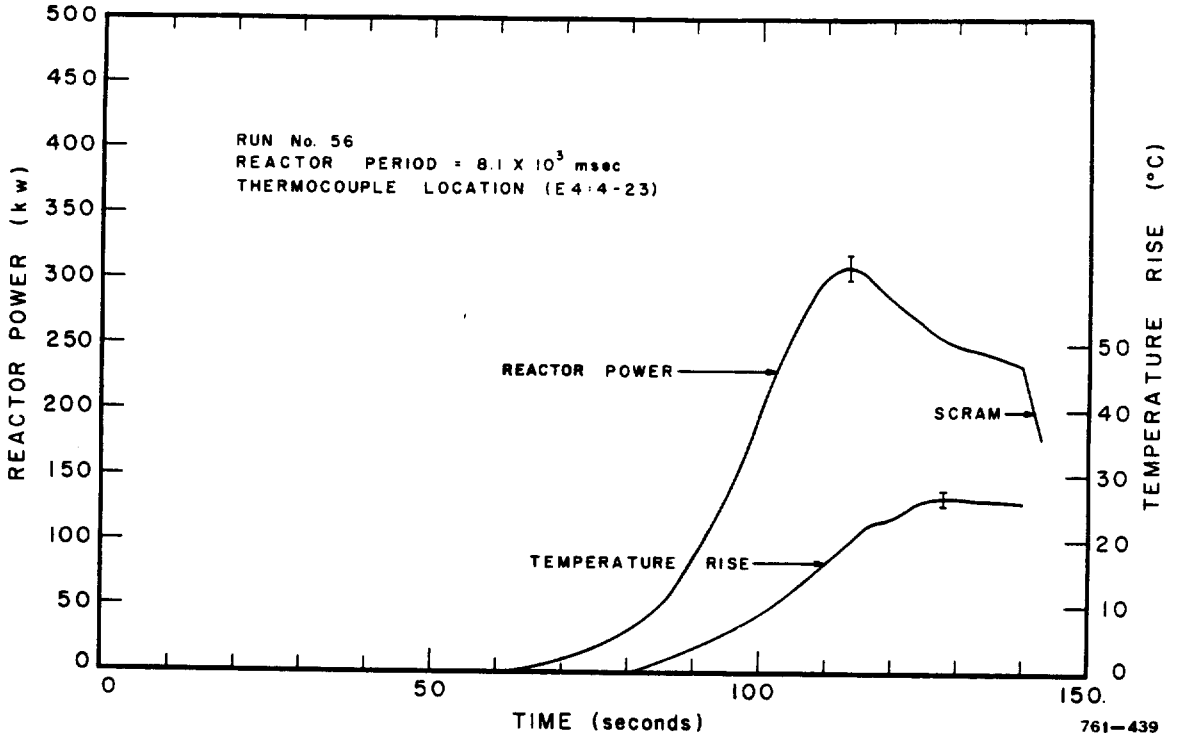

FIG. B-5 RUN 56 – 8.1-SEC-PERIOD TEST.

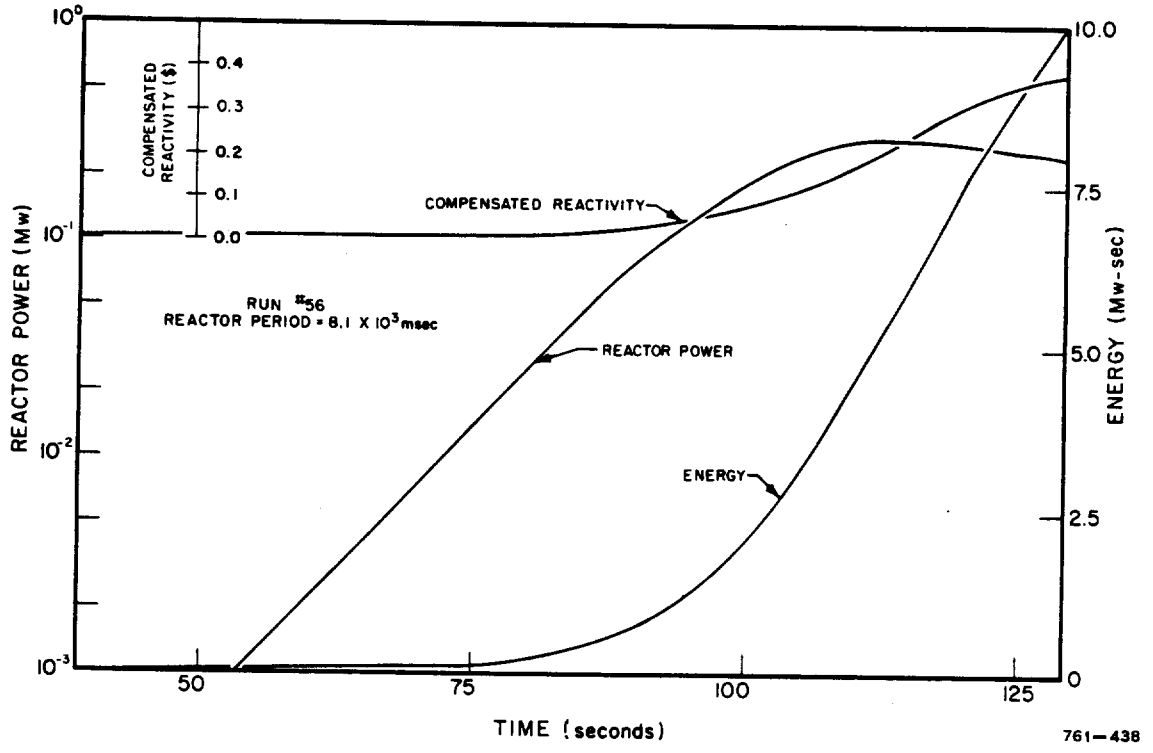

FIG. B-6 RUN 56 – 8.1-SEC-PERIOD TEST.

1133308

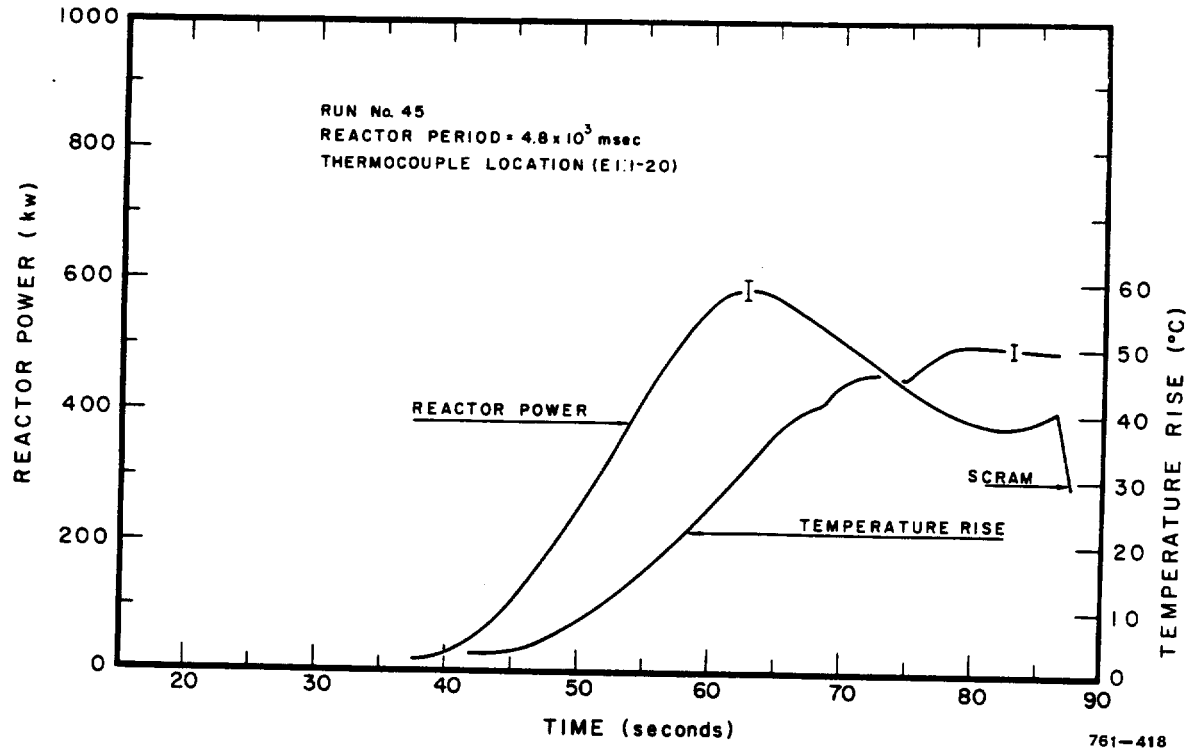

FIG. B-7 RUN 45 – 4.8-SEC-PERIOD TEST.

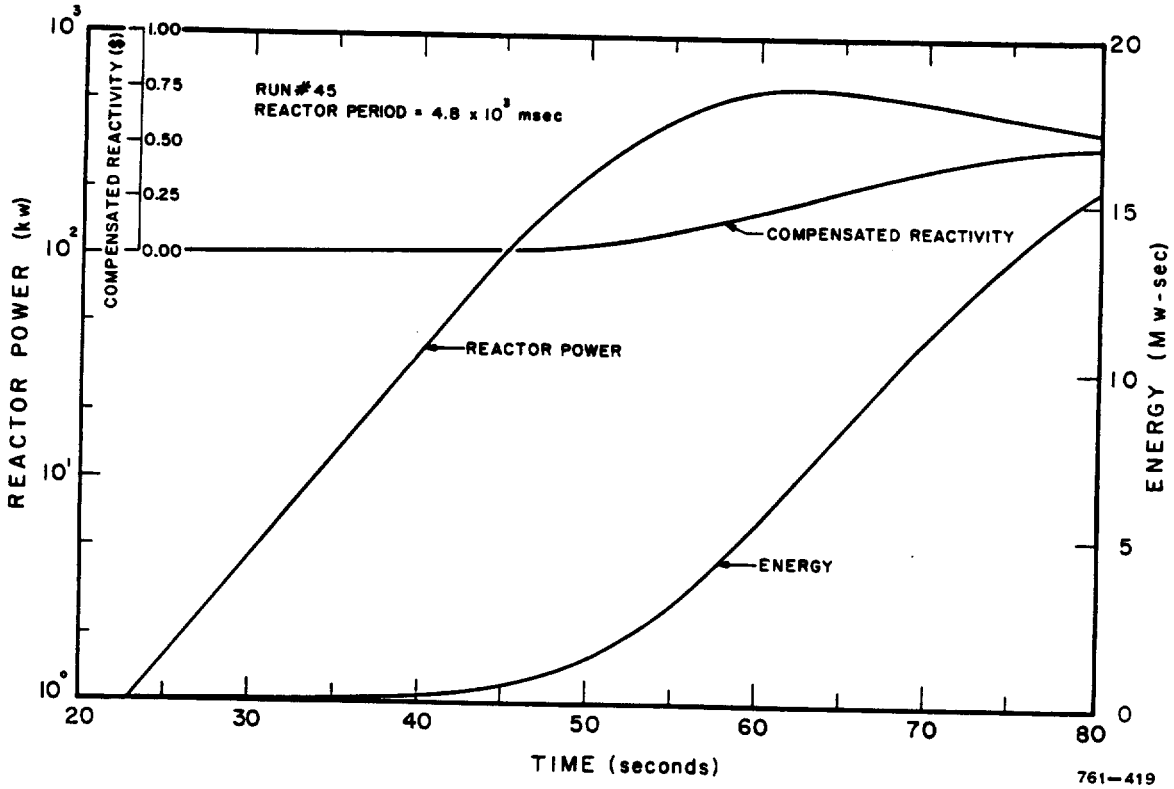

FIG. B-8 RUN 45 – 4.8-SEC-PERIOD TEST.

1133309

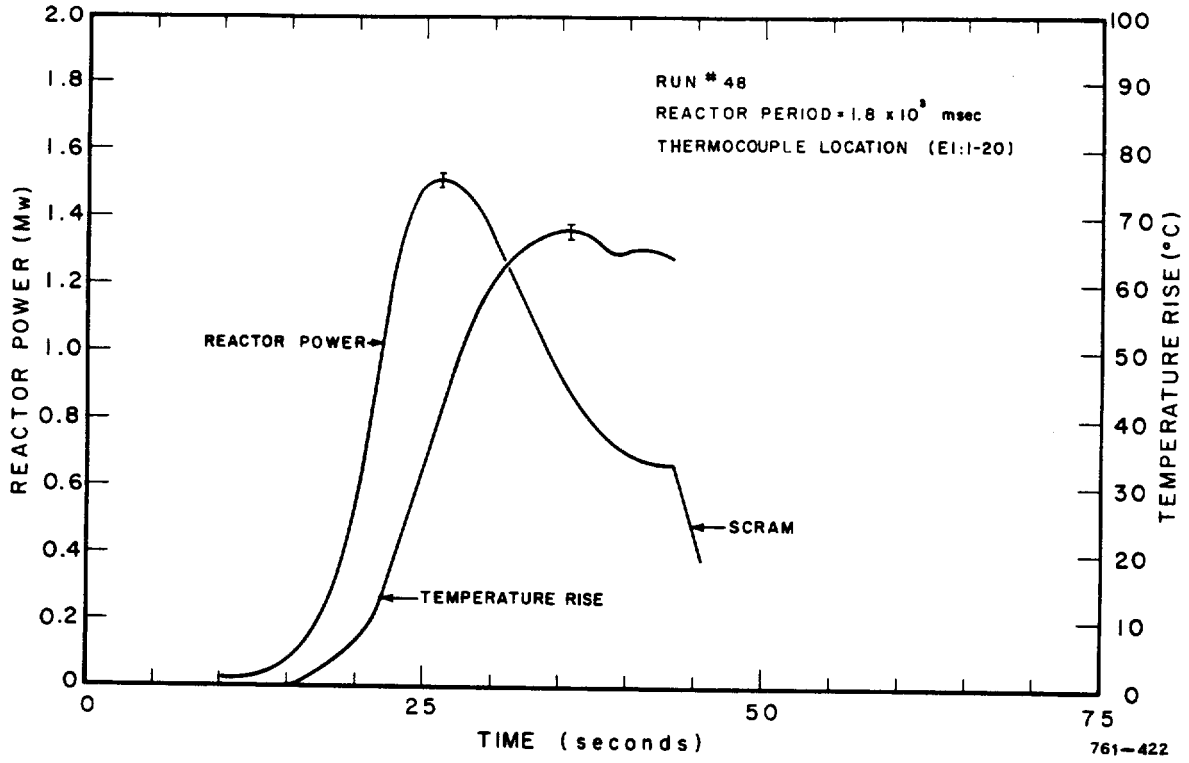

FIG. B-9 RUN 48 – 1.8-SEC-PERIOD TEST.

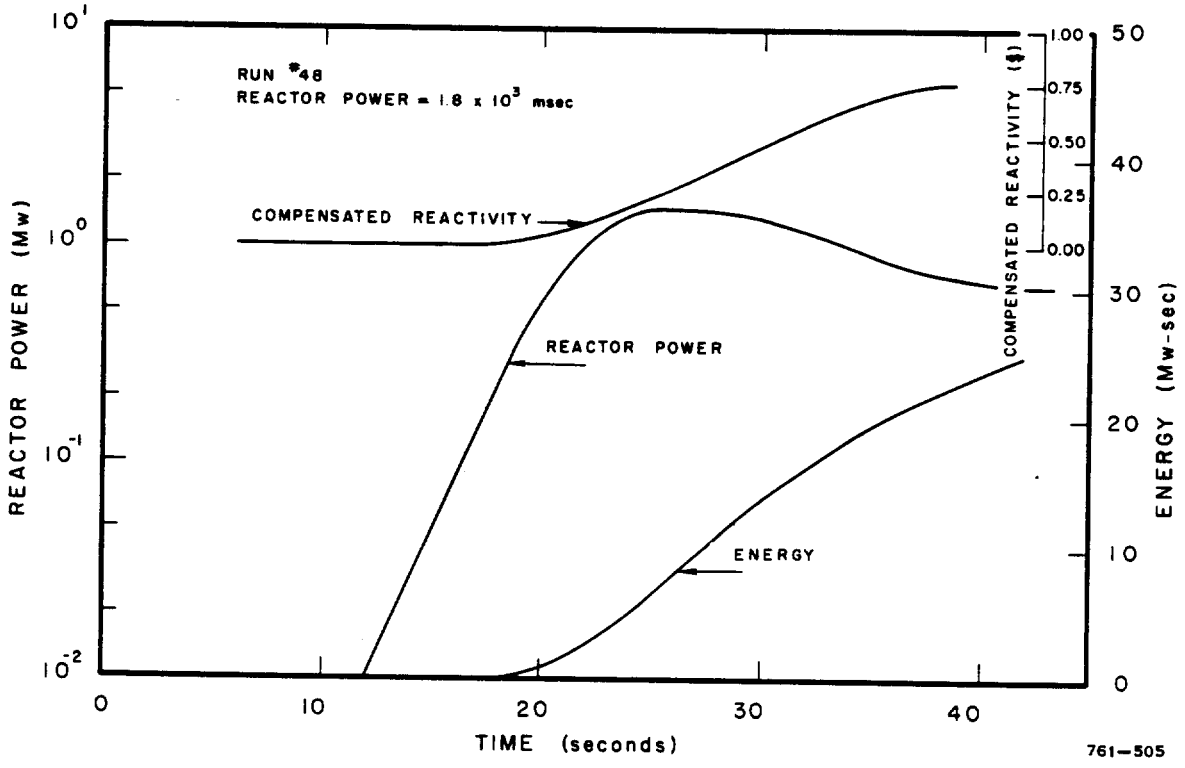

FIG. B-10 RUN 48 – 1.8-SEC-PERIOD TEST.

1133310

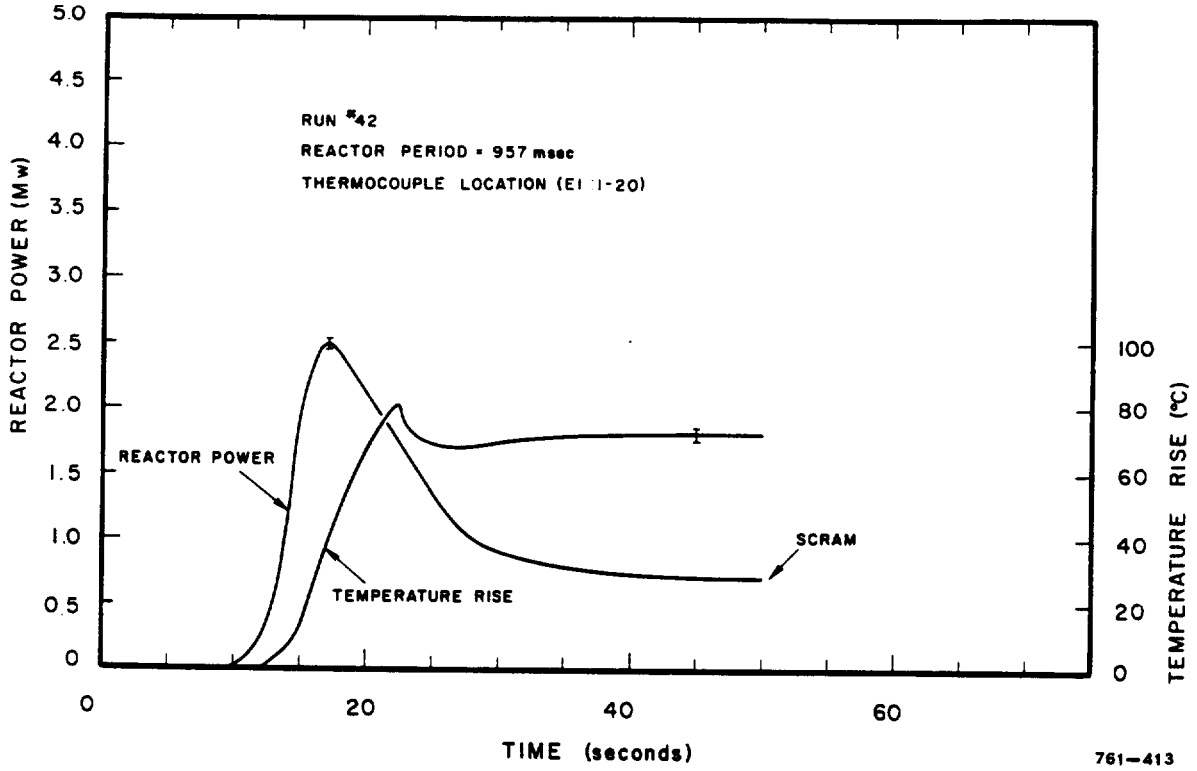

FIG. B-11 RUN 42 – 957-MSEC-PERIOD TEST.

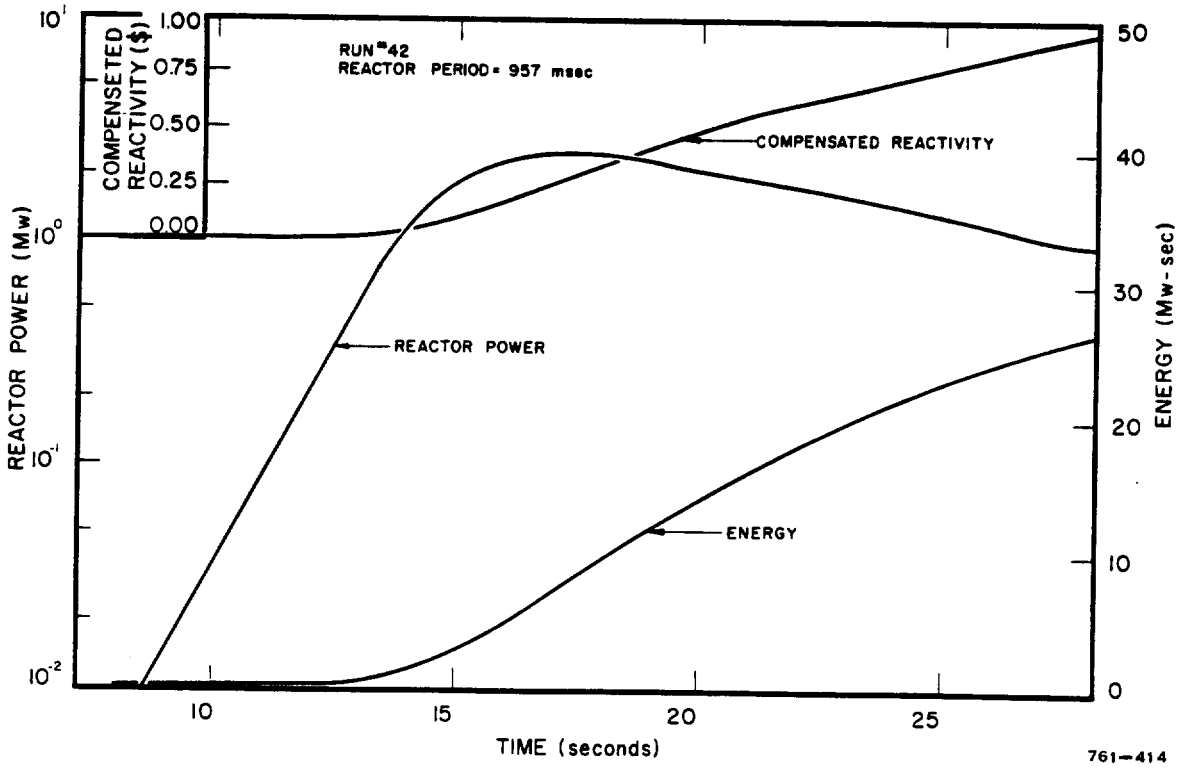

FIG. B-12 RUN 42 – 957-MSEC-PERIOD TEST.

1133311

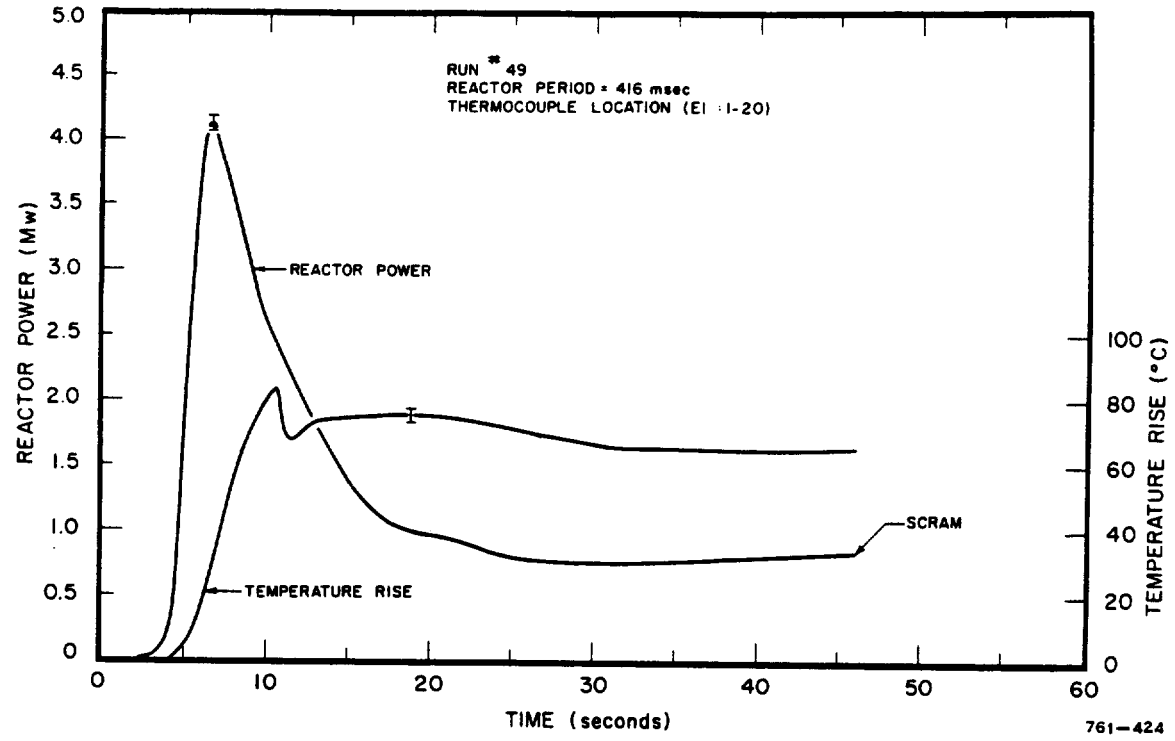

FIG. B-13 RUN 49 – 416-MSEC-PERIOD TEST.

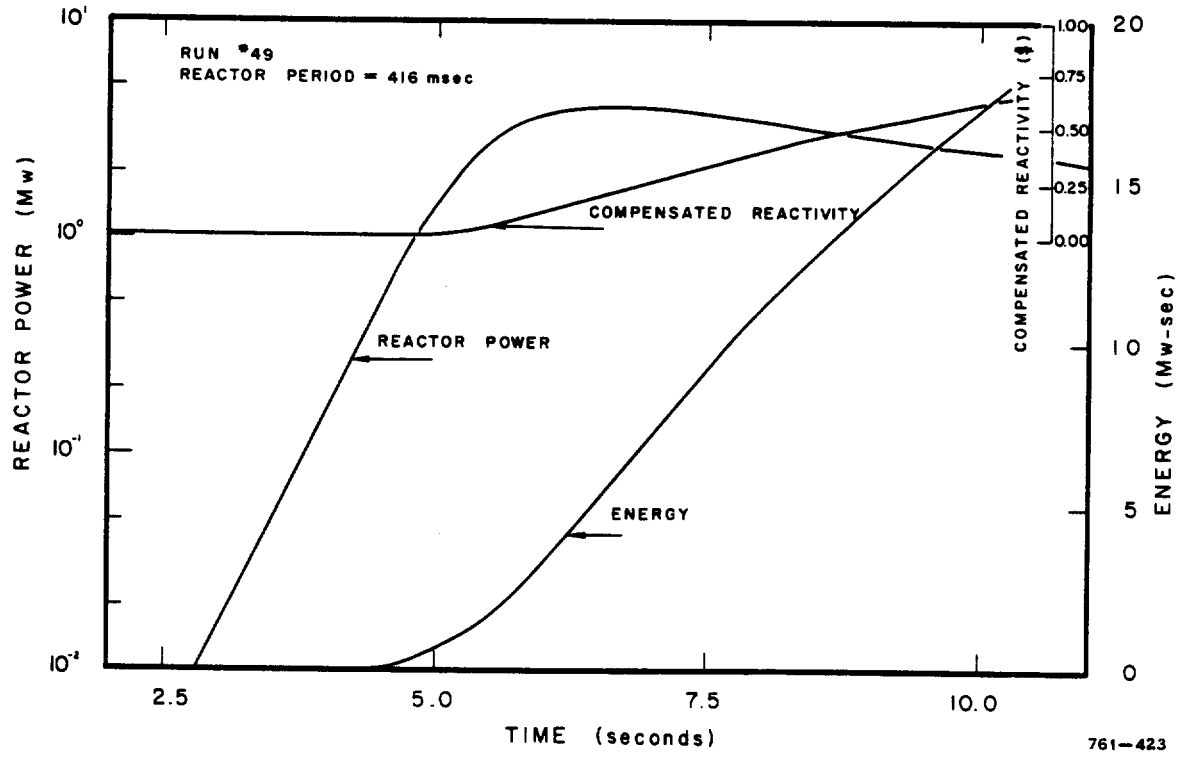

FIG. B-14 RUN 49 – 416-MSEC-PERIOD TEST.

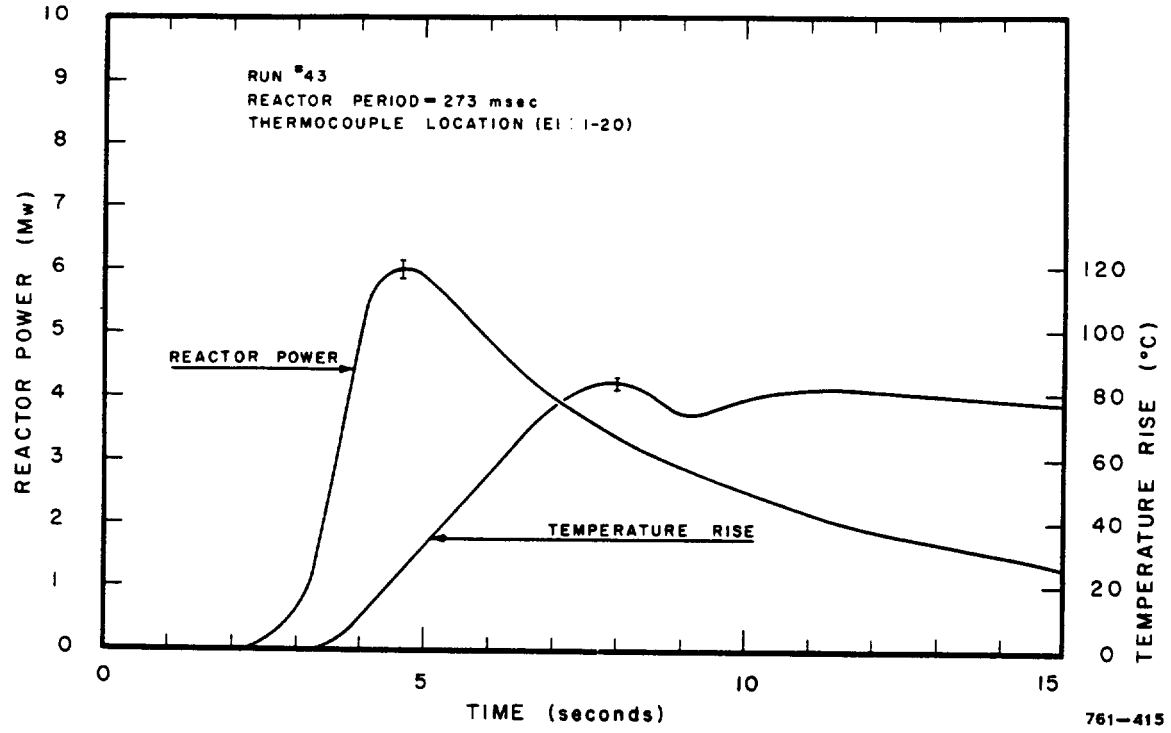

FIG. B-15 RUN 43 - 273-MSEC-PERIOD TEST.

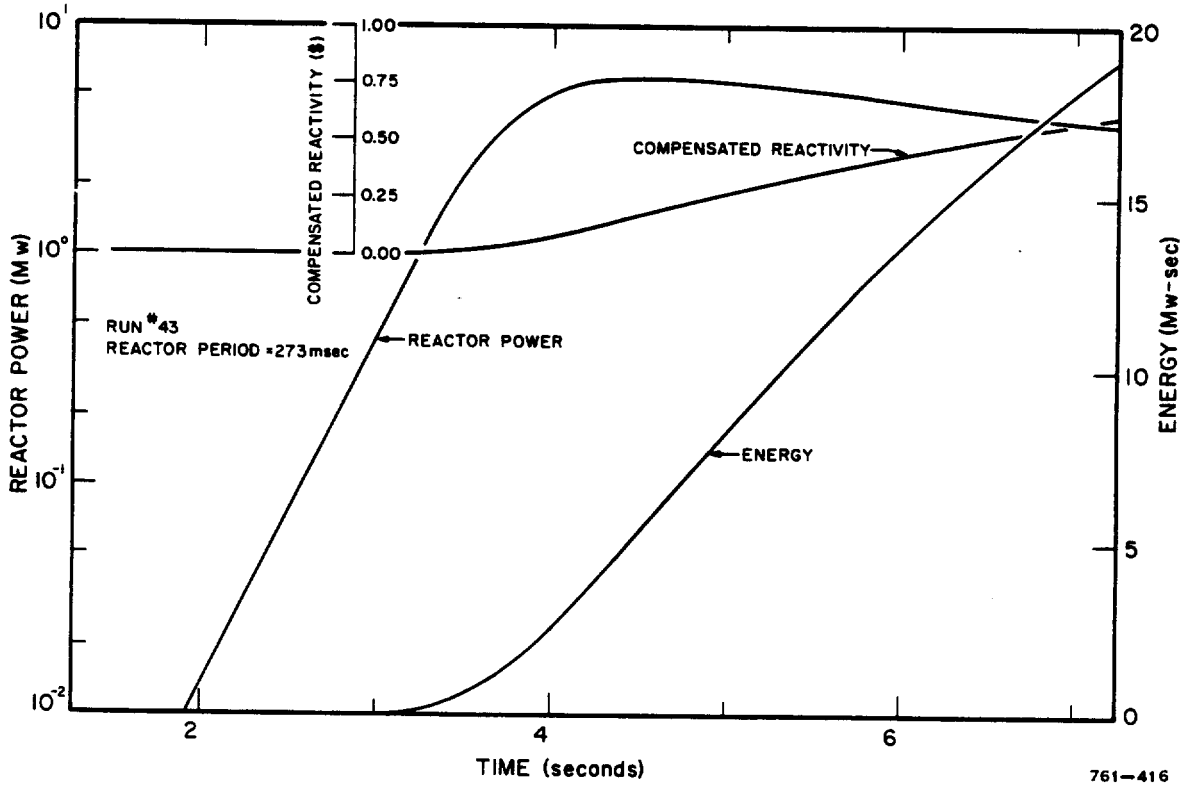

FIG. B-16 RUN 43 - 273-MSEC-PERIOD TEST.

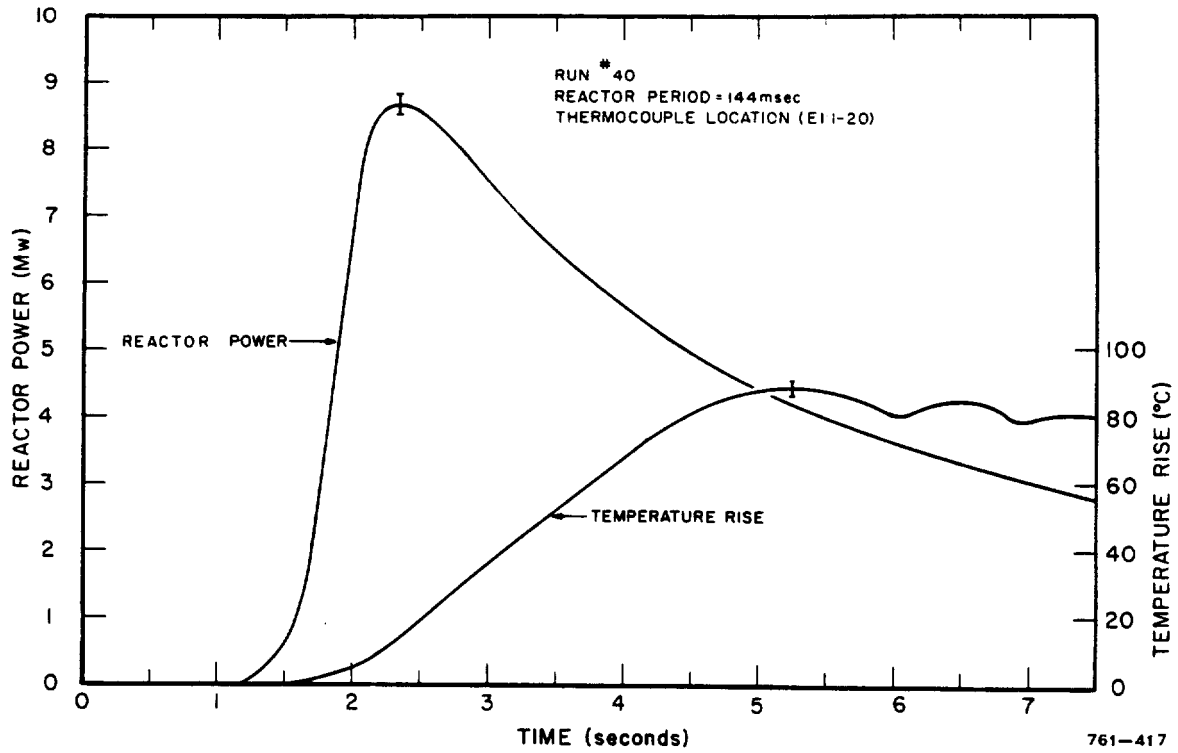

FIG. B-17 RUN 40 – 144-MSEC-PERIOD TEST.

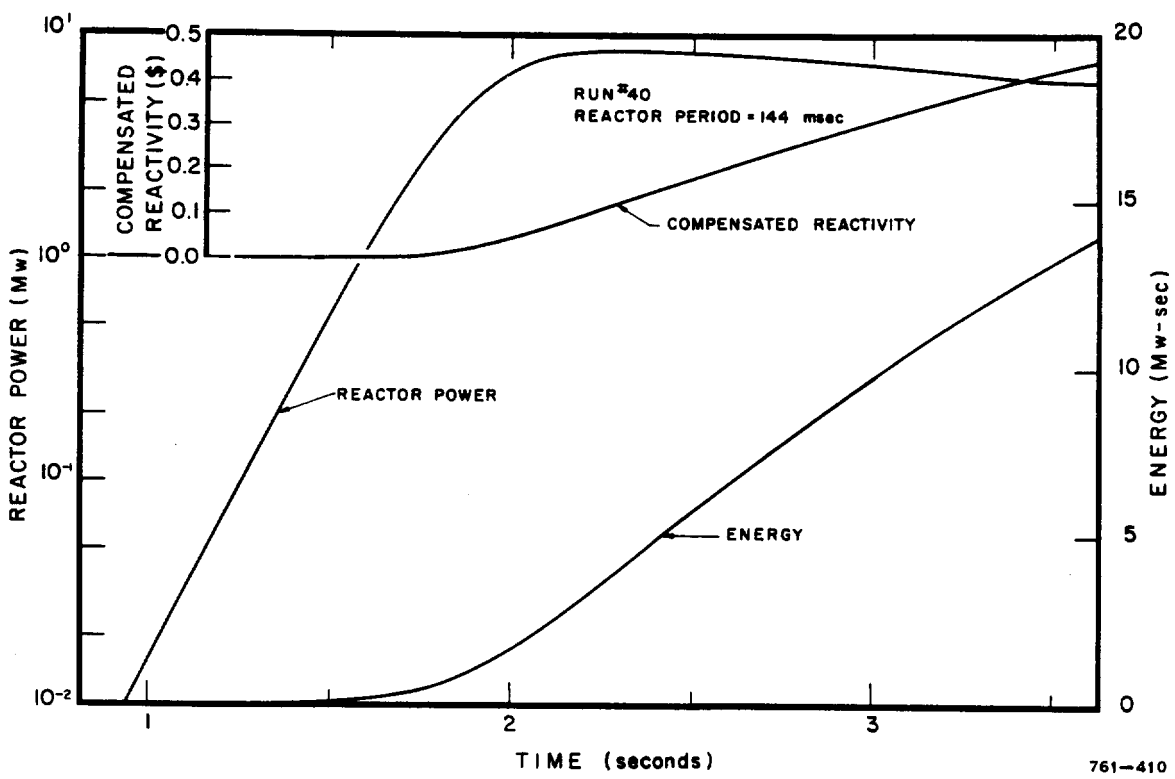

FIG. B-18 RUN 40 – 144-MSEC-PERIOD TEST.

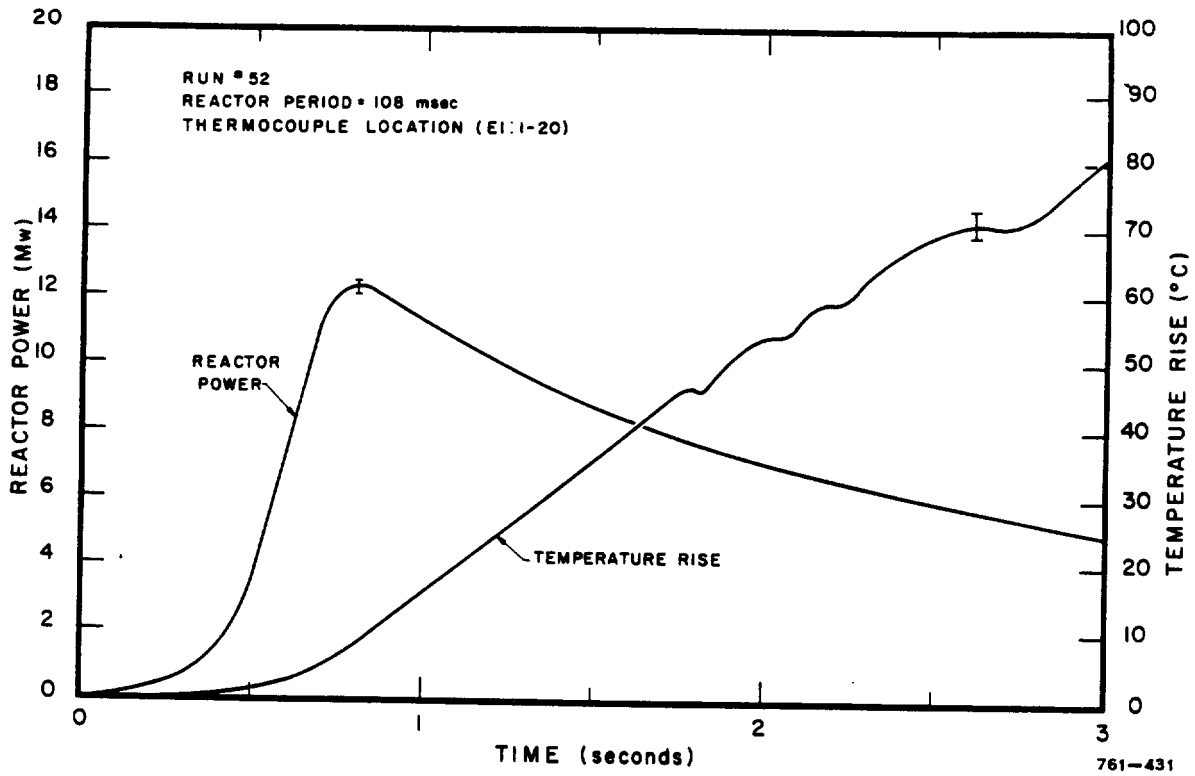

FIG. B-19 RUN 52 - 108-MSEC-PERIOD TEST.

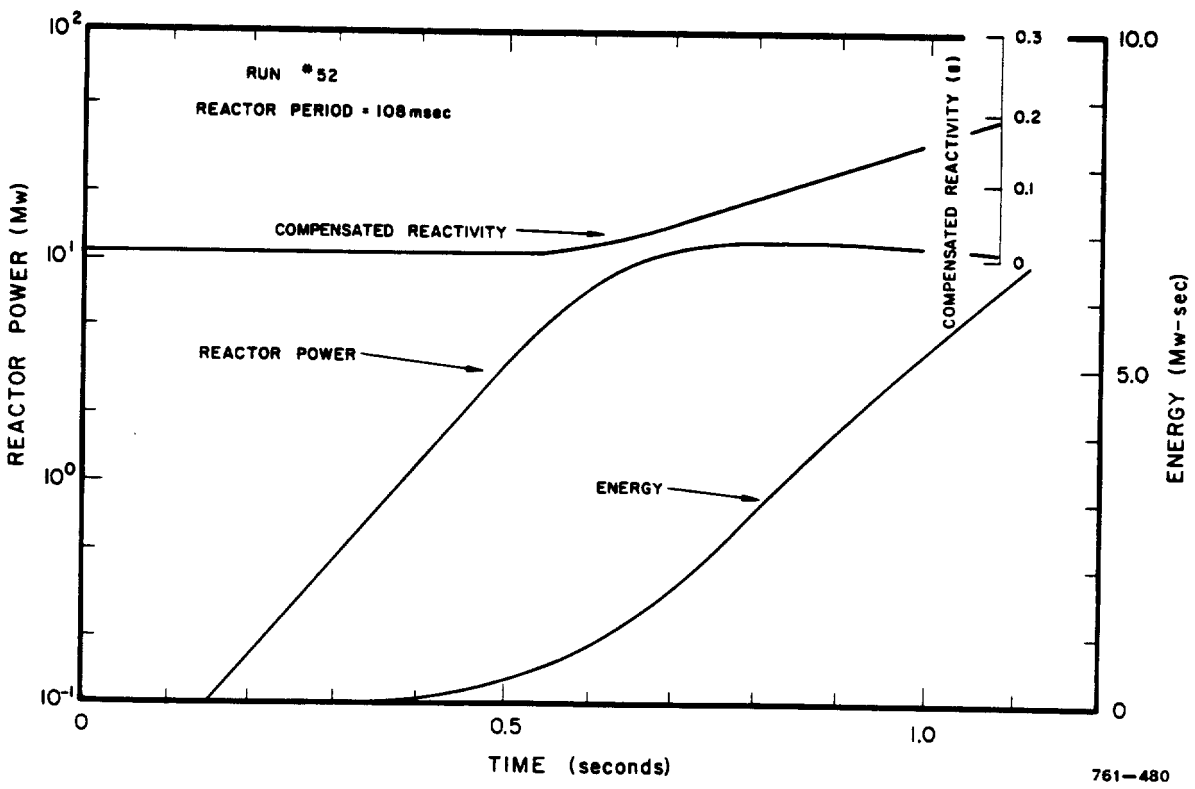

FIG. B-20 RUN 52 - 108-MSEC-PERIOD TEST.

1133315

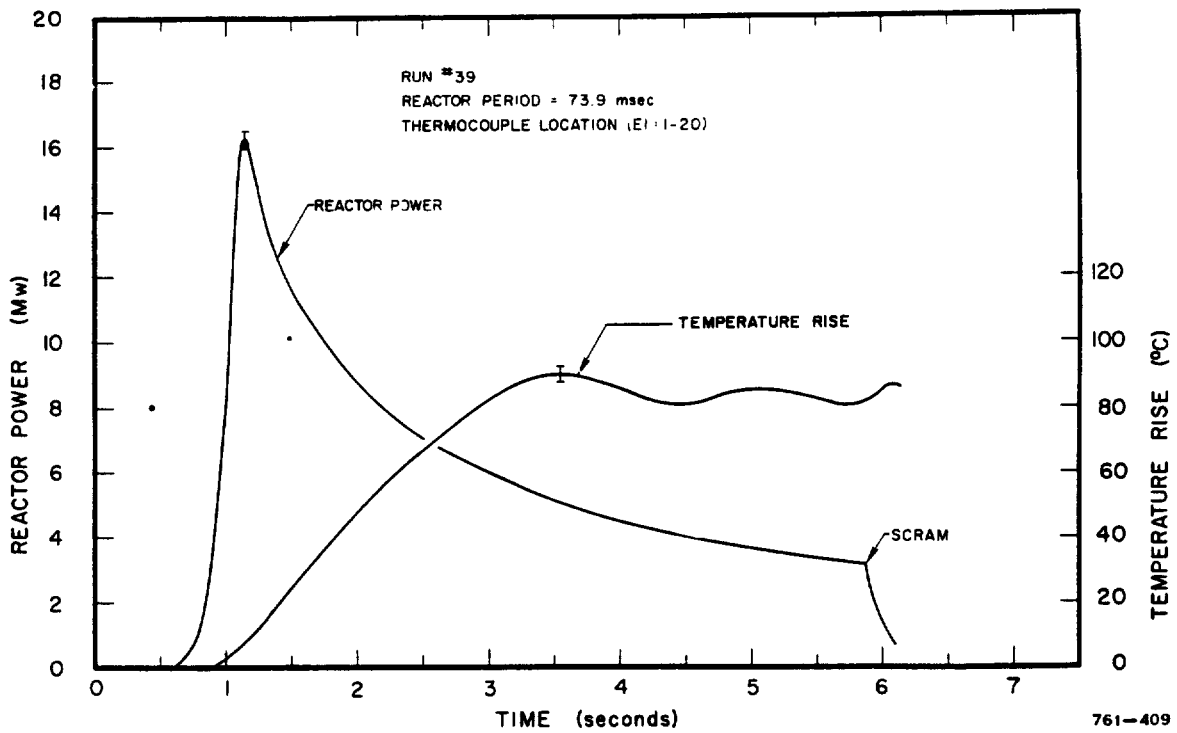

FIG. B-21 RUN 39 – 73.9-MSEC-PERIOD TEST.

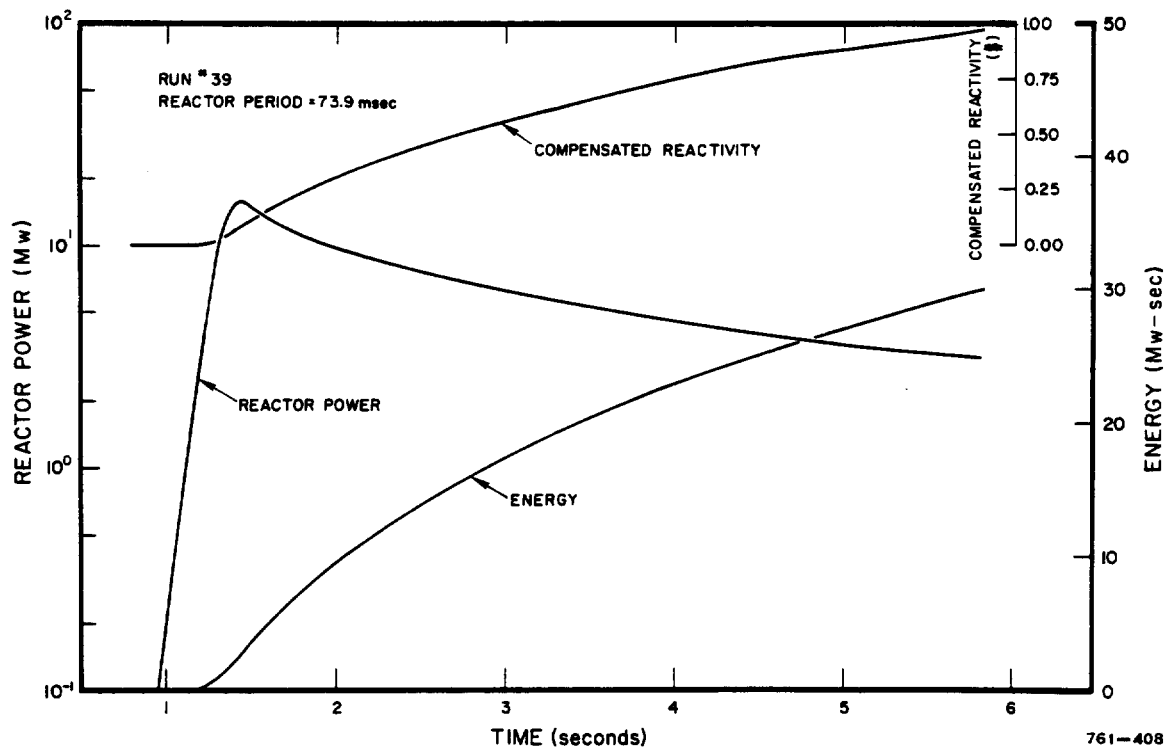

FIG. B-22 RUN 39 – 73.9-MSEC-PERIOD TEST.

1133316

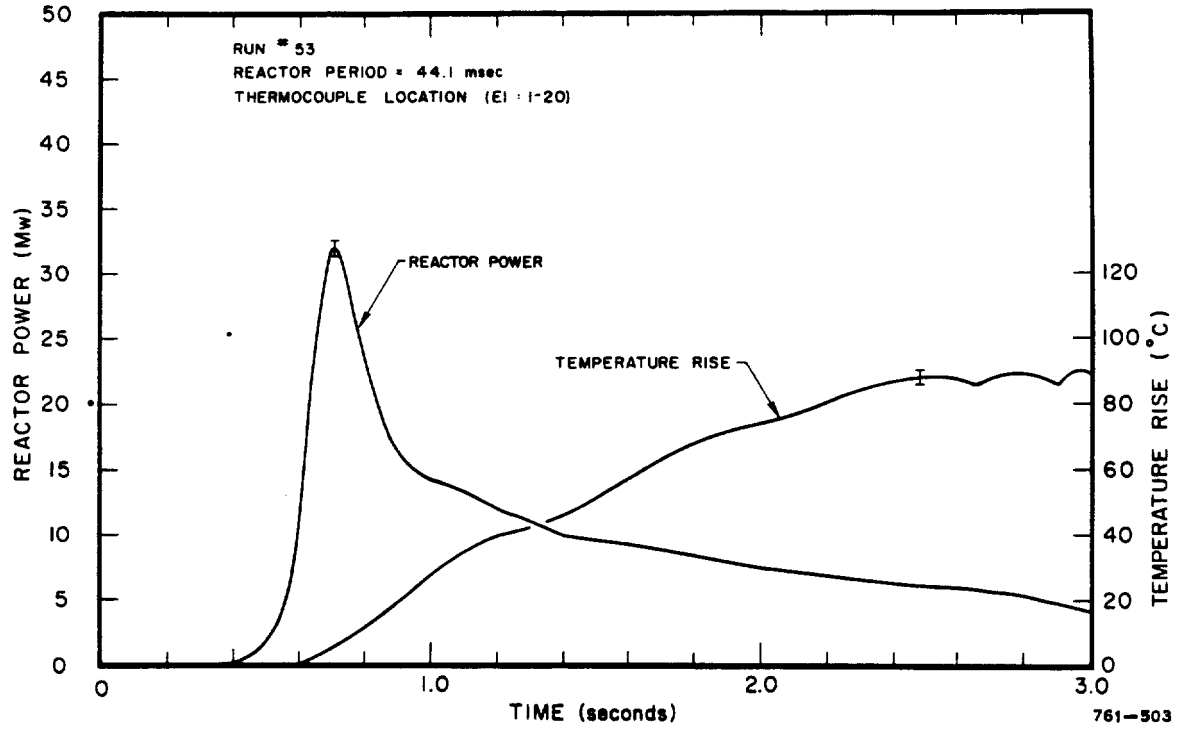

FIG. B-23 RUN 53 – 44.1-MSEC-PERIOD TEST.

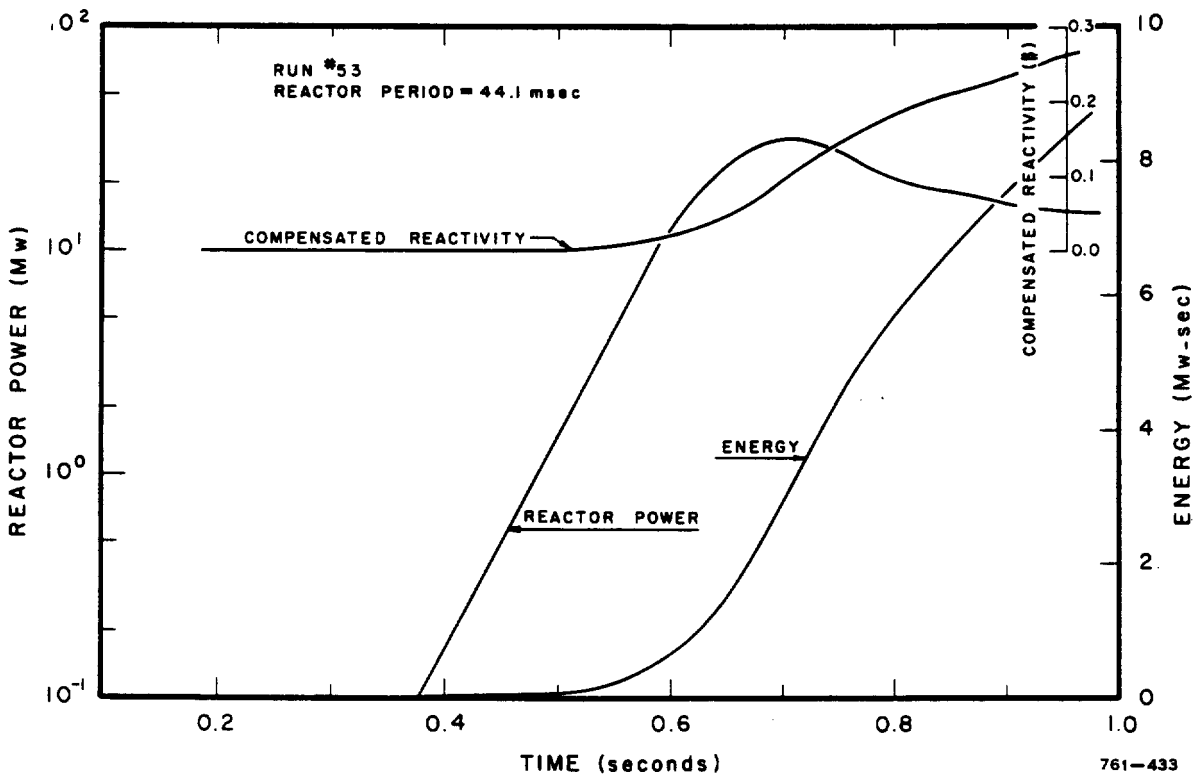

FIG. B-24 RUN 53 – 44.1-MSEC-PERIOD TEST.

1133317

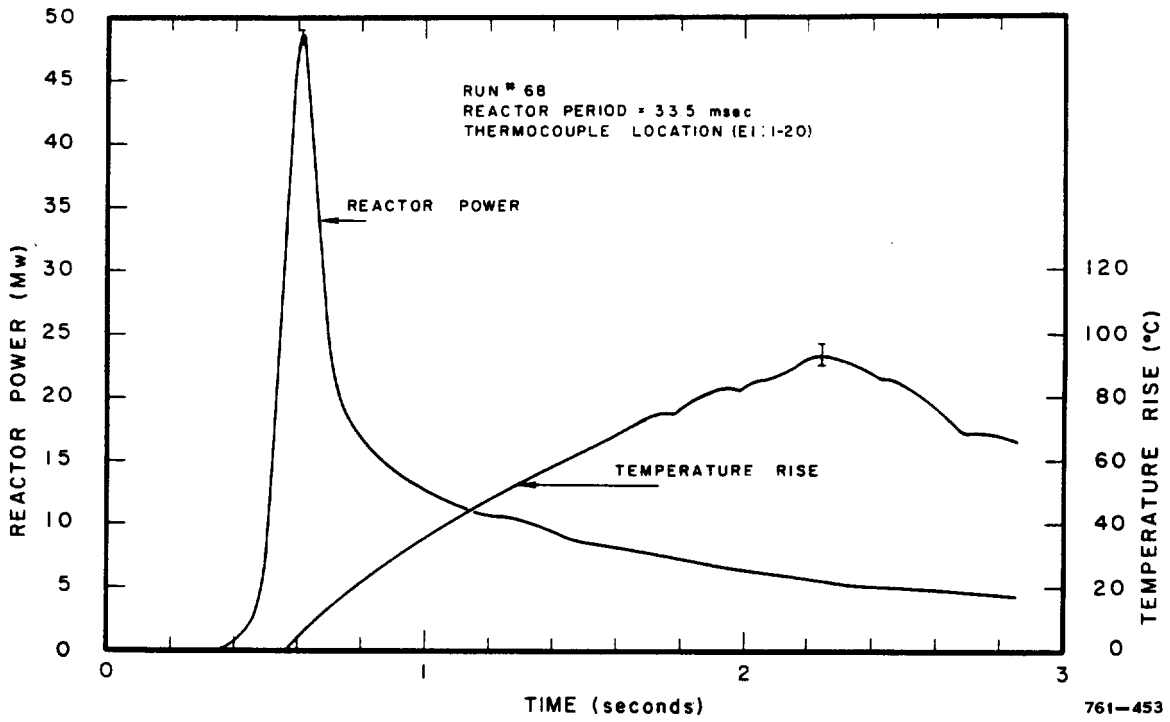

FIG. B-25 RUN 68 – 33.5-MSEC-PERIOD TEST.

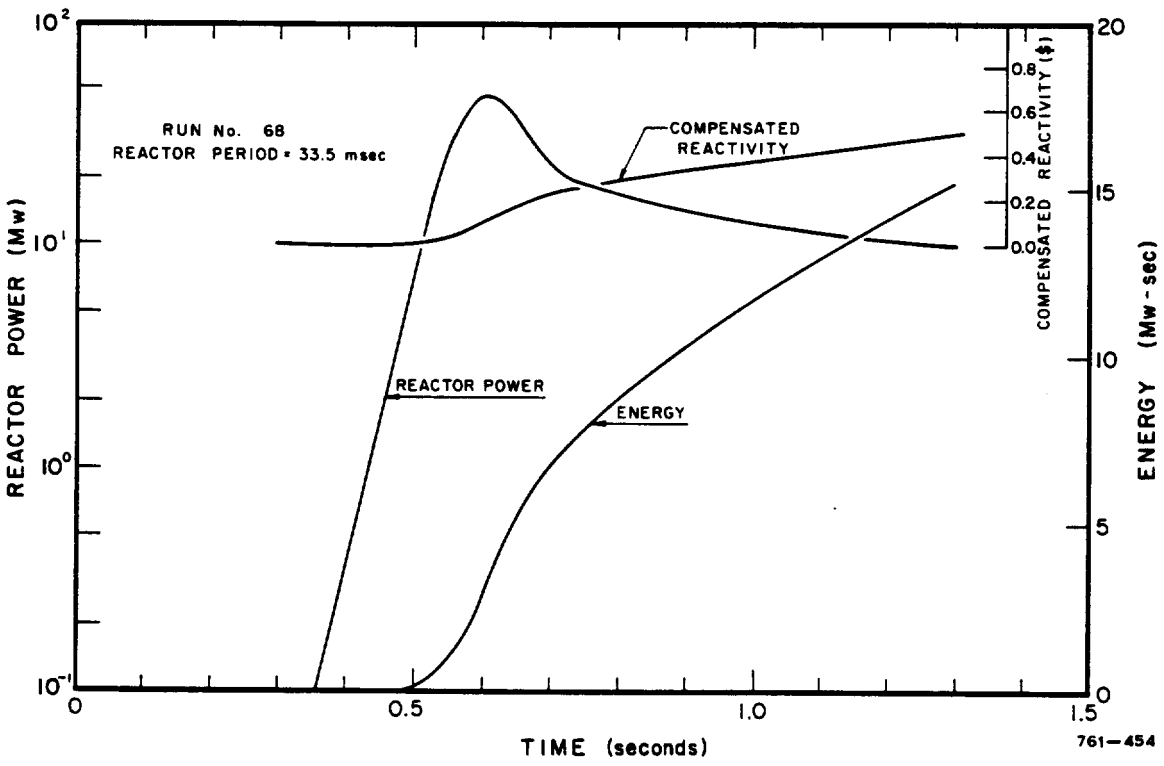

FIG. B-26 RUN 68 – 33.5-MSEC-PERIOD TEST.

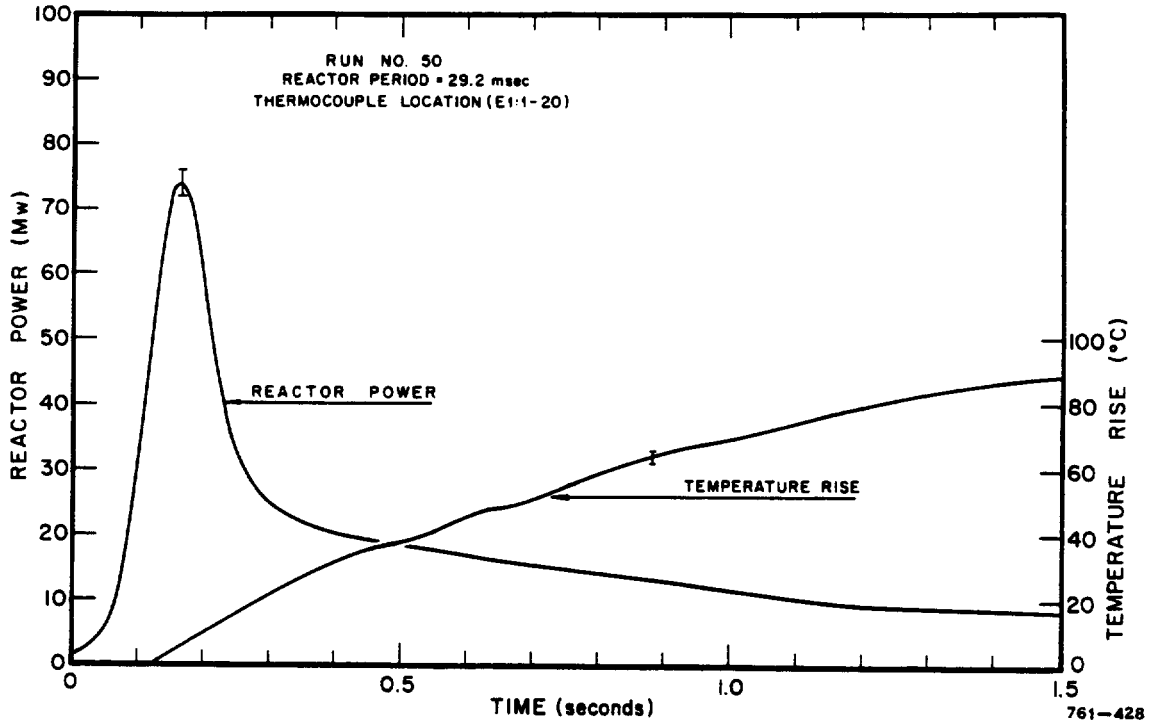

FIG. B-27 RUN 50 – 29.2-MSEC-PERIOD TEST.

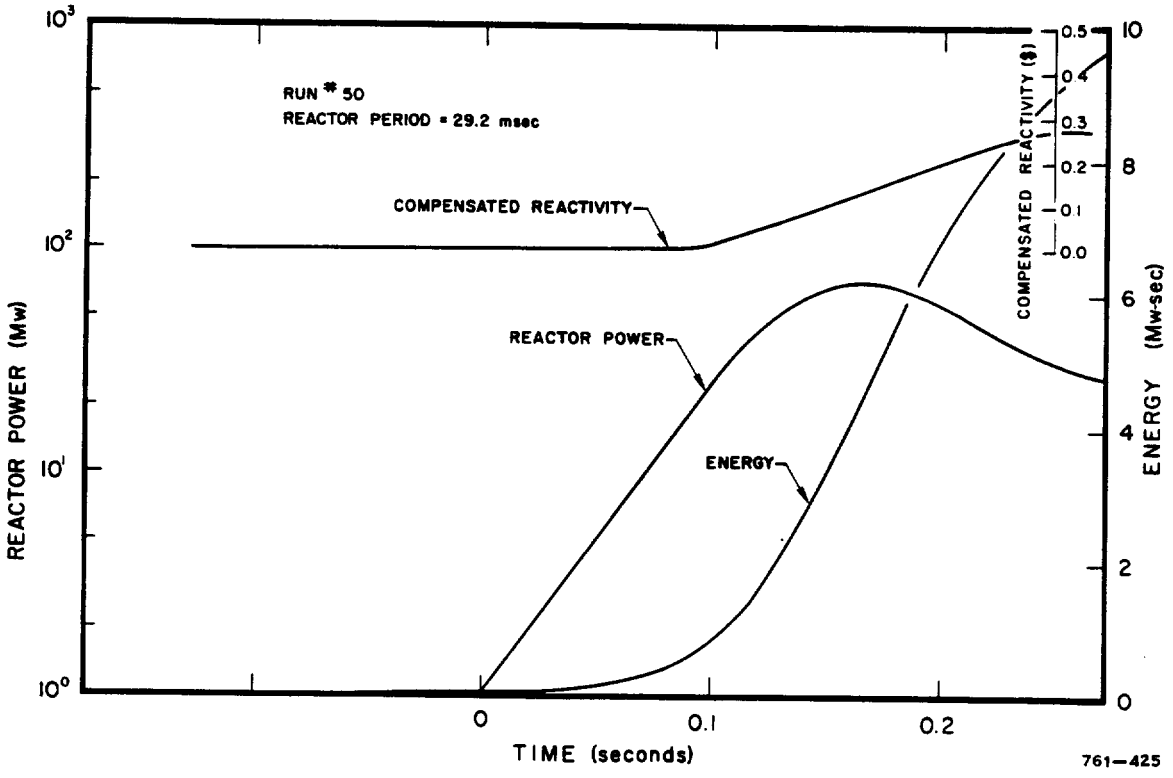

FIG. B-28 RUN 50 – 29.2-MSEC-PERIOD TEST.

1133319

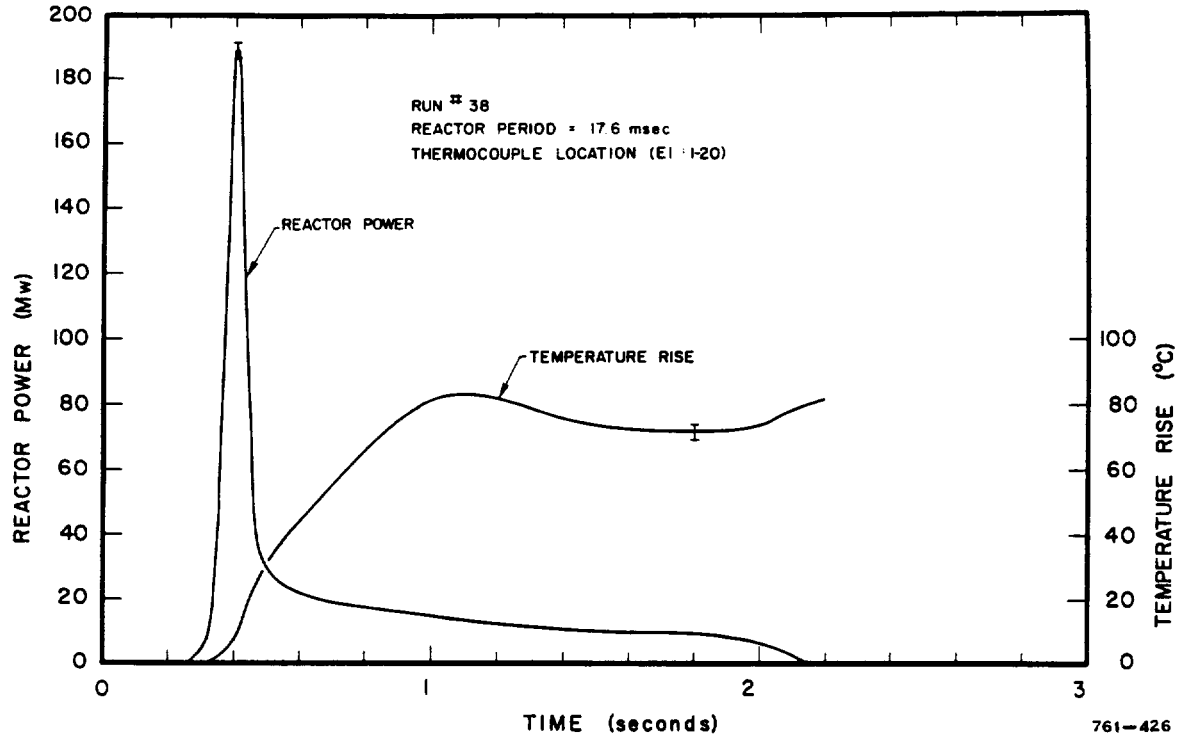

FIG. B-29 RUN 38 – 17.6-MSEC-PERIOD TEST.

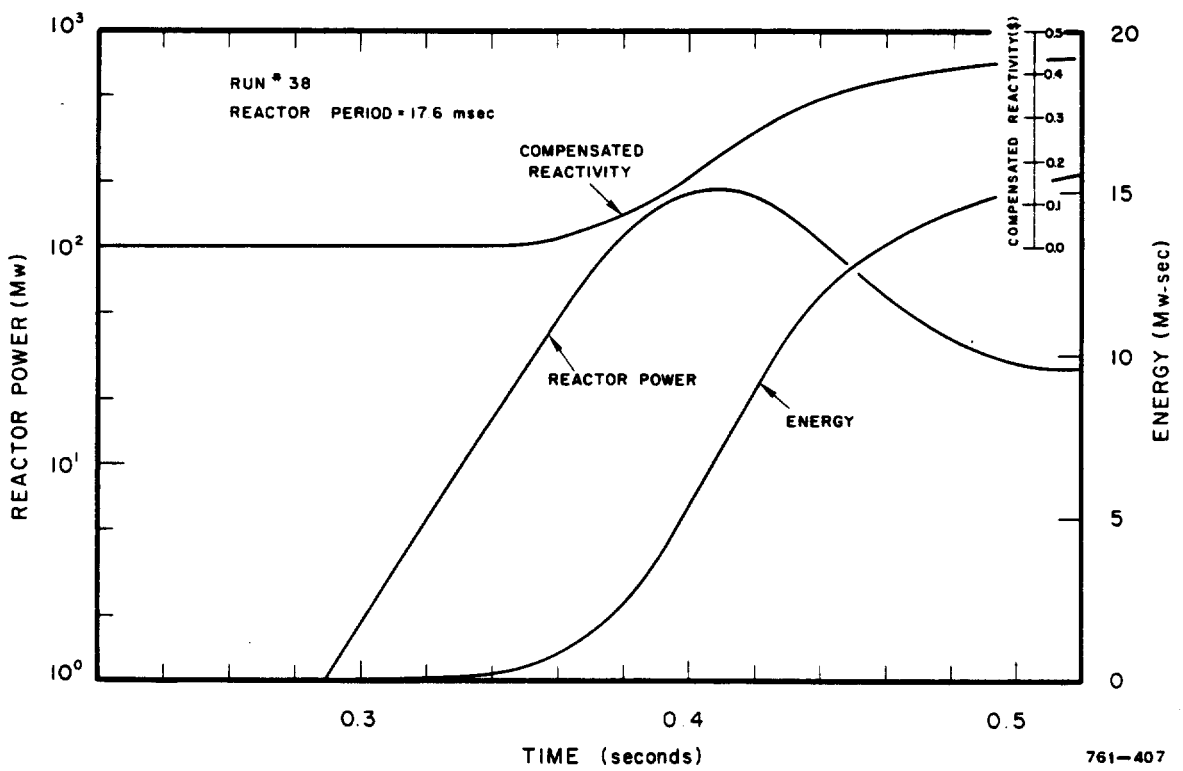

FIG. B-30 RUN 38 – 17.6-MSEC-PERIOD TEST.

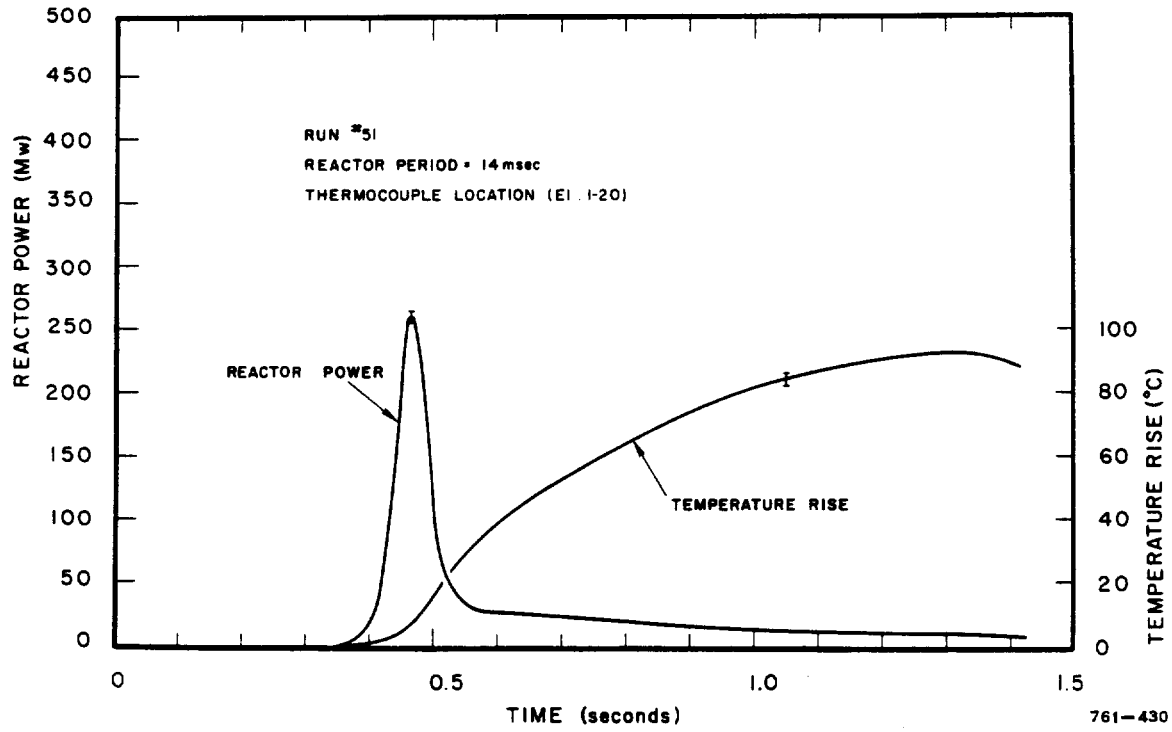

FIG. B-31 RUN 51 – 14.0-MSEC-PERIOD TEST.

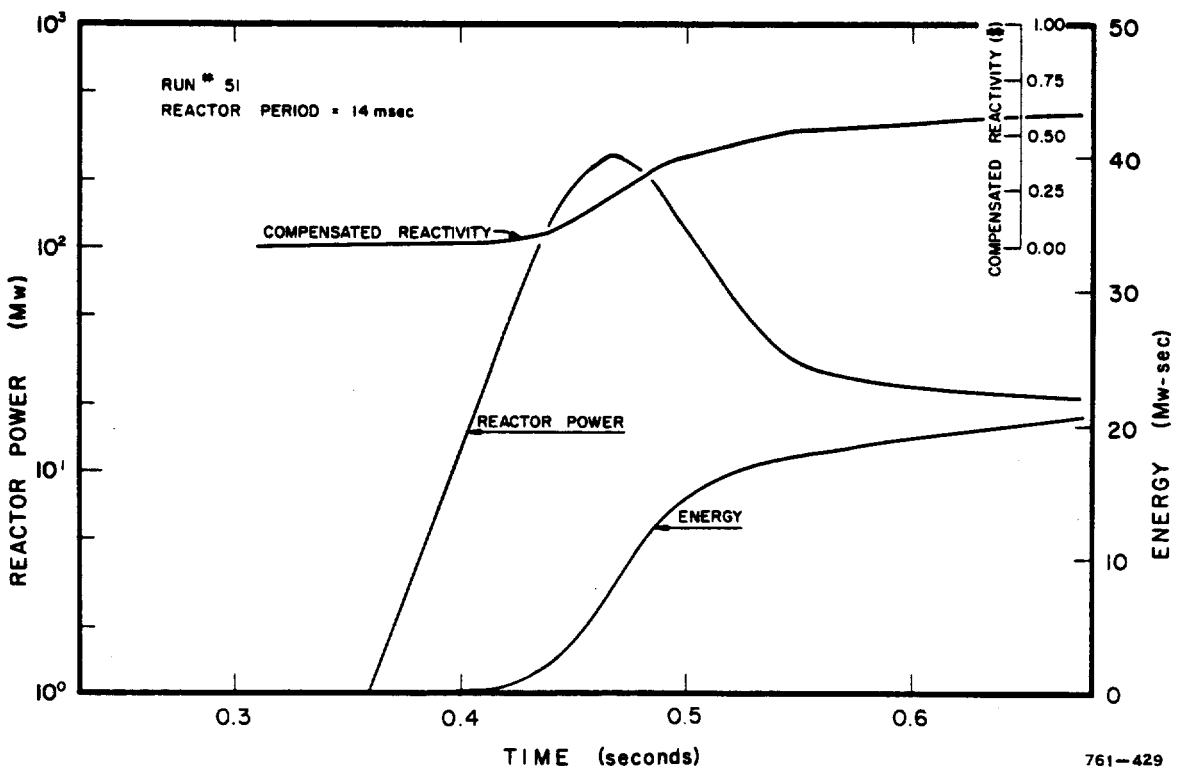

FIG. B-32 RUN 51 – 14.0-MSEC-PERIOD TEST.

1133321

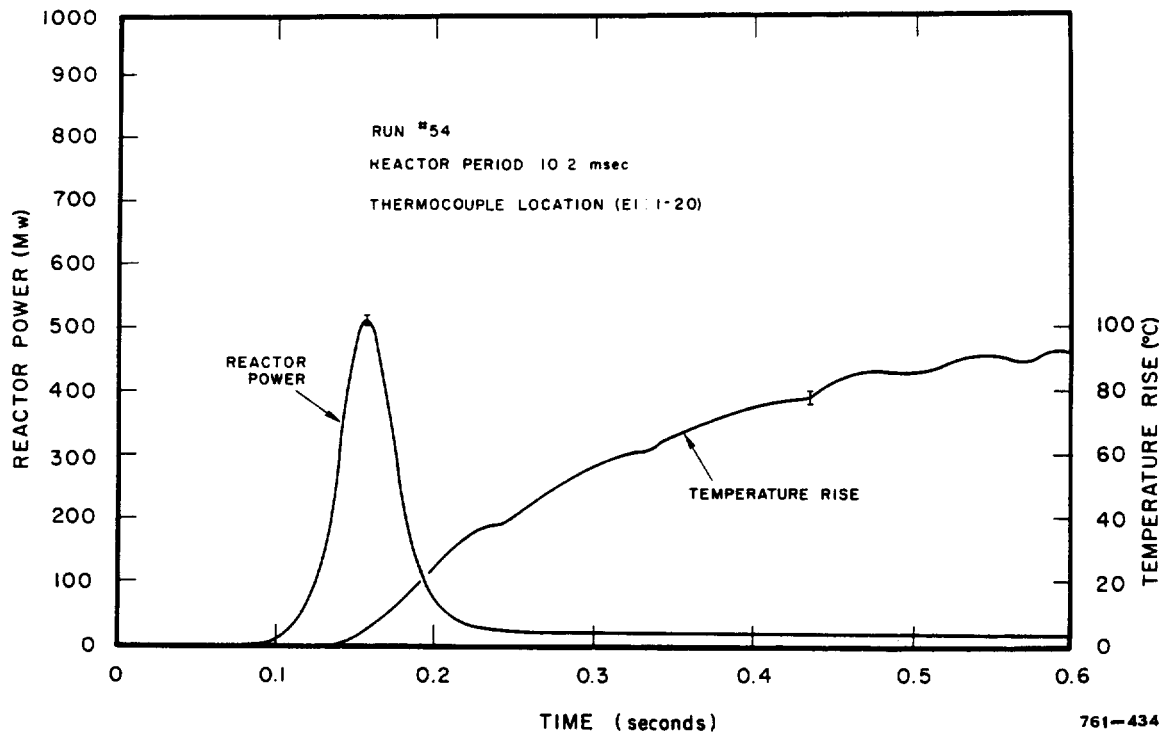

FIG. B-33 RUN 54 — 10.2-MSEC-PERIOD TEST.

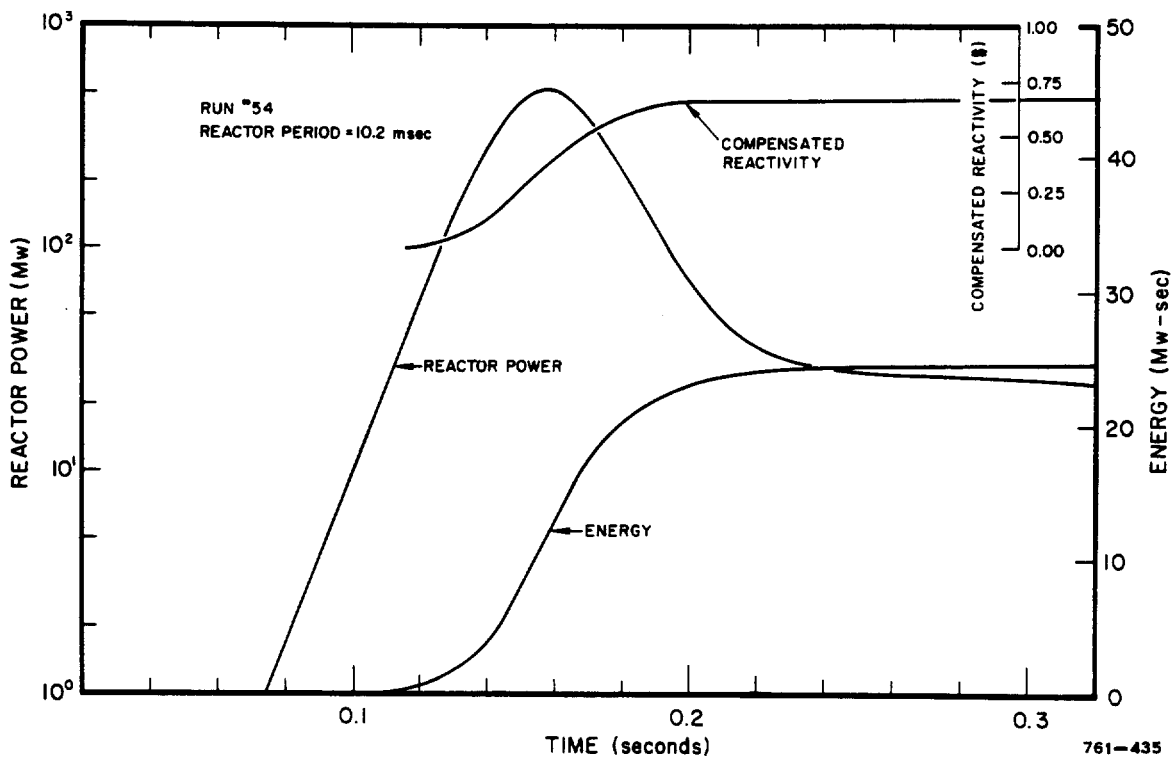

FIG. B-34 RUN 54 — 10.2-MSEC-PERIOD TEST.

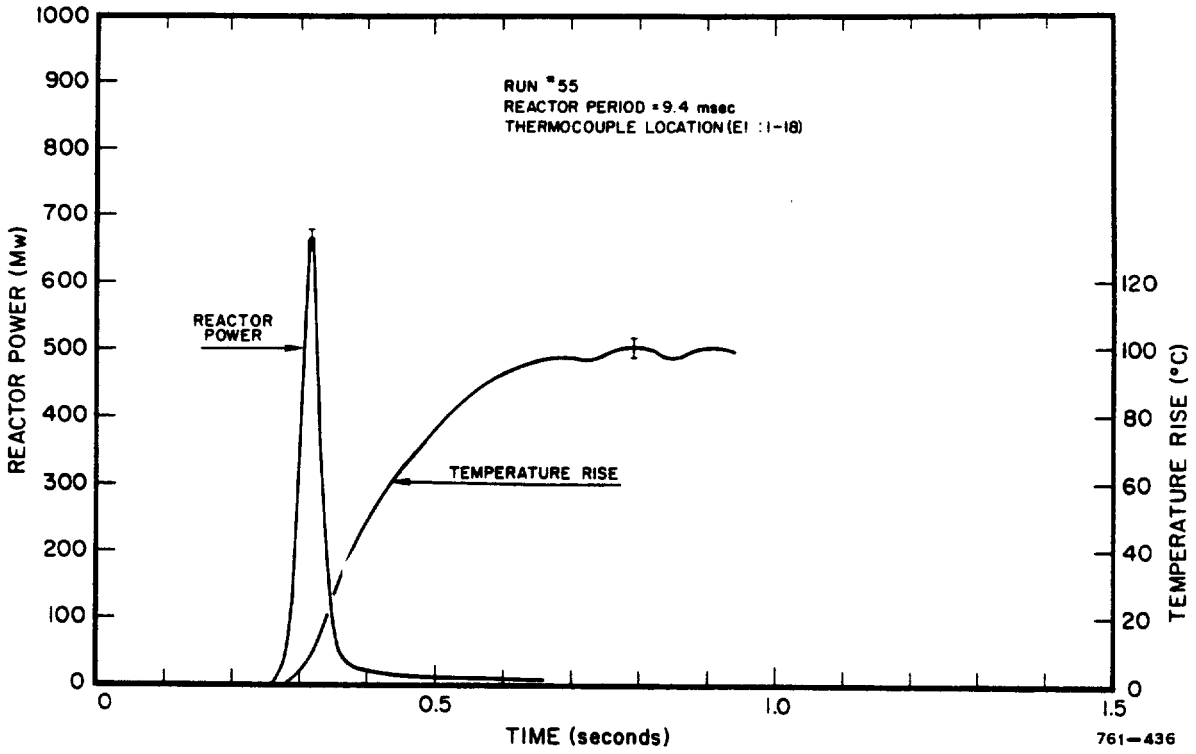

FIG. B-35 RUN 55 - 9.4-MSEC-PERIOD TEST.

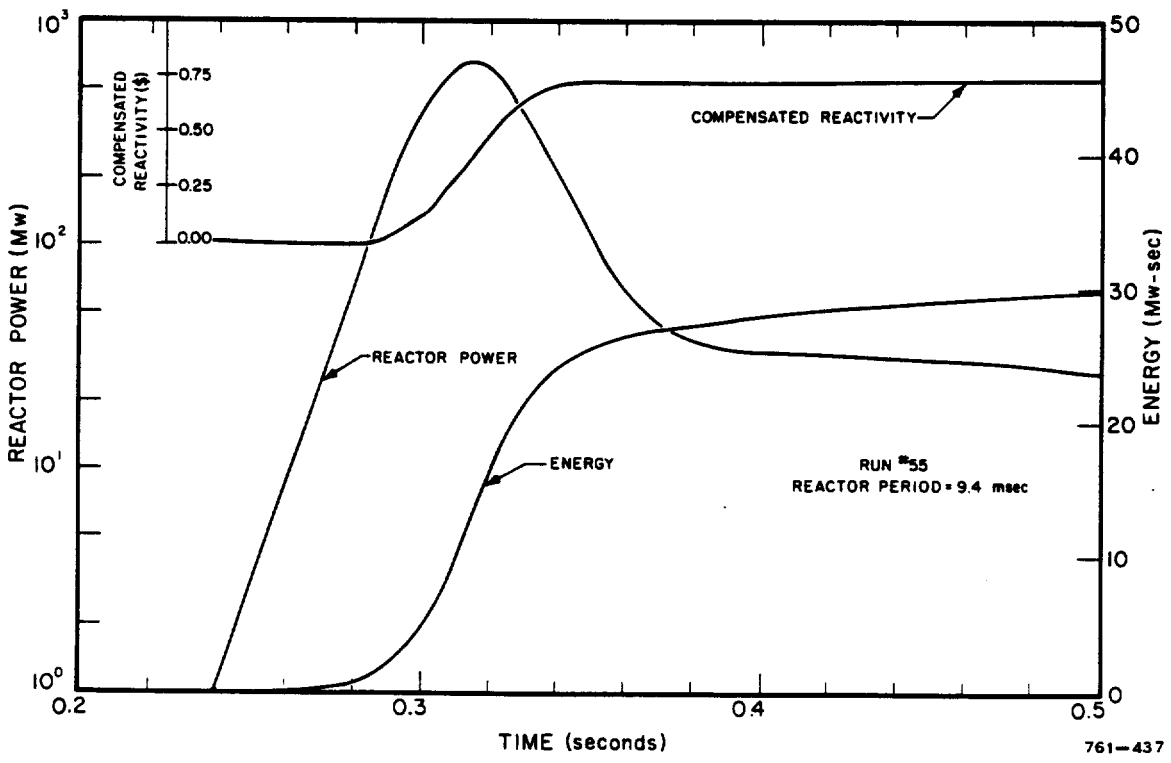

FIG. B-36 RUN 55 - 9.4-MSEC-PERIOD TEST.

1133323

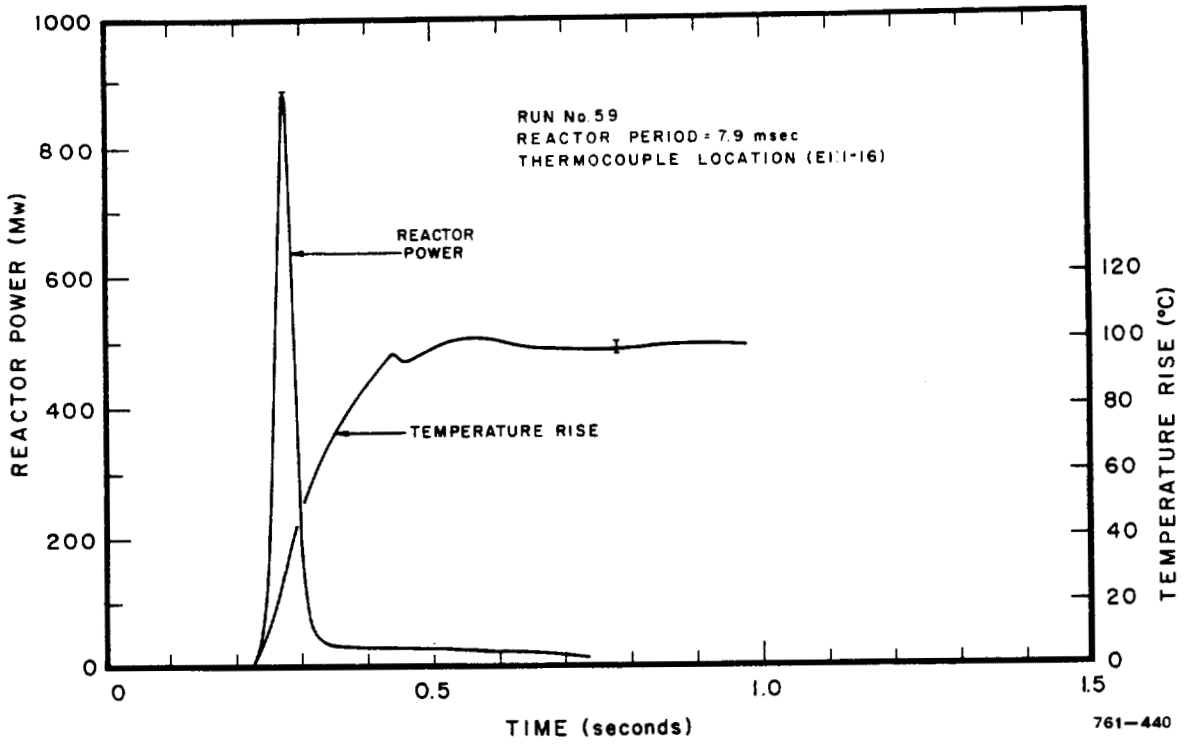

FIG. B-37 RUN 59 – 7.9-MSEC-PERIOD TEST.

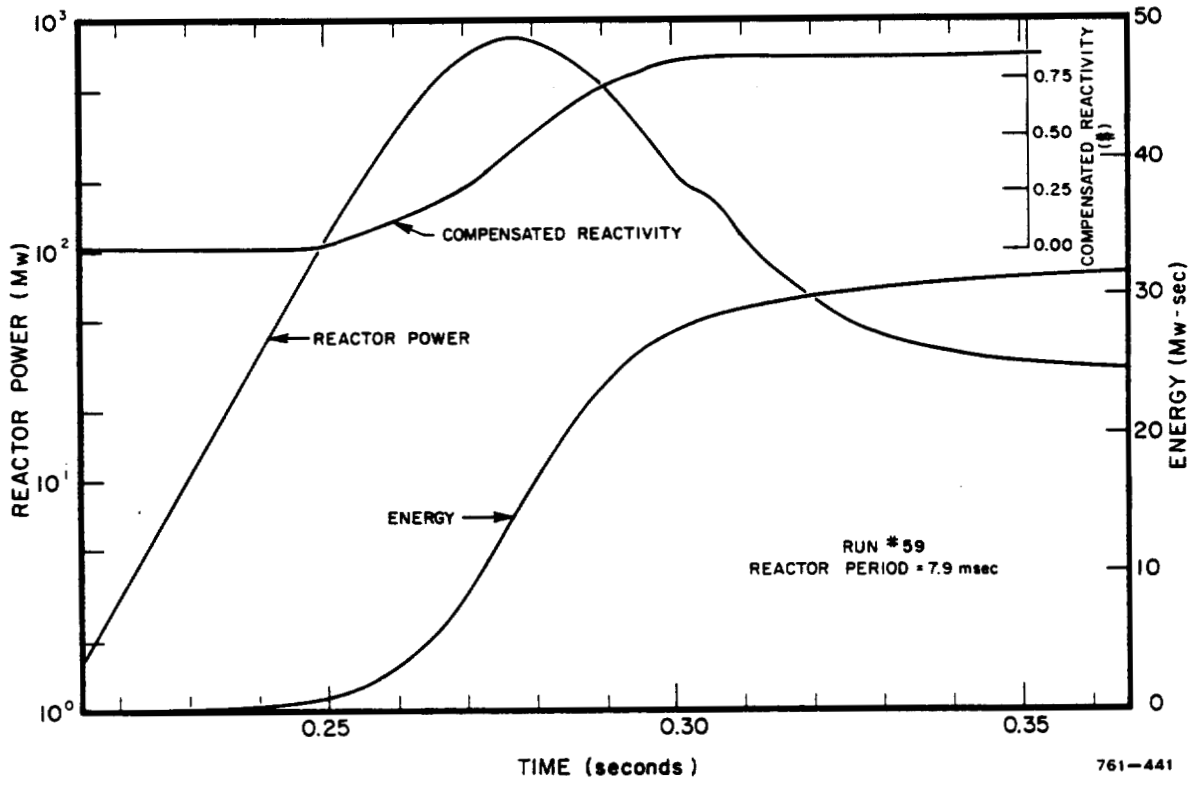

FIG. B-38 RUN 59 – 7.9-MSEC-PERIOD TEST.

1133324

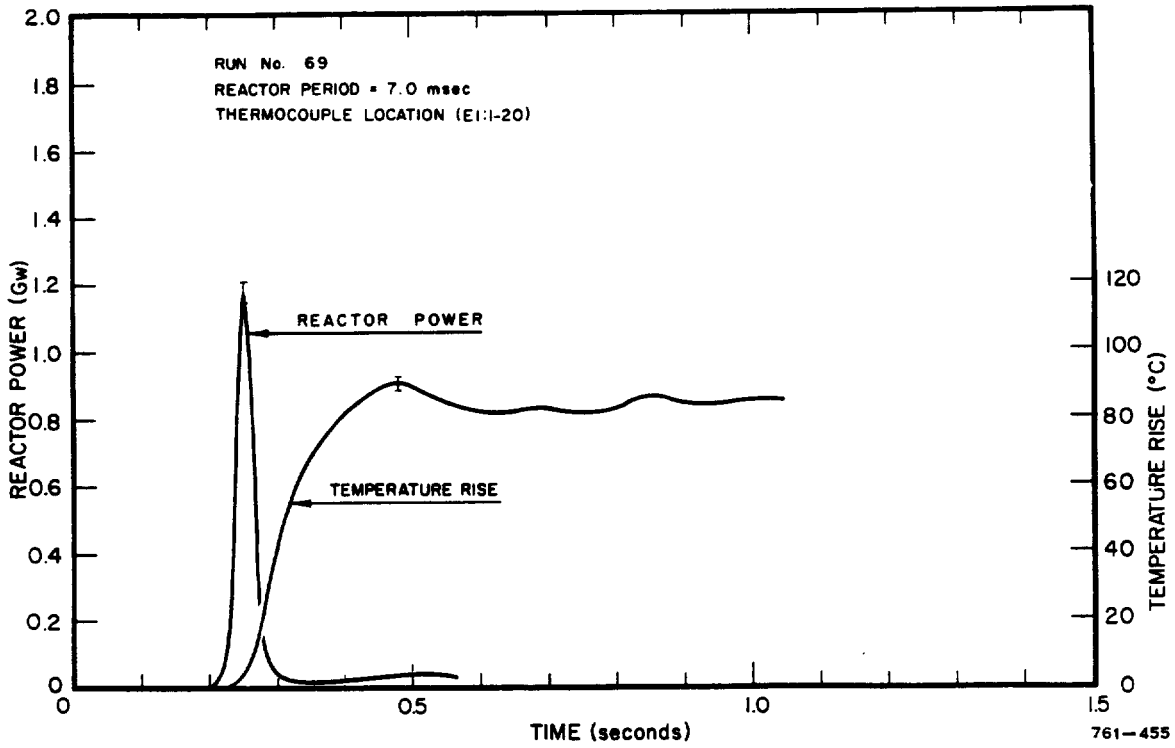

FIG. B-39 RUN 69 – 7.0-MSEC-PERIOD TEST.

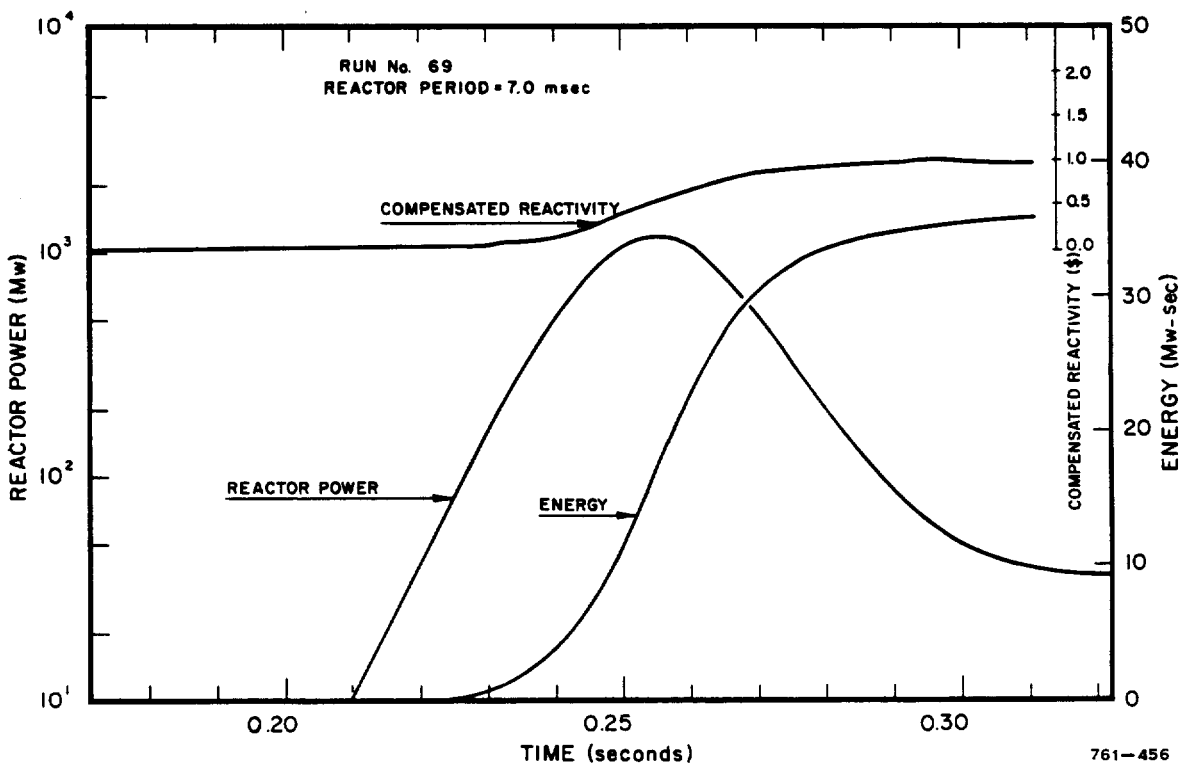

FIG. B-40 RUN 69 – 7.0-MSEC-PERIOD TEST.

1133325

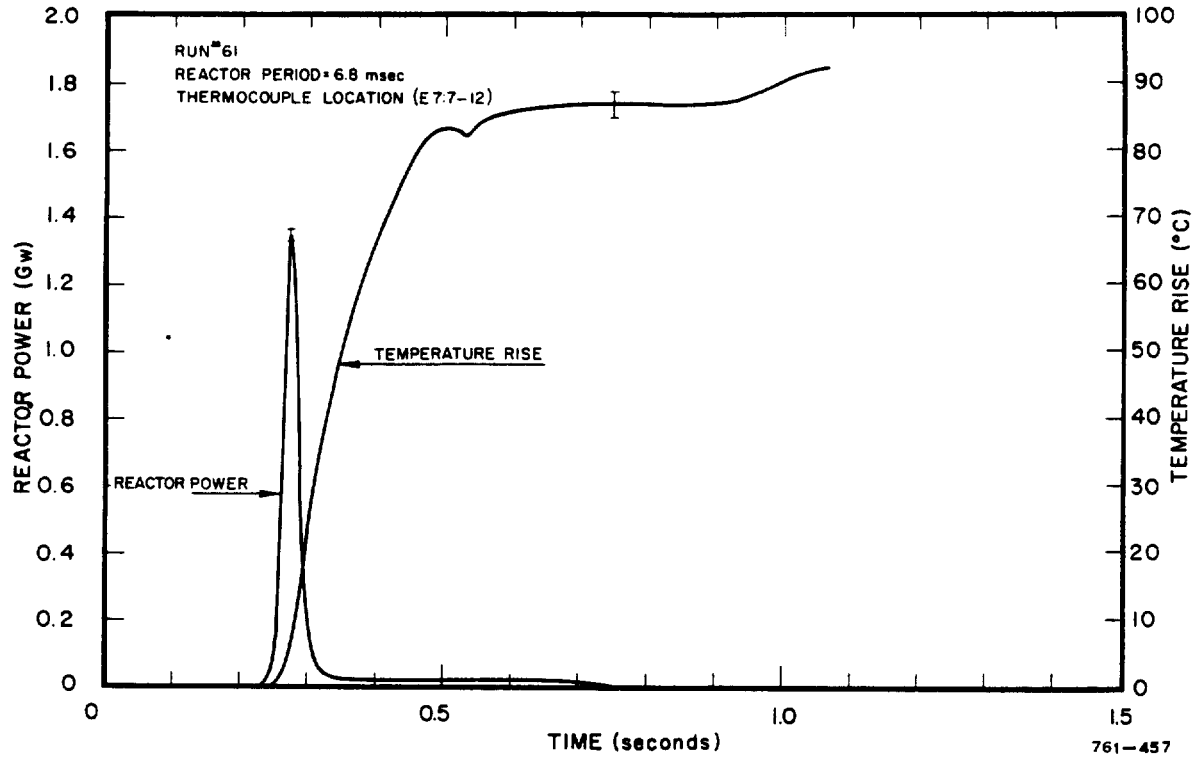

FIG. B-41 RUN 61 - 6.8-MSEC-PERIOD TEST.

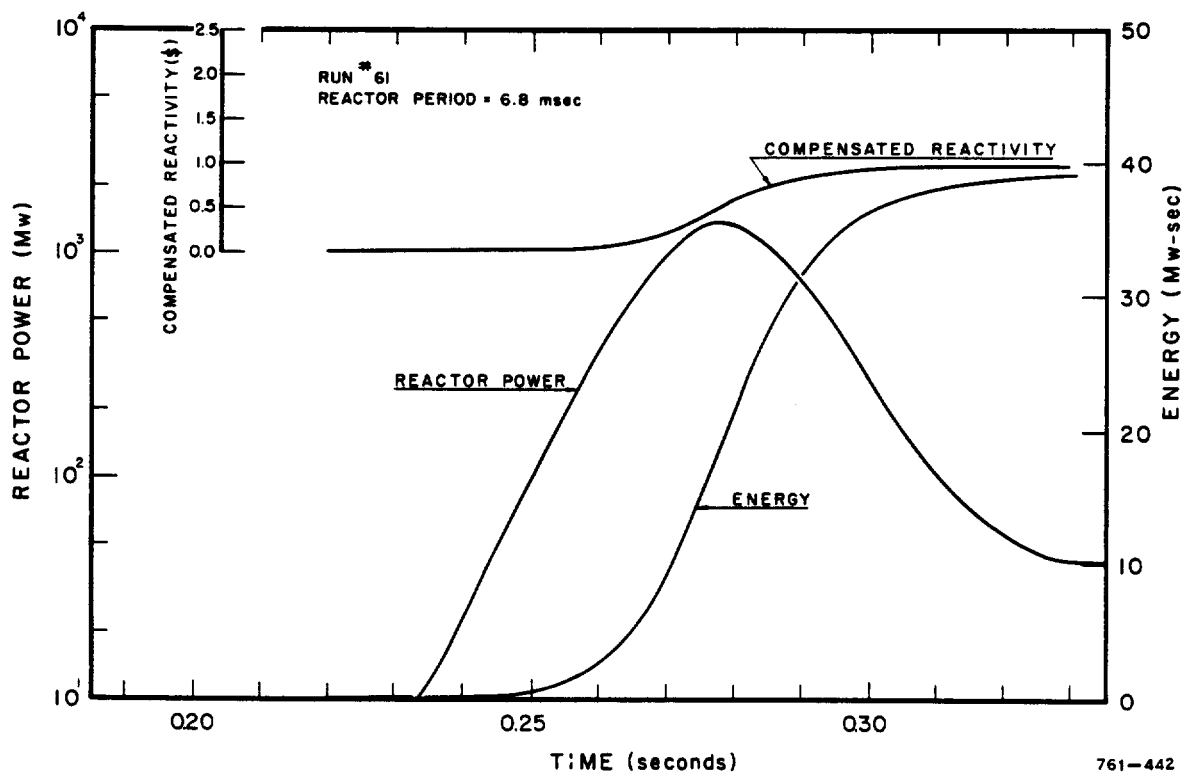

FIG. B-42 RUN 61 - 6.8-MSEC-PERIOD TEST.

1133326

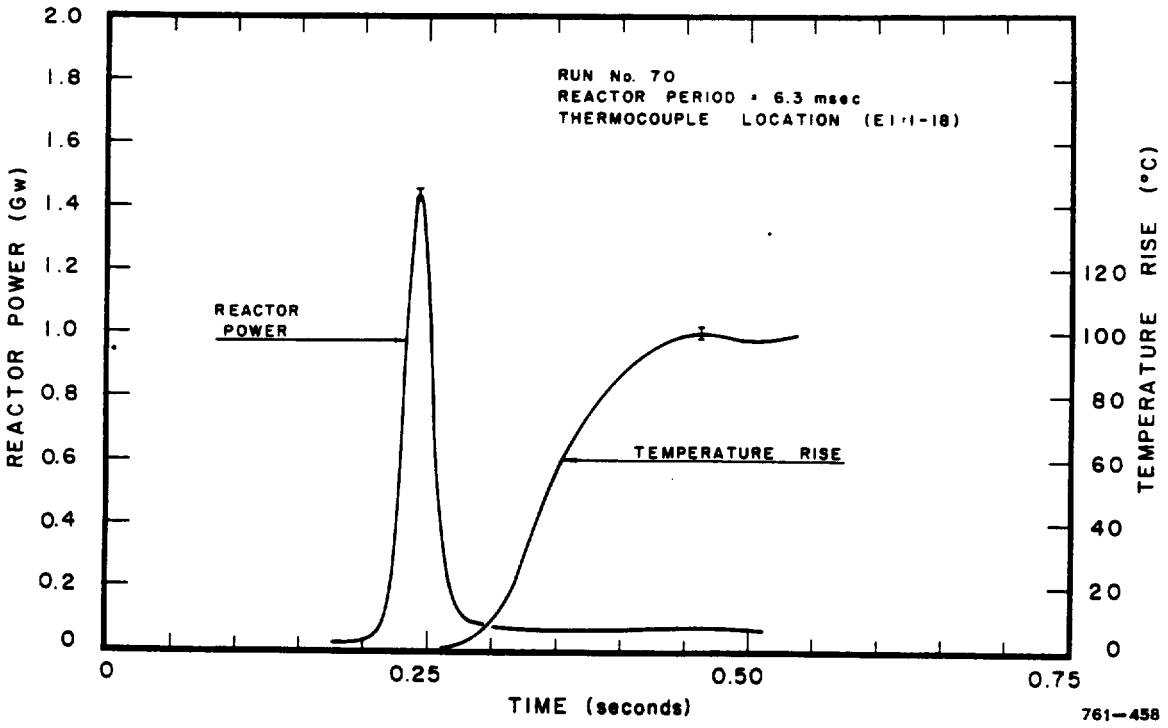

FIG. B-43 RUN 70 – 6.3-MSEC-PERIOD TEST.

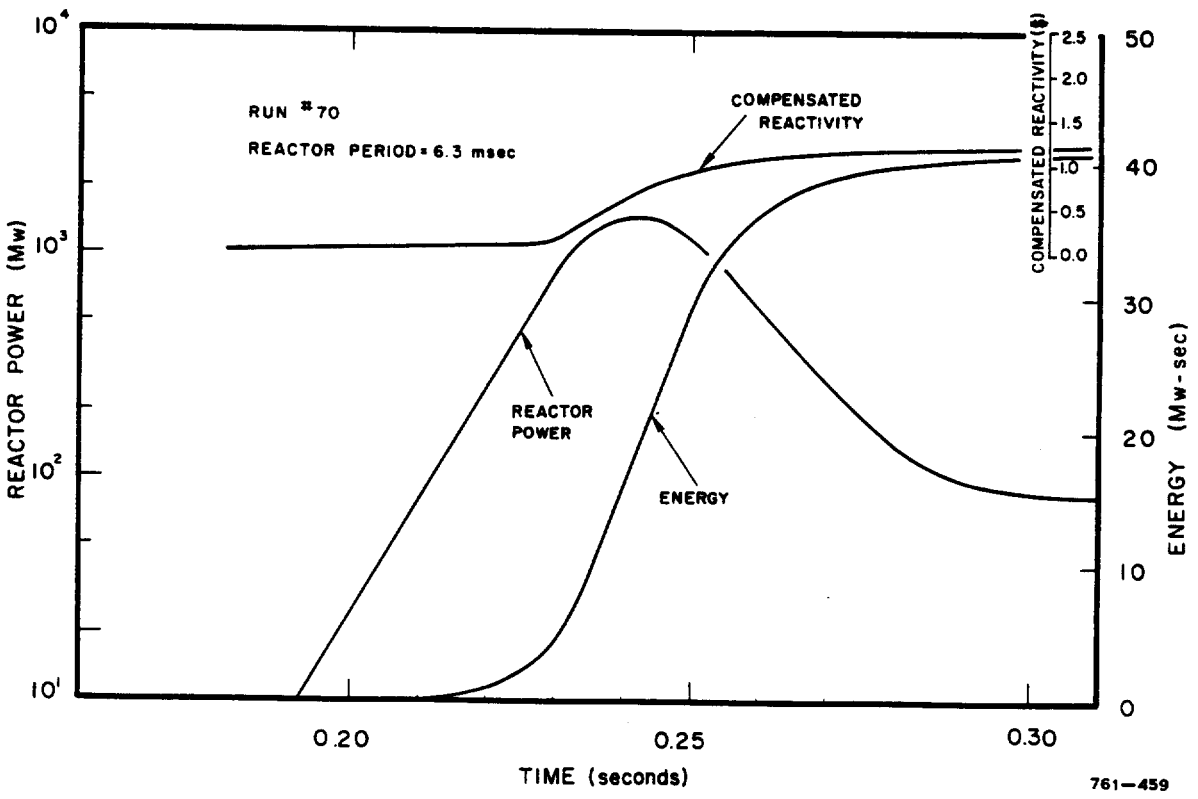

FIG. B-44 RUN 70 – 6.3-MSEC-PERIOD TEST.

1133327

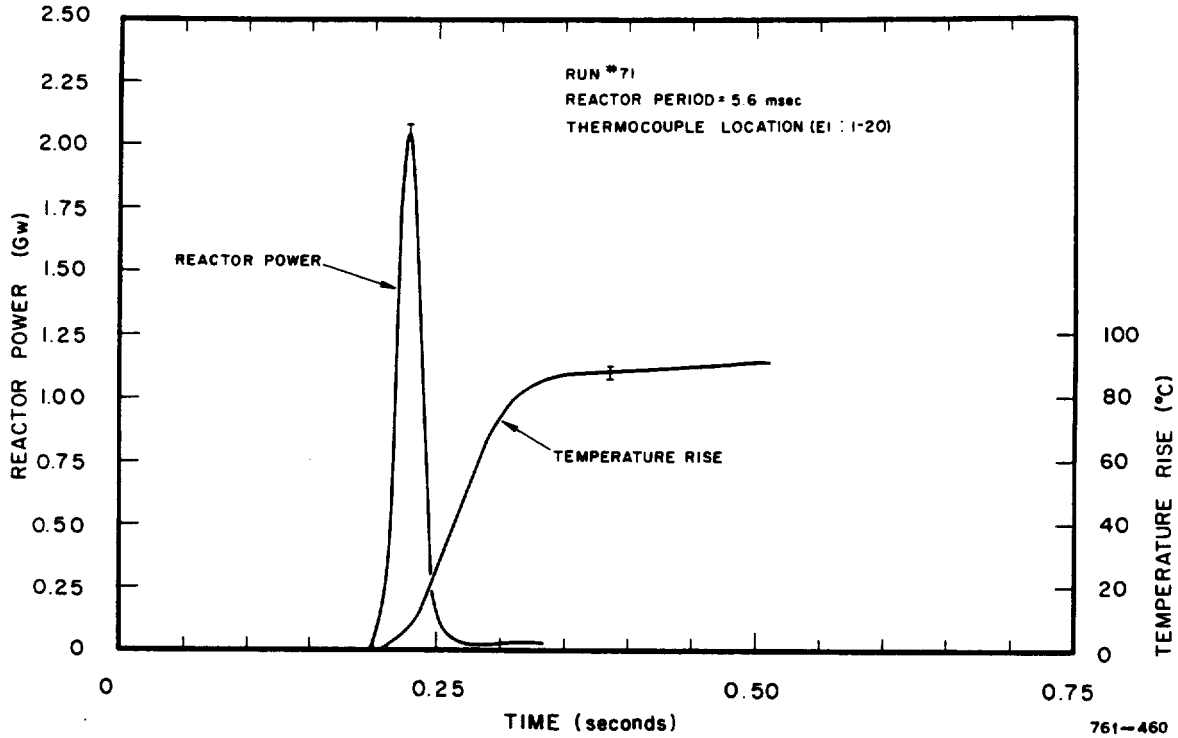

FIG. B-45 RUN 71 – 5.6-MSEC-PERIOD TEST.

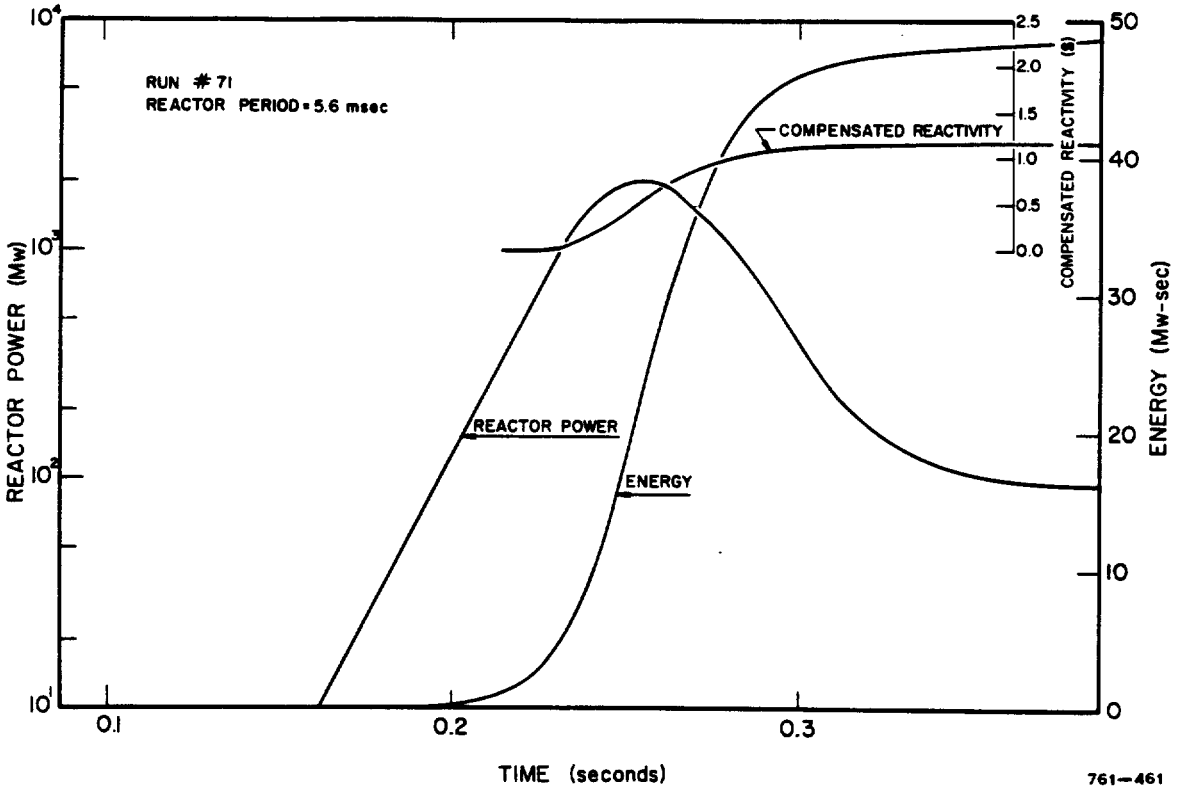

FIG. B-46 RUN 71 – 5.6-MSEC-PERIOD TEST.

1133328

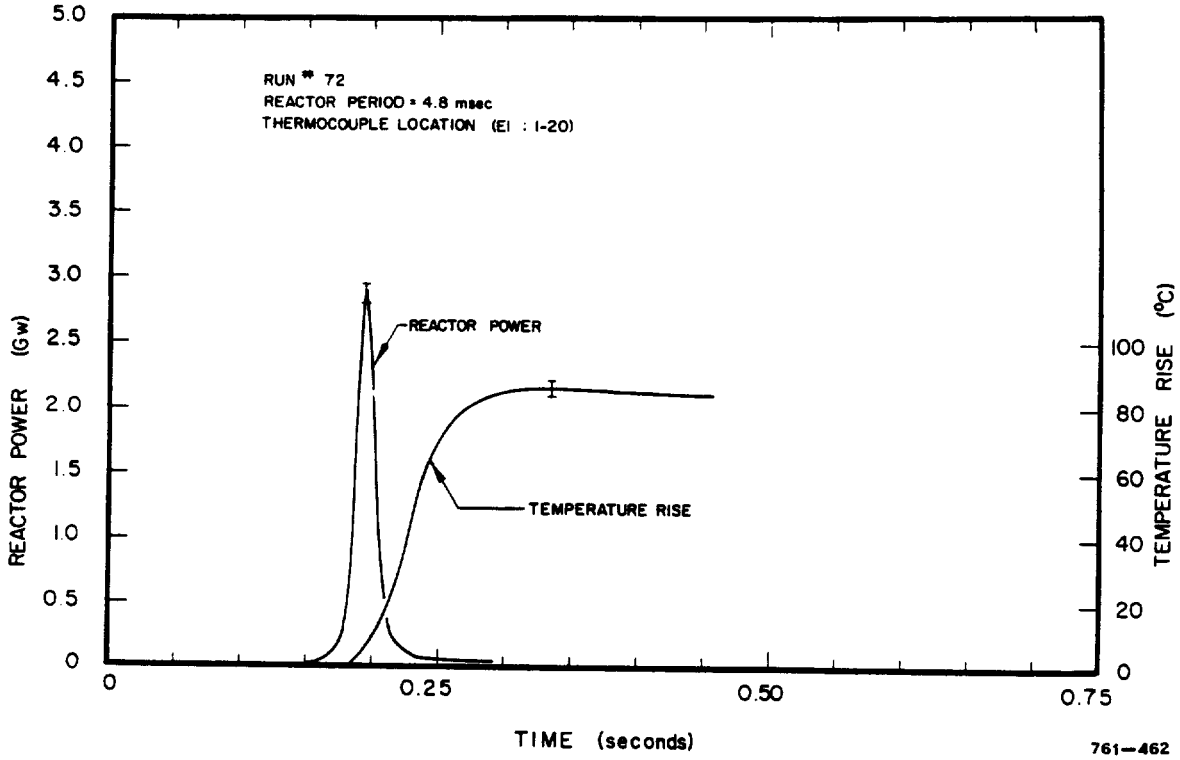

FIG. B-47 RUN 72 – 4.8-MSEC-PERIOD TEST.

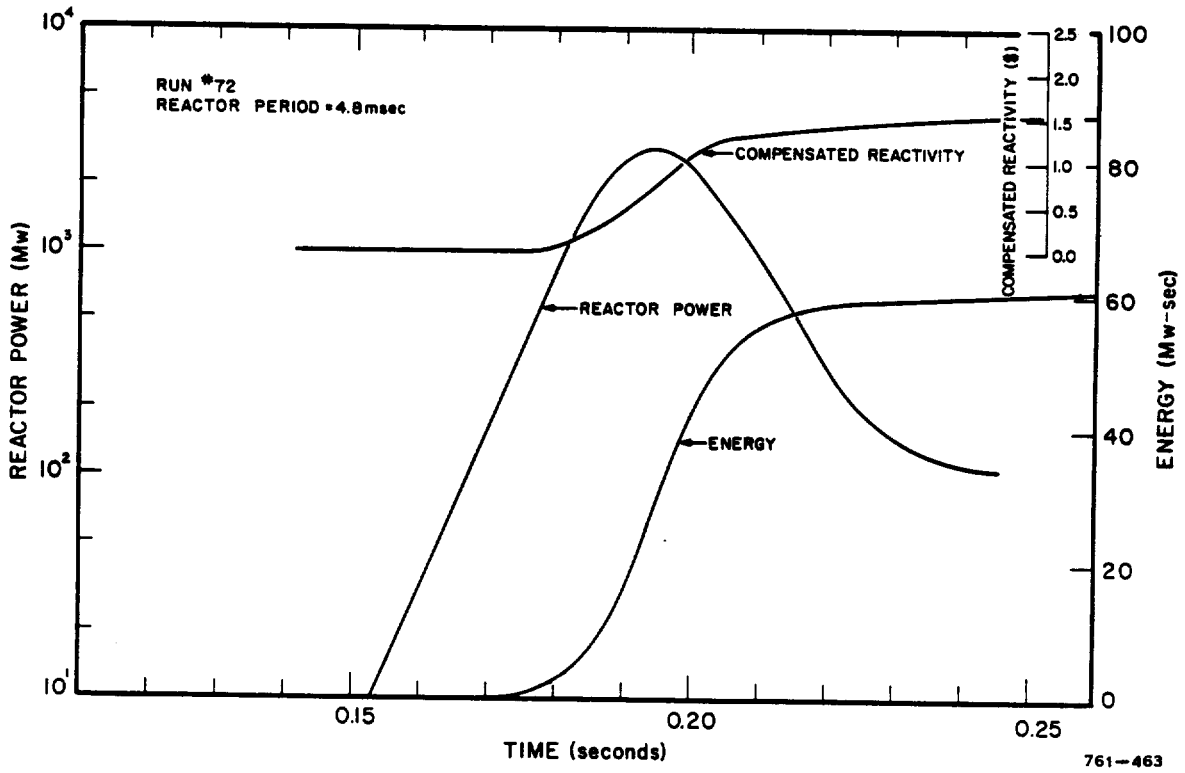

FIG. B-48 RUN 72 – 4.8-MSEC-PERIOD TEST.

1133329

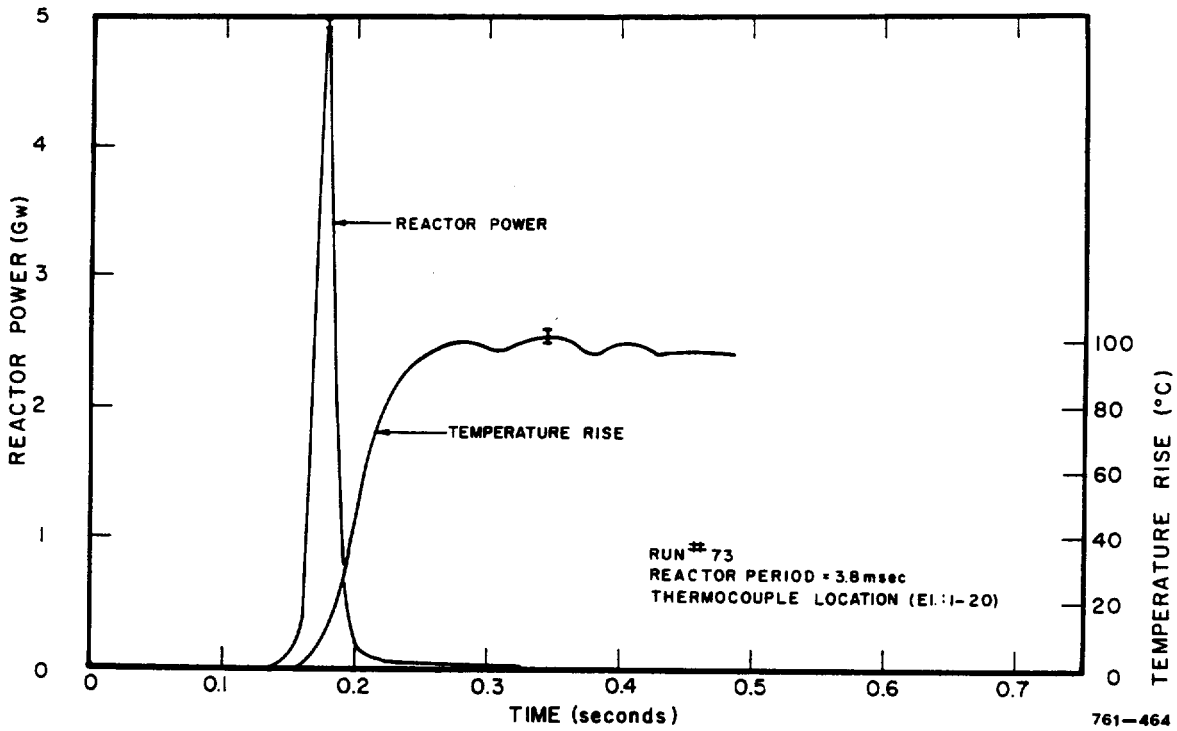

FIG. B-49 RUN 73 — 3.8-MSEC-PERIOD TEST.

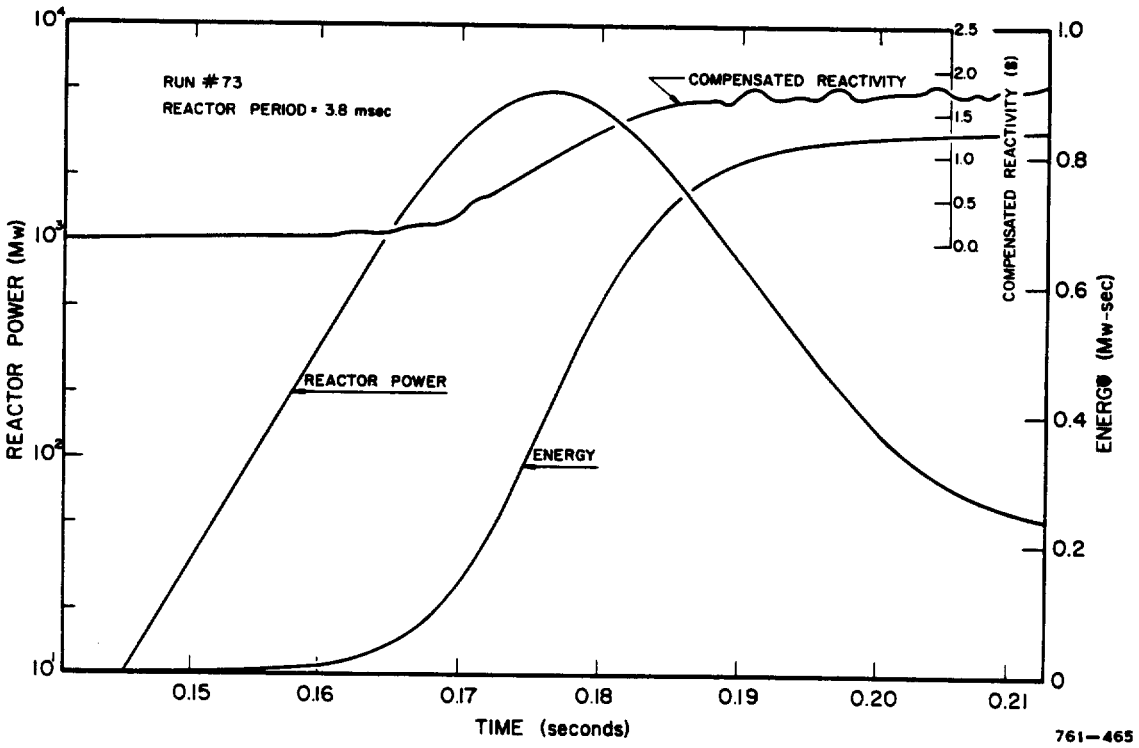

FIG. B-50 RUN 73 — 3.8-MSEC-PERIOD TEST.

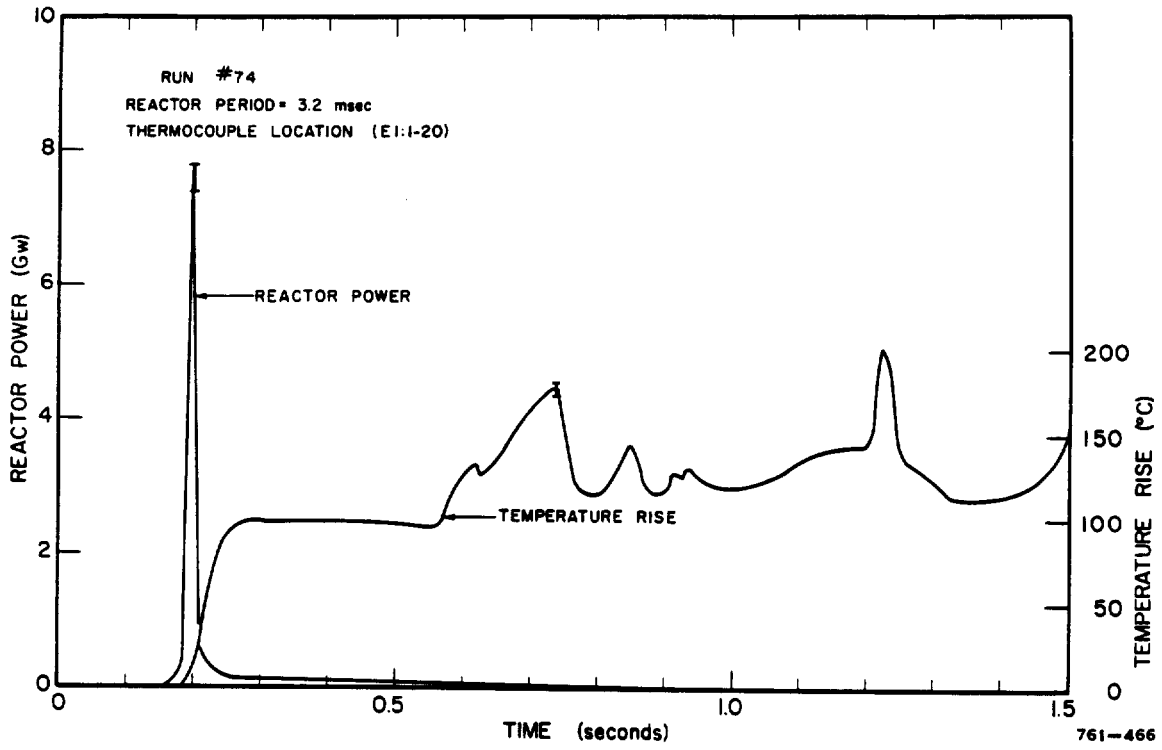

FIG. B-51 RUN 74 – 3.2-MSEC-PERIOD TEST.

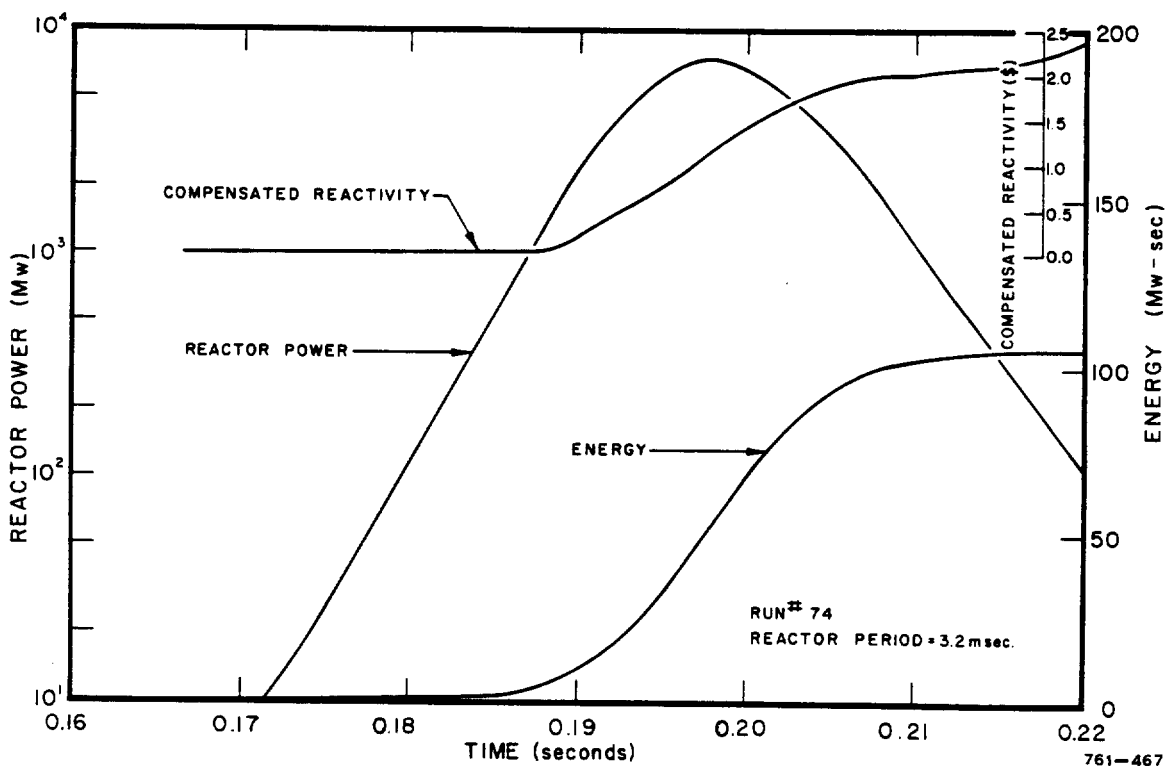

FIG. B-52 RUN 74 – 3.2-MSEC-PERIOD TEST.

APPENDIX C

PLOTS OF PEAK POWER, TOTAL ENERGY AT TIME OF PEAK POWER, AND COMPENSATED REACTIVITY AT TIME OF PEAK POWER VS INVERSE PERIOD, FOR CONSTRAINED AND UNCONSTRAINED SPERT I OXIDE CORES

1133332

INTENTIONAL BLANK PAGE NO. 78

1133333

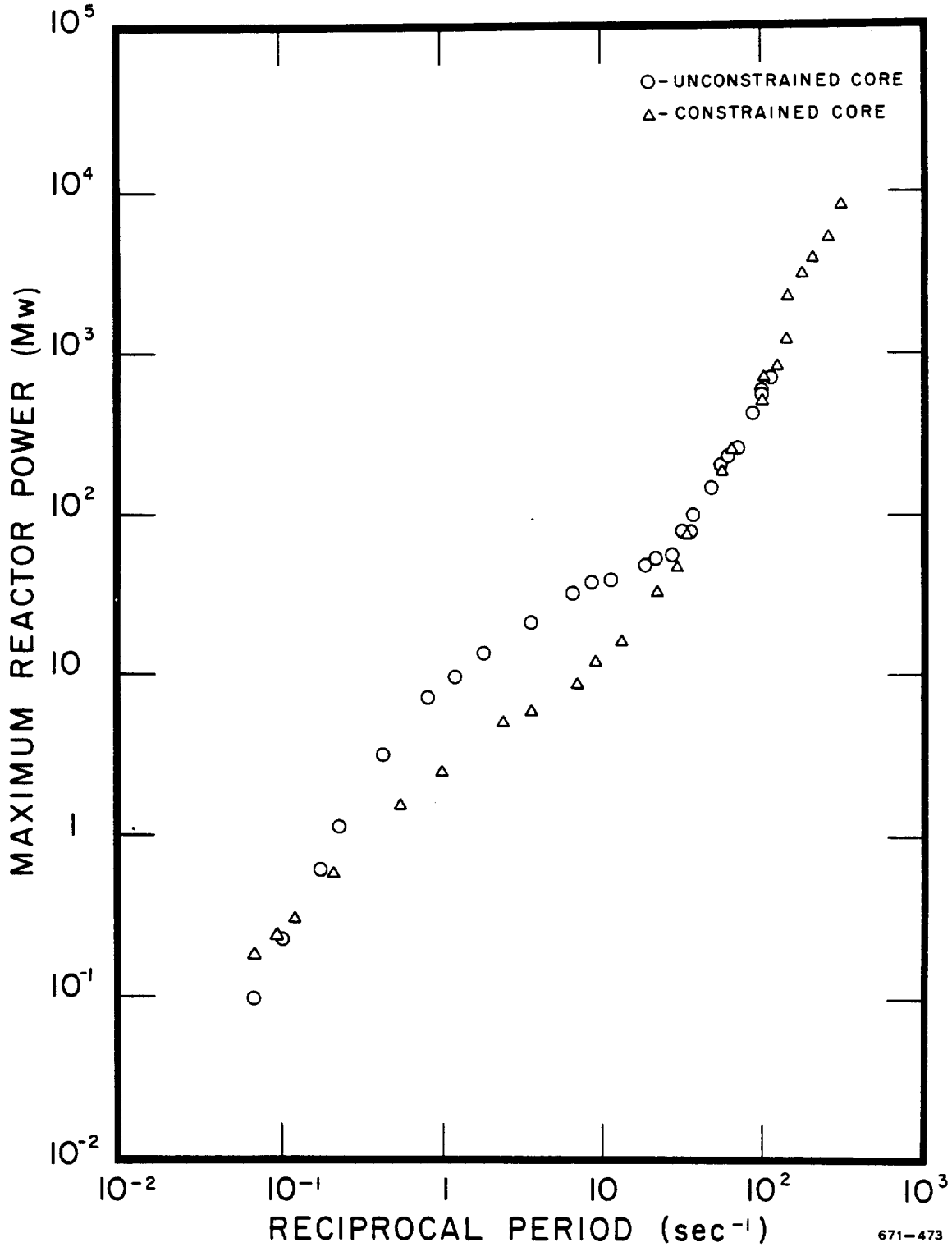

FIG. C-1 PEAK POWER VS INVERSE REACTOR PERIOD.

1133334

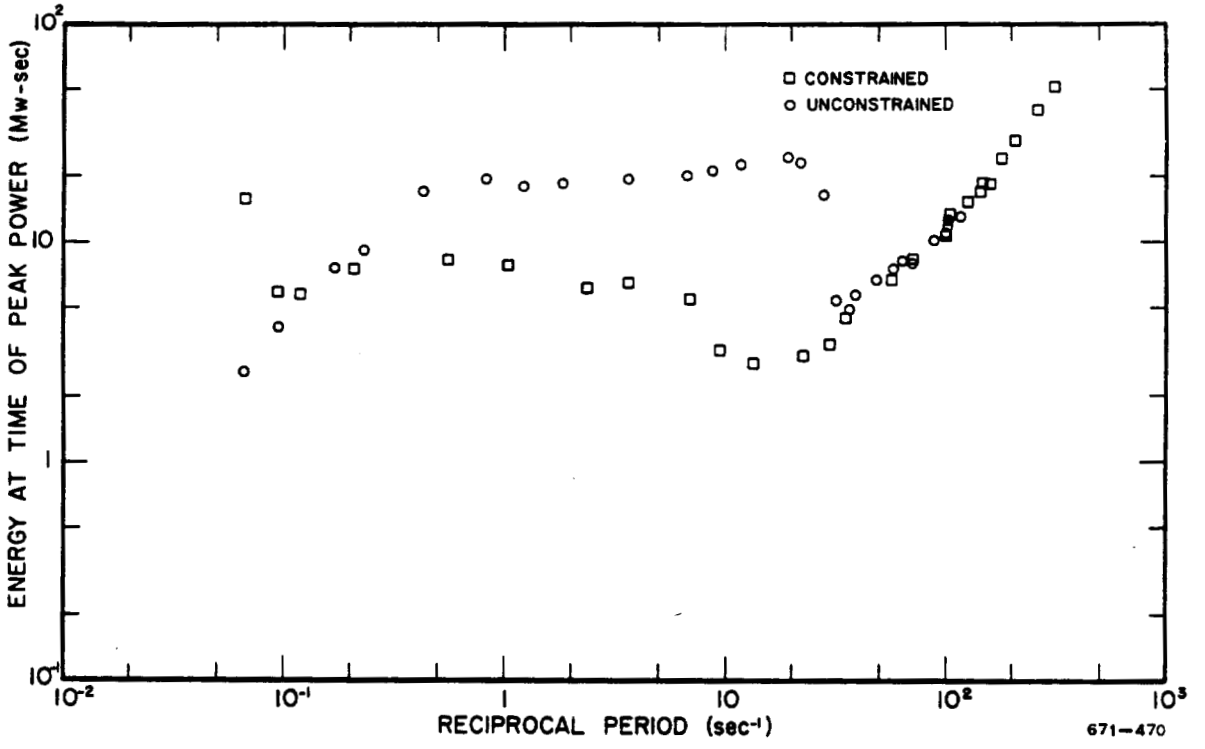

FIG. C-2 ENERGY AT TIME OF PEAK POWER VS INVERSE REACTOR PERIOD.

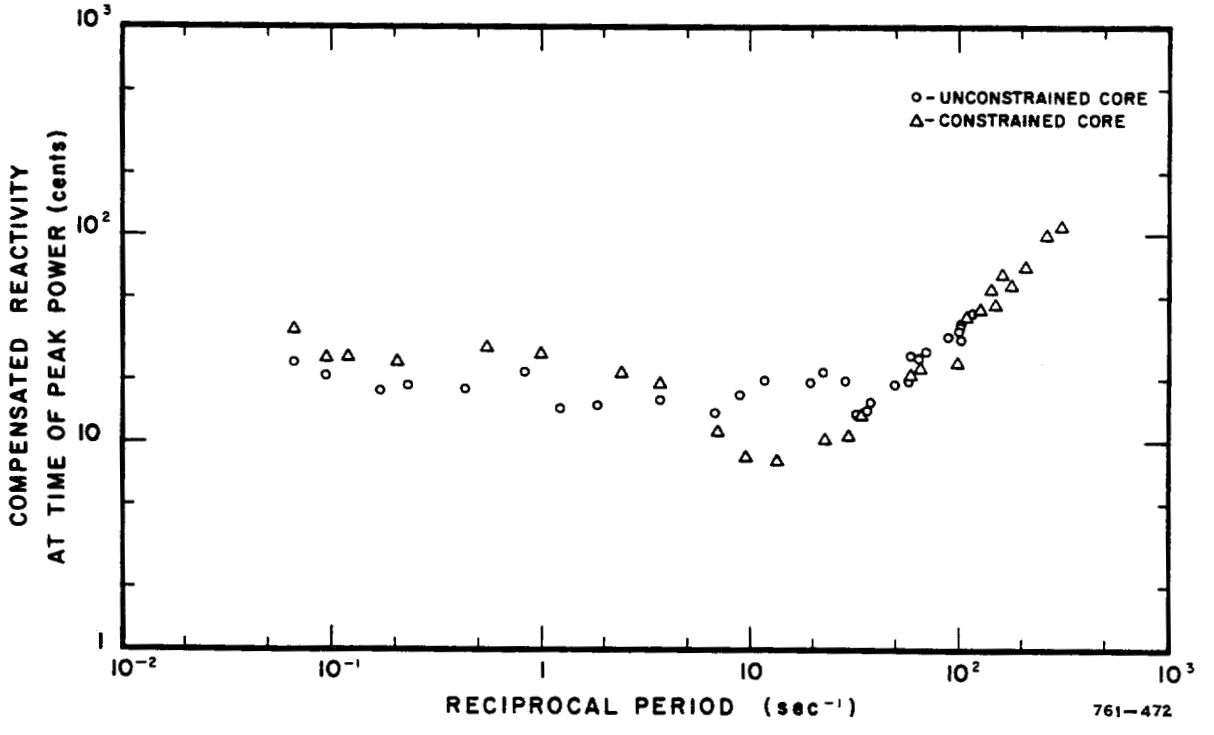

FIG. C-3 COMPENSATED REACTIVITY AT TIME OF PEAK POWER VS INVERSE REACTOR PERIOD.

1133335

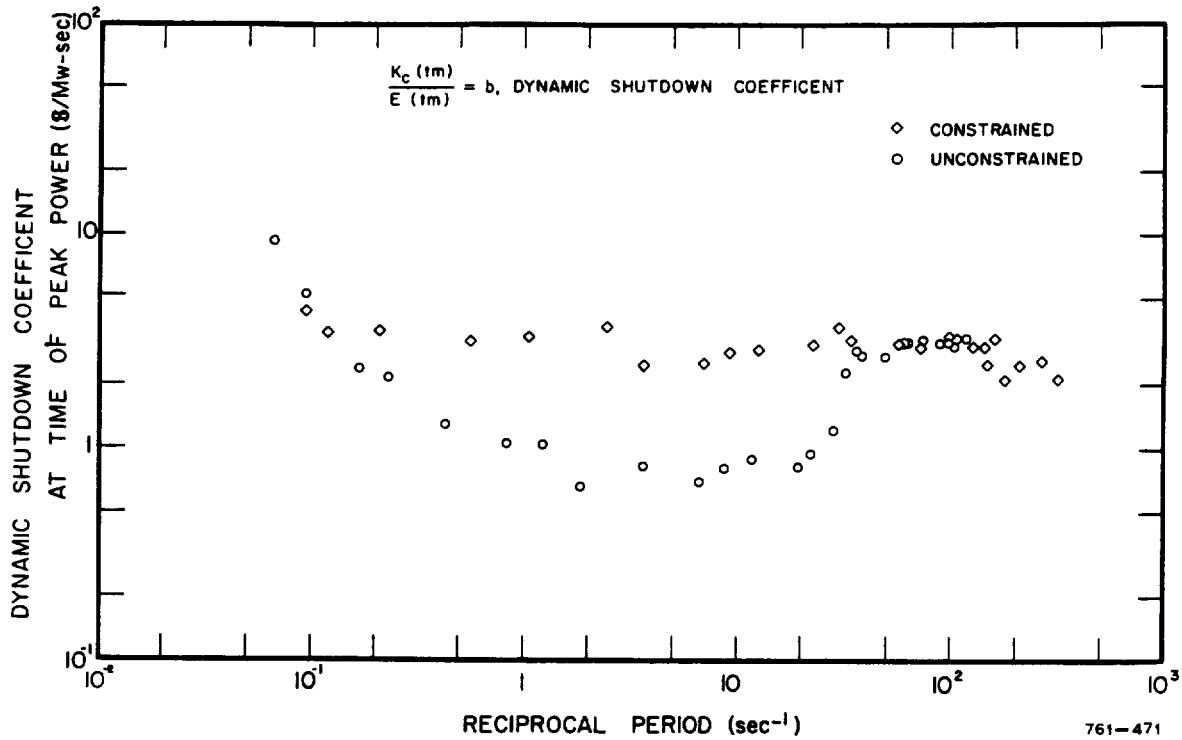

FIG. C-4 DYNAMIC SHUTDOWN COEFFICIENT VS INVERSE REACTOR PERIOD.

113333b

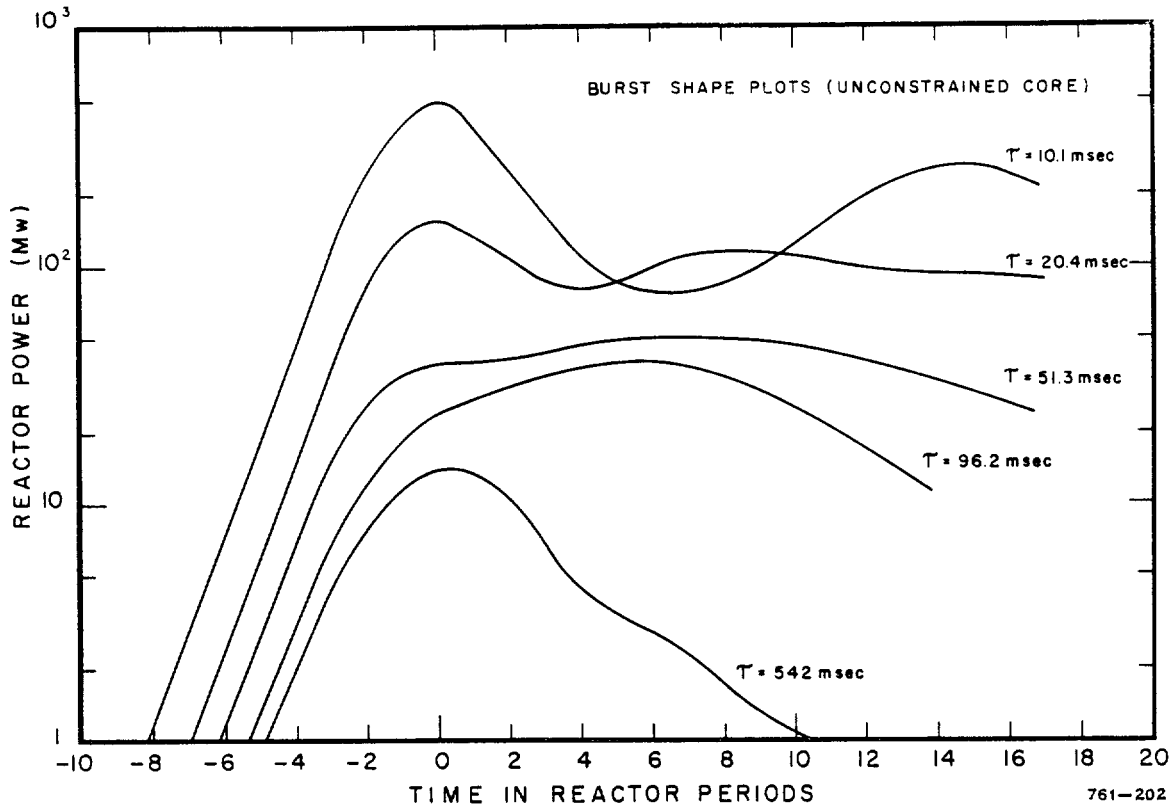

FIG. C-5 POWER-BURST-SHAPE PLOTS (UNCONSTRAINED OXIDE CORE).

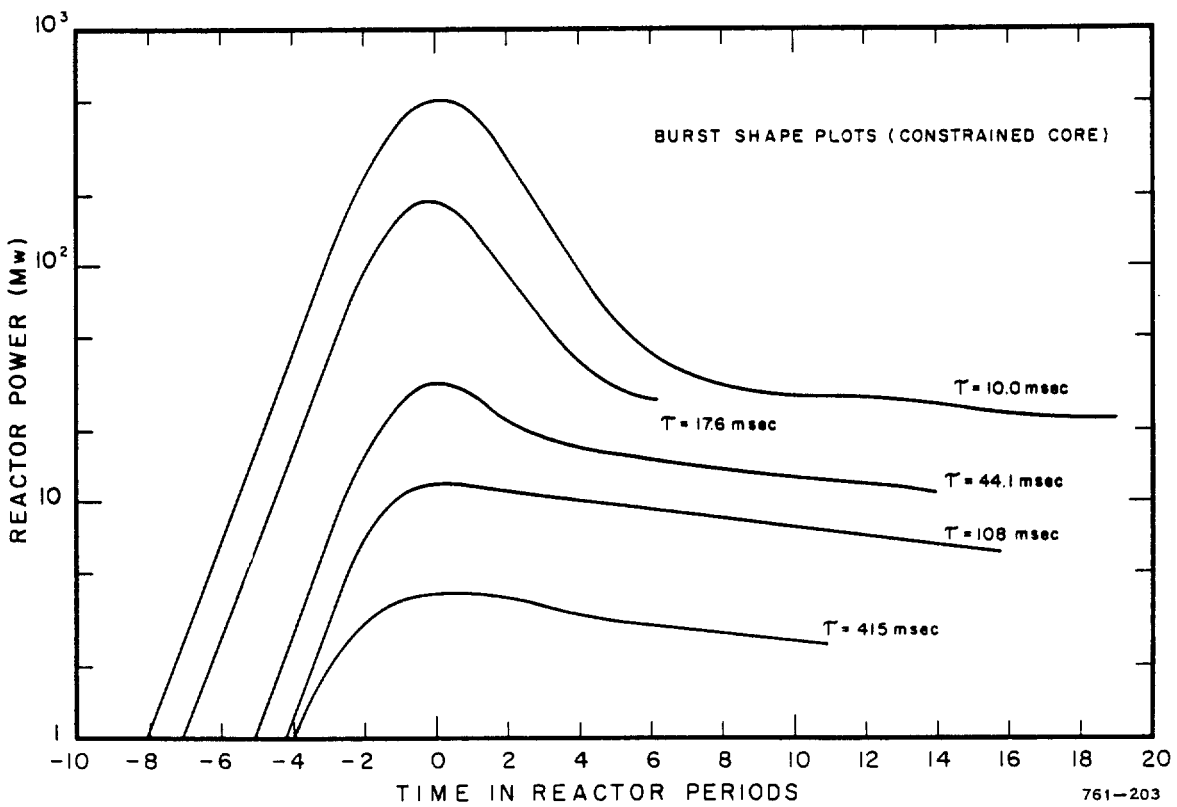

FIG. C-6 POWER-BURST-SHAPE PLOTS (CONSTRAINED OXIDE CORE).

1133337

APPENDIX D

SUMMARY TABLES OF KEY DATA, FOR THE CONSTRAINED AND UNCONSTRAINED SPERT I OXIDE CORES

1133338

INTENTIONAL BLANK PAGE NO. 84

1133339

TABLE II

SUMMARY TABLE OF KEY DATA, FOR UNCONSTRAINED CORE

Figure No.	Run No.	τ (msec)	α (sec^{-1})	$\phi(t_m)$ (Mw)	$E(t_m)$ (Mw-sec)	θ_m (°C)	$\theta(t_m)$ (°C)	Thermo-couple Location	(t_m-t_o)	Reactivity Insertion (ϕ)	Reactivity Compensated at $\phi(t_m)$(ϕ)
A-1	64	15.2×10^3	0.066	0.098	2.58	11.7	10.8	E4:4-17	216.5	30.6	24.2
A-3	3	10.5×10^3	0.095	0.210	4.07	30.7	24.0	E1:1-20	116.0	36.0	21.5
A-5	5	5.9×10^3	0.170	0.690	7.60	57.7	45.0	E1:1-20	57.4	47.8	18.0
A-7	63	4.3×10^3	0.232	1.14	9.20	60.0	48.5	E1:1-20	66.7	54.1	19.5
A-9	6	2.3×10^3	0.430	3.25	17.1	92.0	84.0	E1:1-20	30.5	65.1	22.0
A-11	7	1.2×10^3	0.833	7.07	19.3	101.0	88.0	E1:1-20	14.9	76.0	20.0
A-13	8	822	1.22	9.82	17.9	96.5	86.8	E1:1-20	12.4	80.5	19.0
A-15	9	542	1.85	13.7	18.3	100.0	90.0	E1:1-20	8.2	84.7	12.0
A-17	10	273	3.66	20.9	11.1	100.0	79.0	E1:1-20	4.67	90.3	16.0
A-19	11	150	6.67	32.7	7.1	94.5	73.0	E1:1-20	2.55	95.3	14.0
A-21	12	114	8.77	37.7	6.4	100.7	78.0	E1:1-20	2.30	97.6	17.0
A-23	13	84.2	11.8	39.6	5.3	104.3	78.0	E1:1-20	1.87	99.3	20.0
A-25	14	51.8	19.3	48.1	5.52	95.2	60.0	W7:1-20	1.47	102.9	19.6
A-27	15	45.2	22.1	53.7	5.38	100.0	76.0	E1:1-20	1.24	104.5	22.0
A-29	16	35.5	28.2	64.3	5.67	100.0	29.0	E1:1-20	0.92	106.4	20.0
A-31	17	31.2	32.1	77.4	5.41	102.3	12.3	E1:1-20	0.632	108.4	14.0
A-33	62	27.4	36.5	77.8	4.9	91.2	46.0	E1:1-20	0.620	110.0	14.0
A-35	18	25.8	38.7	101.0	5.77	102.3	5.8	E1:1-20	0.53	111.0	15.5
A-37	19	20.4	49.0	146.0	6.69	107.2	5.8	E1:1-20	0.51	114.4	18.0
A-39	21	17.2	58.1	198.0	7.57	108.2	7.0	E1:1-20	0.423	117.7	23.0
A-41	22	15.7	63.7	239.0	8.16	104.0	6.8	E1:1-20	0.420	119.9	25.3
A-43	27	14.2	70.4	260.0	7.88	110.2	6.3	E1:1-20	0.380	123.0	27.0
A-45	28	11.2	89.3	428.0	10.2	109.2	4.0	E4:4-20	0.324	129.0	32.0
A-47	29	10.1	99.0	494.0	11.0	107.5	8.0	E1:1-20	0.300	132.0	34.0
A-49	65	9.7	103.0	622.0	12.6	97.2	10.0	E1:1-18	0.325	134.0	37.0
A-51	66	9.7	103.0	571.0	11.9	92.0	5.0	E1:1-20	0.320	134.0	38.0
A-53	75	9.7	103.0	546.0	11.9	106.0	8.0	E1:1-20	0.410	134.0	32.0
A-55	30	8.5	118.0	720.0	13.0	109.0	7.0	E1:1-20	0.26	140.0	43.0

NOMENCLATURE

τ	Reactor period
α	Inverse reactor period
$\phi(t_m)$	Peak power
$E(t_m)$	Energy release to time of peak power
θ_m	Maximum fuel plate surface temperature
$\theta(t_m)$	Fuel plate surface temperature at time of peak power
t_m	Time of peak power
t_o	Time or contact of falling transient rod with shock absorber

1133340

TABLE III

SUMMARY TABLE OF KEY DATA, FOR CONSTRAINED CORE

Figure No.	Run No.	τ (msec)	α (sec^{-1}	$\phi(t_m)$ (M_w)	$E(t_m)$ (Mw-sec)	θ_m (°C)	$\theta(t_m)$ (°C)	Thermo-couple Location	(t_m-t_o)	Reactivity Insertion (ϕ)	Reactivity Compensated at $\phi(t_m)$(ϕ)
B-1	47	$15x10^3$	0.067	0.185	15.7	32.0	31.0	E1:1-20	262.0	30.6	35.5
B-3	41	$10.5x10^3$	0.095	0.240	5.93	35.6	24.9	E1:1-20	140.22	36.8	26.0
B-5	56	$8.1x10^3$	0.12	0.310	5.76	26.0	20.0	E1:4-23	114.0	40.7	20.0
B-7	45	$4.8x10^3$	0.21	0.590	7.51	50.0	30.7	E1:1-20	63.0	50.3	26.4
B-9	48	$1.8x10^3$	0.56	1.52	8.36	68.7	43.0	E1:1-20	25.5	65.9	26.5
B-11	42	957	1.05	2.48	7.82	82.0	36.0	E1:1-20	17.17	75.5	26.0
B-13	49	416	2.41	4.14	6.14	84.0	35.5	E1:1-20	7.53	85.5	22.6
B-15	43	273	3.67	6.01	6.50	84.0	23.0	E1:1-20	4.46	89.0	16.0
B-17	40	144	6.96	8.70	5.45	88.5	12.0	E1:1-20	2.175	94.5	13.5
B-19	52	108	9.26	12.11	3.21	81.0	8.0	E1:1-20	1.395	96.4	9.0
B-21	39	73.9	13.5	15.9	2.79	91.0	8.0	E1:1-20	1.14	99.3	8.0
B-23	53	44.1	22.7	32.3	3.02	90.5	6.0	E1:1-20	0.900	102.3	9.25
B-25	68	33.5	29.9	48.6	3.40	92.5	5.0	E1:1-20	0.615	105.3	12.6
B-27	50	29.2	34.2	74.4	4.49	88.0	7.0	E1:1-20	0.607	107.4	14.0
B-29	38	17.6	56.8	190.0	6.76	85.0	8.0	E1:1-20	0.407	116.7	20.6
B-31	51	14.0	71.4	259.0	8.40	93.0	8.0	E1:1-20	0.468	118.2	24.6
B-33	54	10.2	98.1	515.0	10.76	92.0	4.5	E1:1-20	0.337	129.0	36.0
B-35	55	9.4	106.0	669.0	13.51	97.8	9.5	E1:1-20	0.316	135.0	43.8
B-37	59	7.9	127.0	869.0	15.12	102.0	34.0	E1:1-20	0.275	140.0	45.0
B-39	69	7.0	143.0	1126.0	16.93	91.5	9.0	E1:1-20	0.254	145.0	50.0
B-41	61	6.8	147.0	1345.0	18.69	93.5	10.0	E7:7-12	0.276	148.0	45.0
B-43	70	6.3	159.0	1440.0	18.35	99.5	2.0	E1:1-18	0.241	151.0	60.0
B-45	71	5.6	179.0	2010.0	24.0	88.5	6.0	E1:1-20	0.226	161.0	50.0
B-47	72	4.8	208.0	2820.0	29.0	87.5	8.0	E1:1-20	0.194	172.0	70.0
B-49	73	3.8	263.0	4930.0	40.0	99.0	10.0	E1:1-20	0.185	190.0	102.5
B-51	74	3.2	313.0	7480.0	51.3	179.0	16.0	E1:1-20	0.198	210.0	107.5

NOMENCLATURE

τ	Reactor period
α	Inverse reactor period
$\phi(t_m)$	Peak power
$E(t_m)$	Energy release to time of peak power
θ_m	Maximum fuel plate surface temperature
$\theta(t_m)$	Fuel plate surface temperature at time of peak power
t_m	Time of peak power
t_o	Time of contact of falling transient rod with shock absorber

1133341

RECEIVED
PHILLIPS PETROLEUM CO.
OCT 11 1968
TECHNICAL LIBRARY

PHILLIPS 66

1133342